NenuFAR : instrument description and science case

V5, 10/10/2014

NenuFAR : instrument description and science case

Authors list

(**French** / Foreign co-authors)

&

Supporting scientists & Others

M. Atemkeng (Univ. Cape, SA)

S. Azarian (ONERA)

M. Barsuglia (APC)

A. Bonafede (Hamburg Obs.)

F. Boone (IRAP)

A. Bosma (LAM)

R. Boyer (L2S)

M. Branchesi (INAF)

C. Briand (LESIA)

B. Cecconi (LESIA)

S. Célestin (LPC2E)

D. Charrier (Subatech)

E. Chassande-Mottin (APC)

A. Coffre (USN)

I. Cognard (LPC2E)

F. Combes (LERMA)

S. Corbel (Univ. Paris-Diderot, CEA)

C. Courte (ESBAT)

A. Dabbech (Lagrange, OCA)

R. Dallier (Subatech)

L. Denis (USN)

C. Dumez-Viou (USN)

M. N. El Korso (LEME, Univ. Paris Ouest)

E. Falgarone (ENS)

I. Falkovych (IRA Kharkov) †

A. Ferrari (Lagrange, OCA)

C. Ferrari (Lagrange, OCA)

K. Ferrière (IRAP)

C. Fevotte (Lagrange, OCA)

A. Fialkov (ENS)

M. Fullekrug (Univ. Bath)

E. Gérard (GEPI)

J. N. Girard (CEA/AIM)

J.-M. Grießmeier (LPC2E)

B. Guiderdoni (CRAL)

L. Guillemot (LPC2E)

J. Hessels (ASTRON)

A. Konovalenko (IRA Kharkov)

L. Koopmans (Kapteyn Univ.)

V. Kondratiev (ASTRON)

L. Lamy (LESIA)

T. Lanz (Lagrange, OCA)

P. Larzabal (ENS Cachan)

M. Lehnert (IAP)

F. Levrier (ENS Paris)

A. Loh (Univ. Paris-Diderot, CEA)

G. Macario (Lagrange, OCA)

J.-J. Maintoux (RETRAM)

J. Maintoux (RETRAM)

L. Martin (Subatech)

D. Mary (Lagrange, OCA)

S. Masson (LESIA)

M.-A. Miville-Deschenes (IAS)

D. Oberoi (MIT)

M. Panchenko (SRI Graz)

M. Pandey-Pommier (CRAL)

A. Petiteau (APC)

J.-L. Pinçon (LPC2E)

B. Revenu (Subatech)

F. Rible (RETRAM)

C. Richard (Lagrange, OCA)

H. O. Rucker (SRI Graz)

P. Salomé (LERMA)

B. Semelin (LERMA)

M. Serylak (Univ. Oxford)

M. Sidorchuk (IRA Kharkov)

O. Smirnov (Univ. Cape, SA)

B. Stappers (Univ. Manchester)

C. Taffoureau (USN)

M. Tagger (LPC2E)

C. Tasse (GEPI)

G. Theureau (LPC2E)

P. Tokarsky (IRA Kharkov)

S. Torchinsky (USN)

O. Ulyanov (IRA Kharkov)

W. van Driel (GEPI)

I. Vasylieva (LESIA & IRA Kharkov)

J. Vaubaillon (IMCCE)

F. Vazza (Hamburg Obs.)

S. Vergani (GEPI)

M. Was (LAPP)

R. Weber (PRISME / Polytech)

V. Zakharenko (IRA Kharkov)

P. Zarka (LESIA)

The NenuFAR project

P. Zarka, M. Tagger, L. Denis, J. Girard, C. Tasse, & the NenuFAR-France team[1]

1. Introduction

Radioastronomy experiences a period of rapid change, with many new radiotelescopes under study, construction, commissioning or operation (LOFAR, LWA, MWA, MeerKAT, ASKAP, SKA[2]). They bring in an increase in sensitivity and resolution by orders of magnitude, over wide fields of view (FoV), thanks to the development of new technologies in the fields of telecommunication and massive parallel computation. This instrumental revolution will have a major impact in 21st century astrophysics and in fundamental physics, much beyond what radioastronomy can usually do.

The project NenuFAR – New extension in Nançay upgrading LOFAR – is both a major extension of the LOFAR array (the LOFAR Super Station – LSS) and a standalone large low-frequency (LF) instrument. NenuFAR is the generic name for the entire project, whereas its two facets will be named hereafter NenuFAR/LSS and NenuFAR/Standalone. NenuFAR/LSS will dramatically increase LOFAR's total sensitivity and image resolution, whereas NenuFAR/Standalone will provide high instantaneous beamformed sensitivity down to 10 MHz, as well as coarse imaging in a broad FoV (as discussed in section 7 below, an minor evolution of the design will actually permit imaging to be not so coarse for stable broadband sources).

These capabilities will allow astronomers to address such fundamental scientific questions as : (i) What is the nature of the processes that couple the stellar winds to the planetary systems? (this applies to our solar system as well as to exoplanets) (ii) What is the spatial structure and dynamics of the interstellar warm plasma in the Milky way? (iii) What are the populations and physical processes underlying the unveiled Impulsional Universe? (iv) What were the physical processes controlling the evolution of the baryonic matter at very high redshift ($z>10$) ? And (v) How did the Universe take its local shape over cosmic time scales ?

2. Concept

The original concept of NenuFAR is briefly described in [Zarka et al., 2012], and further detailed in the following chapters 3 to 7. NenuFAR consists of adding to the standard Nançay LOFAR station (FR606) 96 LF tiles. Each tile is a regular hexagonal cluster of 19 crossed-dipole antennas, analogically phased (it is hereafter noted MA_{19} for « 19-antennas mini-array »). The 96 MA_{19} will be included in a disk of 400 m in diameter (~5 Dutch LOFAR station diameters or ~6 European LOFAR station diameters [van Haarlem et al., 2013]). Thus NenuFAR will gather 96x19 = 1824 dual-polarized antennas, equivalent to the whole Dutch LOFAR-LBA, but in a compact configuration. The frequency range of operation (~10-85 MHz) will include the main LOFAR-LBA range 30-80 MHz and extend it to lower frequencies with largely increased sensitivity (LOFAR-LBA can be used to observe down to 10 MHz but with low sensitivity).

The analog output signals from the 96 MA_{19} (96 tiles x 2 polarizations), adequately amplified, will be split in two signal paths:

- One path will feed the 96 dual-polarization receivers (RCUs) of the LOFAR backend via its spare (LBL) input (10-90 MHz), making NenuFAR a high-sensitivity LOFAR-compatible

[1] See author list of the NenuFAR-Science-Case document.
[2] See list of acronyms and abbreviations

« super-LBA station » (NenuFAR/LSS mode). The signal will then be processed as those of the LBA field of FR606, i.e. digitized, channelized (with polyphase filters, in ~200 kHz subbands), beamformed (the FR606 beamforming software will be adapted to take into account the characteristics of NenuFAR antennas), and the resulting complex streams will be sent to LOFAR's central correlator in Groningen to be correlated with all other stations' LBA signals, or to be further channelized (by FFT, to <1 kHz resolution) in "single-station" mode.

- The second signal path will feed a dedicated, specifically designed, Standalone NenuFAR backend. This backend will digitize the 96 x 2 MA_{19} signals, channelize them in 200 kHz or 100 kHz subbands, and form 2 beams in 2 arbitrary pointing directions within the analog FoV of the MA_{19}, each over the whole NenuFAR bandwidth (~10-85 MHz). The (complex) outputs of the beamformer can in turn feed a post-backend/computer (such as ARTEMIS [Armour et al., 2011]) that ingests high resolution station data and locally computes high-resolution time-frequency planes including parametric dedispersion, RFI mitigation, etc. In addition, the Standalone NenuFAR backend will export the subband signals (full resolution, complex) to a dedicated correlator, in order to compute cross-correlations (visibilities) between MA_{19} at high rate, permitting to do Standalone imaging with NenuFAR (with high sensitivity but modest resolution, see below).

NenuFAR will not be by itself a powerful imaging instrument. Combined with LOFAR, NenuFAR/LSS will bring the following significant improvements :

- Long LOFAR baselines (>1000 km) make possible for the first time high spatial resolution images (with sub-arcsec resolution) in degree-scale FoV. Those including NenuFAR will be √19 times more sensitive than with the standard FR606 LBA field. As errors on calibration of the instrumental and ionospheric effects are the main limiting factor for high resolution imaging, adding extra sensitivity to long baselines will help calibration (especially direction-dependent solutions for correcting ionospheric effects). Because most sources are resolved on international baselines, high resolution imaging will generally meet signal-to-noise limitations, so that a more sensitive station such as NenuFAR/LSS will represent an advantage, by giving access to many more calibrators, improving wide field LF imaging at arcsec resolution. The first step will be to image bright MSSS sources in order to construct high spatial resolution models for wide field calibration. Sensitive high resolution wide-field imaging in the LBA range with LOFAR+NenuFAR will permit to study black hole formation and AGN activity at moderate redshifts ($z<1$), details of star formation in nearby galaxies (resolving star formation clumps up to $z=1$-2), and conduct extragalactic surveys in dense extragalactic fields already observed by LOFAR (where strong calibrators are available). High resolution full polarization observations (provided that the absolute ionospheric Faraday rotation is properly calibrated) will be very valuable to image small-scale magnetic fields via rotation measure measurements without depolarization due to spatial integration, and study shocks in the hot intergalactic medium at galactic haloes to cluster scales (where 0.1-1 Mpc shocks have been detected). Detection of time-correlated scintillation effects between distant LOFAR stations (including NenuFAR) will also provide the possibility to perform 3D tomographic reconstruction of the ionospheric structure. These observations can be performed with NenuFAR and LOFAR international stations only, when the Dutch LOFAR is busy and not available.
- Correlation of signals from the MA_{19} within NenuFAR will provide 96x95/2=4560 baselines, ~25% of which are 2 to 3 times shorter than a LOFAR station diameter − the shortest baseline presently available − , but far more sensitive than the antenna-to-antenna baselines within a standard LOFAR station. These measurements at short (u,v) spacings, poorly sampled in the current LOFAR low band hardware, are crucial for the imaging of large-scale structures. Specifically they will permit the study of the warm plasma radio emission from the Milky Way and large structures within it. LOFAR+NenuFAR will thus permit to study the ISM at both large and small scales, in addition to pulsar measurements.

In Standalone mode, its high instantaneous beamformed sensitivity with full polarization capability

in several (≥2) beams will make NenuFAR/LSS a powerful detector of unresolved LF radiosources (flare stars, exoplanets and Solar system planets, pulsars, RRATs…). It is shown in chapter 8 of this document (by Fialkov et al.) to be well adapted to the search and study of the dark ages/cosmic dawn signal. Coupled to an ARTEMIS-like post-backend, it will be very powerful for blind transient searches. The dedicated correlator will permit to build images at ~0.5° to 4° resolution (see below) in the 10°-60° MA_{19} analog beam, at timescales ~1 sec, permitting to conduct efficiently systematic searches and blind transient searches in large FoV with good sensitivity.

Both backends will be usable in parallel, permitting to conduct simultaneously observation programs within LOFAR (when international LBA stations are requested) and in Standalone mode, with the only constraint that both programs concern targets within the analog FoV of the MA_{19} (see details below). Both backends will also produce low-rate spectral and correlation subband statistics, that can be used for NenuFAR's calibration as well as for monitoring (instrument health, RFI environment, sky maps).

A design study conducted from 10/2009 to 2/2013 allowed us to define and test all the elements of NenuFAR's design [Girard et al., 2012a ; Girard, 2013]: antenna radiator and preamplifier, MA_{19} topology and phasing, MA_{19} distribution, control/command and dialog with LOFAR. The optimal antenna radiator design was found to be the LWA one [Hicks et al., 2012], that we adapted to our environment. The preamplifier is an original design with improved characteristics. Details are given in chapter 3 (Girard et al.), and all technical studies and reports are available at http://nenufar.obs-nancay.fr/ (lss / anr090509). The construction of NenuFAR was also fully costed at ~5 M€, and a site study was conducted by the Office National des Forêts that authorized the necessary tree cuts and terrain preparation (~13 hectares) necessary to build NenuFAR.

The LOFAR Transient Buffer Boards (TBB) of FR606 and analog RAM in the dedicated receiver will permit full waveform capture at 5 nsec resolution from all MA_{19} for snapshots of a few seconds. It will also be possible to record the waveform of the beamformed NenuFAR signal for longer durations.

The science objectives of NenuFAR, briefly listed in [Zarka et al., 2012], are detailed in chapters 8 to 23 of this document. They include searches and studies of exoplanets and binary or eruptive stars, pulsars and Rotating RAdio Transients (RRATs), the structure of the Galactic Interstellar Medium (ISM), galaxy formation and pre-EoR dark ages cosmological signal, the « impulsional » Universe, Transient Luminous Events (TLE) in the Earth and planetary atmospheres, and Solar system physics.

3. Operation and data policy in LSS & Standalone modes

NenuFAR can be used either as part of the LOFAR network as a super-sensitive LBA station improving LOFAR's global sensitivity and imaging capabilities, especially toward low frequencies (NenuFAR/LSS mode), or as a standalone instrument with large instantaneous sensitivity (~2x LOFAR's core) oriented toward coherent beamformed observations and coarse imaging (NenuFAR/Standalone mode). The two modes can be used in parallel within the instantaneous MA_{19} FoV. It will also be possible to make sub-arrays of any number of MA_{19} point in specific directions.

Only a fraction of LOFAR observations request the use of international stations such as FR606 (≤1/3 presently, but this number will increase with the availability of long baselines calibrators and pipeline [Moldon et al., 2014]). When these observations are performed in the LBA range (≤half of the above quoted observations), the users will have the choice to select the FR606 LBA field, or the

NenuFAR antenna field (eventually, the latter will be systematically more interesting). The observed field, and consequently the analog pointing of the MA_{19}, will be defined by the ongoing LOFAR program. In that case, NenuFAR/Standalone observations will be possible in the same MA_{19} FoV.

In all other cases, i.e. when LOFAR observations are performed in the HBA range or do not request the use of international stations, Standalone use of NenuFAR will be possible without restriction. The Standalone use of an international LOFAR station by its owner country is guaranteed by contract for a minimum of 10% of the time, but the numbers above show that it is actually the case ≥50% of the time. The dedicated Standalone receiver will permit unrestricted observations ~3/4 of the time, and observations within a MA_{19} FoV fixed by a LOFAR program for the rest of the time.

In LSS mode, NenuFAR will be available as a LOFAR international station (as an alternative to the standard LBA), part of the ILT and programmed by the LOFAR Program Committee on its semester cycle basis, based on scientific merit. Authorship of papers using this mode will be opened to a NenuFAR Builders list for a limited time, similar to what is done with the LOFAR Builders list.

In stand-alone mode (which uses no LOFAR hardware or signal), NenuFAR will be operated by a French NenuFAR PC, including a member of LOFAR PC for better collaboration. Gradual transition to a common-user facility at least parallel to LOFAR policy is expected (with ~50% open time after 5 years). Following international standards, all observation data will be publicly available after a proprietary period (of e.g. 1 year).

4. Deployment of NenuFAR

Obtaining funding for NenuFAR imposes its realization in phases. The hierarchical design of NenuFAR consists of many identical elements (antennas, MA_{19}, phasing systems, …) and the dedicated receiver itself will have an evolutive architecture, with its number of acquisition/processing boards increasing with the number of MA_{19}.

NenuFAR Phase 1 (hereafter simply NenuFAR-1), whose budget is secured, will consist in the deployment of 24(±2) MA_{19} of 19 dual-polarization antennas, with their specifically designed preamplifiers, phasing systems, control/command systems and dedicated receiver. This phase will also include the preparation of infrastructures for the whole project. With 24x19 = 456 dual-polarized antennas, NenuFAR-1 will have capabilities similar to :

- ~4.7 international LOFAR stations or equivalently ~9.5 Dutch LOFAR stations, i.e. 1.5 times the LOFAR Superterp [van Haarlem et al., 2013];
- ~6 times the Nançay decameter array (NDA) [Boischot et al., 1980];
- ~2 times the LWA1 instrument (256 antennas [Taylor et al., 2012]).

The main differences consist of the hierarchical antenna phasing scheme (digitization of groups of analog-phased-arrays of 19 antennas in NenuFAR-1), the possibilities of operation (standalone only for the LWA1 or NDA, mostly within LOFAR for the Superterp, standalone or with LOFAR for NenuFAR-1), and the expandability of NenuFAR-1 into NenuFAR.

The scientific objectives of NenuFAR-1 overlap those of the whole NenuFAR, but with ~4x lower sensitivity and ~2x lower angular resolution (see detailed technical specifications in chapter 3).

NenuFAR-1 will also have several technical objectives, essentially aimed at demonstrating and fine-tuning the operations and developing the tools for the subsequent full-scale NenuFAR project. In particular, NenuFAR-1 will allow us :

- to optimize gain pattern and bandpass calibration techniques (based on strong natural

sources, noise-loads and/or an emitter in the field) ;
- to quantitatively document first order mutual coupling effects ;
- to set up, test and tune the dialog with LOFAR, both for commanding NenuFAR-1 and for beamforming and returning to the central correlator the signal from the 24 MA_{19} ;
- to build, test and operate the first slice of the dedicated receiver, with 24 dual-polarization inputs ;
- to set up the procedures for external and internal triggering ;
- to set up and operate piggyback programs.

5. Summary of NenuFAR and NenuFAR-1 baseline technical characteristics

NenuFAR

- Number of antennas : 1824, distributed within 96 mini-arrays of 19 antennas each (MA_{19})
  - each MA_{19} is an hexagon physically included in a disk of 25 m diameter
  - the minimum distance between MA_{19} centers is 27.5 m (in order to minimize the overlap of antennas' effective area)
  - NenuFAR will be included in an disk of 400 m in diameter
  - Number of baselines within NenuFAR : 4560
- Frequency range : ~10-85 MHz ; this is also the bandwidth per beam
- Frequency and time resolutions :
  - down to δf = 100 kHz after the 1st polyphase filter stage ; down to ~1 kHz with further (FFT) channelization of the beamformed complex streams
  - down to δt = 5 μsec, with the limitation $\delta f \times \delta t \geq 1$. Waveform snapshots capture mode at 5 nsec resolution (TBB).
- Polarizations : 2 linear polarizations measured by each antenna, NW-SE & SW-NE ; 4 Stokes parameters computed from these 2 measurements
- Declination of pointing : -23° to +90° (corresponding to an elevation ≥20°, at the latitude of Nançay 47.38° N)
- Effective area : $\lambda^2/3$ per antenna, $\sim 600\lambda^2$ for NenuFAR, with an upper limit $\sim 6 \times 10^4$ m^2 due to overlapping of antenna's effective areas below 30 MHz (i.e. for $\lambda \geq 10$ m)
- Field of View :
  - each antenna sees $\sim 2\pi$ sr
  - the instantaneous FoV of a phased MA_{19} is 60° – 8° at 10 – 80 MHz
- Number of beams : 2 (full-band ; possible trade-off N_{beams} vs Δf)
- Angular resolution / pencil beam size / pixel size in standalone imaging : 4° – 0.5° per beam at 10 – 80 MHz (i.e. ~16x16 pixels imaged in the MA_{19} analog beam)
- Sensitivity S_{min} : 2 – 0.5 Jy at 20 – 80 MHz (5σ, 1 sec x 10 MHz, polarized signal)
  31 – 9 mJy at 20 – 80 MHz (5σ, 1 h x 10 MHz, polarized signal)
- Confusion noise at zenith[3] : 50 – 1 Jy at 20 – 80 MHz (for unpolarized signal ; much lower for a polarized signal as randomly distributed polarization angles of faint background sources tend to cancel out net background polarization [e.g. Rohlfs & Wilson, 1996])

NenuFAR-1 : The hypothesis of 24 MA_{19} is taken. The actual number will be 24±2.

- Number of antennas : 456, distributed within 24 mini-arrays of 19 antennas each (MA_{19})
  - each MA_{19} is an hexagon physically included in a disk of 25 m diameter

[3] Theoretical estimate from [Condon, 2005].

    - the minimum distance between MA_{19} centers is 27.5 m (in order to minimize the overlap of antennas' effective area)
    - NenuFAR-1 will be included in an disk of 200 m in diameter
    - Number of baselines within NenuFAR-1 : 276
- Frequency range : ~10-85 MHz ; this is also the bandwidth per beam
- Frequency and time resolutions :
    - down to δf = 100 or 50 kHz after the 1st polyphase filter stage ; down to ~1 kHz with further (FFT) channelization of the beamformed complex streams
    - down to δt = 5 μsec, with the limitation $\delta f \times \delta t \geq 1$. Waveform snapshots capture mode at 5 nsec resolution (TBB).
- Polarizations : 2 linear polarizations measured by each antenna, NW-SE & SW-NE ; 4 Stokes parameters computed from these 2 measurements
- Declination of pointing : -23° to +90° (corresponding to an elevation ≥20°, at the latitude of Nançay 47.38° N)
- Effective area : $\lambda^2/3$ per antenna, $\sim 150\lambda^2$ for NenuFAR-1, with an upper limit $\sim 1.5 \times 10^4$ m^2 due to overlapping of antenna's effective areas below 30 MHz (i.e. for $\lambda \geq 10$ m)
- Field of View :
    - each antenna sees ~2π sr
    - the instantaneous FoV of a phased MA_{19} is 60° – 8° at 10 – 80 MHz
- Number of beams : 2 (full-band ; possible trade-off N_{beams} vs Δf)
- Angular resolution / pencil beam size / pixel size in standalone imaging : 8° – 1° per beam at 10 – 80 MHz (i.e. ~8x8 pixels imaged in the MA_{19} analog beam)
- Sensitivity S_{min} : 8 – 2 Jy at 20 – 80 MHz (5σ, 1 sec x 10 MHz, polarized signal)
  125 – 34 mJy at 20 – 80 MHz (5σ, 1 h x 10 MHz, polarized signal)
- Confusion noise at zenith[3] : 200 – 5 Jy at 20 – 80 MHz (for unpolarized signal ; much lower for a polarized signal)

6. Comparison and Synergies with existing or planned LF instruments

The table compares a few characteristics of **NenuFAR** and **NenuFAR-1** with those of large LF radio instruments (capable of observing below 100 MHz), existing or in project.

The LWA1 and OLWA have characteristics close to ½ x NenuFAR-1 [Taylor et al., 2012]. The OLWA is more image oriented, all 256 antennas (+outliers) being digitized and correlated. NenuFAR-1, owing to its hierarchical design in 24 MA_{19}, is more focussed towards coherent phased array beam observations, with imaging limited by the MA_{19} FoV. NenuFAR-1 is LOFAR-compatble (NenuFAR-1/LSS mode) whereas LWA1 is standalone only.

LOFAR's Superterp, and its related project AARTFAAC [Prasad &Wijnholds, 2012], consisting in an all-sky imager by correlation of the 288 antennas (LBA or HBA) of the 300m Superterp, is also imaging oriented. The larger diameter of the Superterp (300m, i.e. close to that of the full NenuFAR) results in a ~10x smaller FoV. NenuFAR-1, and furthermore NenuFAR, will have more limited imaging capabilities (number of baselines and instantaneous FoV) but a much higher sensitivity.

The NDA, operated since the 1970's in Nançay, is a instrument ~6x smaller than NenuFAR-1 (resp. 24x smaller than NenuFAR), single beam, built from circular polarization antennas, essentially automated and dedicated to systematic observations of Jupiter and the Sun up to 14 hours/day (it was also involved in the development of the CODALEMA experiment). Its observations feed databases that provide the basis for statistical studies and context for spacecraft observations. It has

low sensitivity but is well-calibrated and thus presents interest for cross-calibration with NenuFAR-1 & NenuFAR.

Name	Antennas	Eff. area	Freq. range	Ang. Res.	N beams	Polar.
NDA	144 circ. dipoles	2400 m^2 (*)	10–100 MHz	7.5◦ (*)	1 beam	4 Stokes
UTR-2	2040 dipoles	143000 m^2	8–32 MHz	0.5◦	5 beams	1 lin. polar.
VLA	27 dish.× 25 m	~2000 m^2	73–74.5 MHz	0.5’	1 beam	4 Stokes
LWA (LWA1)	256 X dipoles	~8000 m^2 (*)	10–88 MHz	6◦ (*)	4 beams ×20 MHz	4 Stokes
OLWA	256 X dipoles (→2000)	~8000 m^2 (*) (→ 65000 m^2)	10(28)–88 MHz	≤5◦ (*) (→ ≤1°)	Full-sky imaging	4 Stokes
NenuFAR-1	**456 X dipoles**	**~15000 m^2 (*)**	**10–85 MHz**	**3° (*)**	**2 beams ×75 MHz**	**4 Stokes**
AARTFAAC-LBA	288 X dipoles	~8000 m^2 (*)	30–80 MHz	2° (*)	All-Sky	4 Stokes
LOFAR-LBA	2688 X dipoles	72000 m^2 (*)	30–80 MHz	2” (*)	8+beams ×4 MHz	4 Stokes
NenuFAR/ Standalone	**1824 X dipoles**	**62000 m^2 (*)**	**0–85 MHz**	**1.5◦ (*)**	**≥2 beams ×75 MHz**	**4 Stokes**
NenuFAR/LSS + LOFAR	**4512 X dipoles**	**134000 m^2 (*)**	**10–80 MHz**	**2” (*)**	**Nbeams → total 48 MHz**	**4 Stokes**
SKA-Low	250000 log-per dipoles	≥3x10^6 m^2	50–350 MHz	<0.1”	Nbeams → total 300 MHz	4 Stokes

Table : A few characteristics of **NenuFAR** and **NenuFAR-1** compared to those of large LF radio instruments (capable of observing below 100 MHz), existing or in project. (*) at 30 MHz.

The UTR-2 radio telescope in Kharkov [Braude et al., 1978] is a much larger instrument (with an effective area larger than LOFAR’s) but it is restricted to frequencies ≤32 MHz and has no polarization capability. A smaller URAN array also operated in Ukraine has characteristics similar to NenuFAR-1, including dual-polarization measurements, but it is an analog instrument whose phased output is acquired by a digital receiver, offering less possibilities than NenuFAR-1 (and furthermore NenuFAR/Standalone and NenuFAR/LSS).

Finally, LOFAR is a large interferometer offering immense possibilities, dominantly imaging-oriented. Being fully multipurpose, it offers few possibilities of large duty cycle observations as it is already involved in large programs (surveys, EoR, pulsar studies…). It provides a frame for the use of NenuFAR/LSS. But NenuFAR/Standalone will offer better possibilities in terms of instantaneous observations in coherent phased array mode.

NenuFAR and NenuFAR-1 thus appears to have specific exploitation areas not redundant with existing instruments. They will offer and benefit from complementarity with the use of these instruments, e.g. complementary longitude coverage with LWA1 and UTR-2, joint use with LOFAR, possibilities of simultaneous observations/detections of weak sources (e.g. with NenuFAR and UTR-2) ensuring a better confidence and a better immunity to local RFI or ionospheric perturbations.

7. Further steps

NenuFAR-1 is the first step in the development of the full NenuFAR project, but also an operational instrument. Its construction will include the elements and infrastructures required by the full-scale project and that cannot be built efficiently in slices (e.g. power lines, integrated antenna amplifiers, terrain preparation and trenches for the inner parts of NenuFAR…). The expansion of NenuFAR-1 will rely upon these bases and be facilitated in terms of technical work and funding requirements. NenuFAR-1 represents 1/3 of the cost of NenuFAR, and should be completed in 2015.

Additional funding for the whole NenuFAR is expected in the coming few years. The full-scale NenuFAR will be a cost-effective large instrument, with unique capabilities, that will serve broadly the French LF community (with international collaborations), and prepare it for SKA (scientifically, with possible technical lessons for SKA-low). The status of SKA pathfinder has been requested (see chapter 2).

As a Standalone instrument, NenuFAR has further planned developments that will expand its capabilities. The initial dedicated receiver will be the beamformer able to export beamformed data to an ARTEMIS-like post-backend and the high-rate subband signals to a dedicated correlator. These 2 "post-backends" are the first planned extensions of NenuFAR.

Another extension, that we will actually consider early in the project (just after Phase 1, in parallel with the rollout of additional MA_{19} in the compact 400m disk), is the construction of a few MA_{19} (2 to 6) up to distances of ~3 km, on existing grounds of the Nançay Radioastronomy station. For stable radio sources with a broad spectrum, rotational multifrequency synthesis will permit to cover well the (u,v) plane up to distances 7 times larger than with baselines ≤400m (Figure 1), immensely improving NenuFAR/Standalone imaging capabilities (angular resolution ~5' at 80 MHz, confusion reduced by a factor 50, i.e. close to the thermal noise at 80 MHz – see Figure 2).

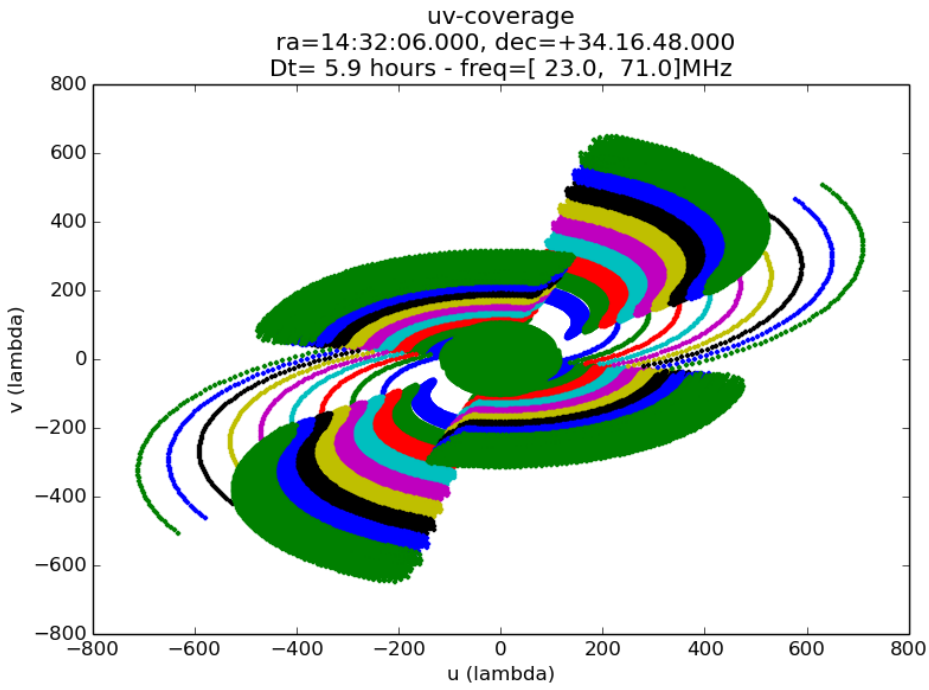

***Fig. 1**: (u,v) coverage of NenuFAR + 2 distant MA_{19} (at resp. ~2 and ~3 km, corresponding to the existing grounds of the extension antennas of the Nançay RadioHeliograph), for ~6 Hours integration and 23 to 71 MHz multifrequency synthesis.*

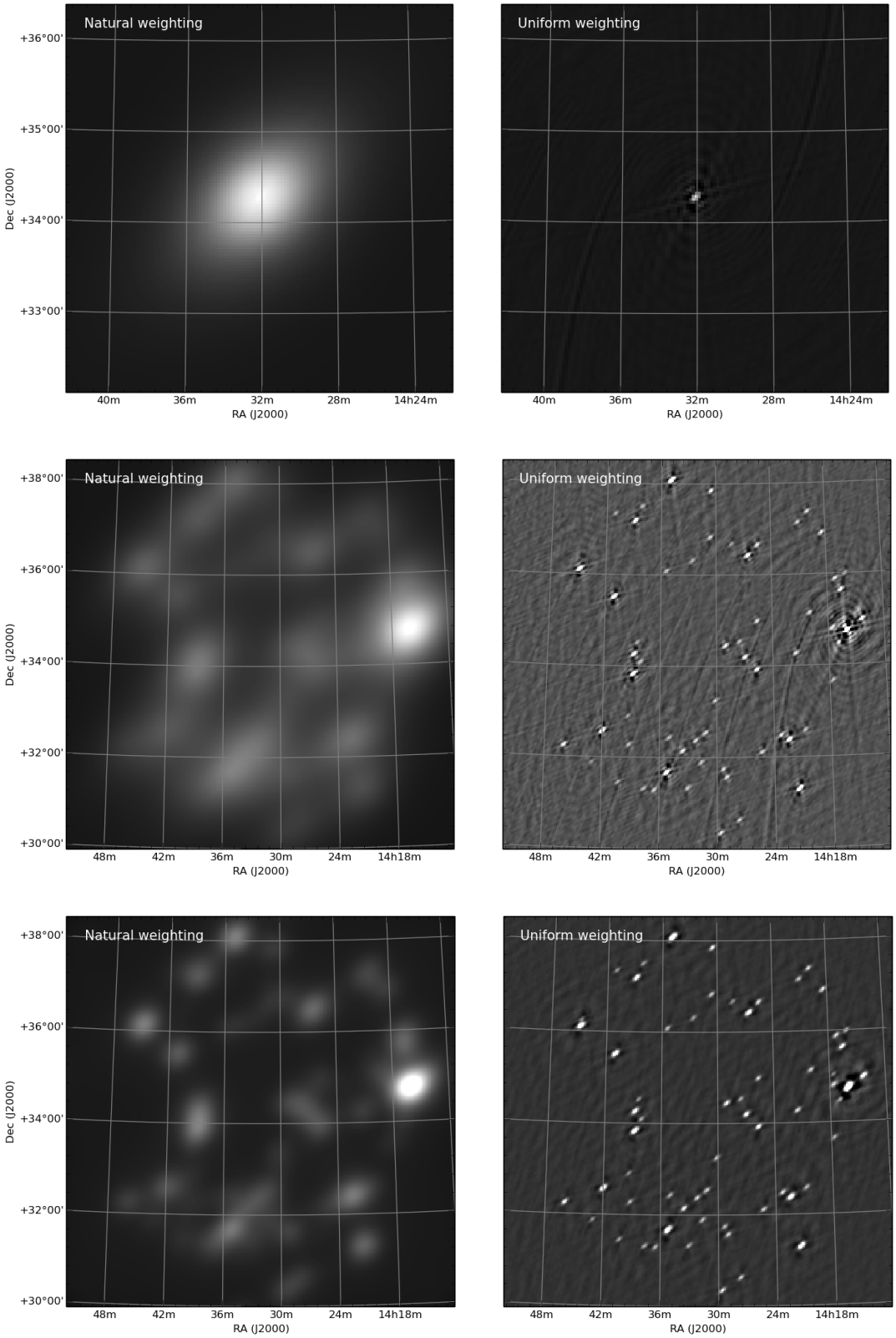

Fig. 2*: (top) PSF corresponding to Fig. 2, with Gaussian weightning (left ~NenuFAR compact core only) and uniform weighting (right) ; (middle) Corresponding simulated image of NVSS sources with spectral slope -0.8 ; (bottom) same as above, after deconvolution.*

The 2 to 6 MA_{19} will come in addition to or part of the 96 total MA_{19}. They will not feed the beamformer, but only the correlator, and thus digitization at the "foot" of each MA_{19} is the best adapted strategy, provided that the ADC are synchronized on a common clock (as for LOFAR's core). The relative sensitivity of the images at resolutions beyond 400m baselines, compared to the

sensitivity on baselines ≤400m, will be proportional to $(N_{distant}/N_{core})^{1/2}$ with N_{core} and $N_{distant}$ being the number of MA_{19} resp. within and beyond the 400m compact core. With N_{core}=6 and $N_{distant}$=90, $(N_{distant}/N_{core})^{1/2}$=26%, thus a large fraction of the whole NenuFAR sensitivity. Such a "low confusion mode" will be very useful for e.g. searches of GRBs or GW counterparts.

Further gradual expansion of the NenuFAR backend and computing power, e.g. based on GPU architecture, will permit to gradually increase NenuFAR's capabilities (e.g. form more full-band beams and thus increase the surveys and blind search capabilities NenuFAR).

Acronyms or Definitions

AARTFAAC	Amsterdam-ASTRON Radio Transients Facility And Analysis Centre
ARTEMIS	Advanced Radio Transient Event Monitor and Identification System
ASKAP	SKA precursor in Australia
CODALEMA	COsmic ray Detection Array with Logarithmic ElectroMagnetic Antennas
EoR	Epoch of Reionization of the early Universe
FFT	Fast Fourier Transform
FoV	Field of View
FR606	The French LOFAR international station (in Nançay)
GRB	Gamma Ray Bursts
GW	Gravitational Waves
HBA	LOFAR High Band Antennas (110-250 MHz)
ISM	InterStellar Medium
LBA	LOFAR Low Band Antennas (30-80 MHz)
LBL	LOFAR Low Band Low antennas (descoped)
LF	Low Frequency
LOFAR	The Low Frequency ARray (NL/Europe)
LSS	LOFAR Super Station mode of NenuFAR
LWA	The Long Wavelength Array (USA)
LWA1	The 1st (and presently only) LWA station
MA_{19}	NenuFAR's Mini-Arrays of 19 antennas
MeerKAT	SKA precursor in South Africa
MSSS	LOFAR's Million Sources Shallow Survey
MWA	The Murchison Widefield Array (80-300 MHz)
NDA	The Nançay Decameter Array
NenuFAR	New extension in Nançay upgrading LOFAR
NenuFAR-1	Phase 1 of NenuFAR
NVSS	NRAO (Nat'l Radio Astronomy Obs.) VLA (Very Large Array) Sky Survey
OLWA	Owens valley LWA
PC	Program Committee
RAM	Random Access Memory
RCU	LOFAR's Receiver Units
RFI	radio Frequency Interference
RRATs	Rotating RAdio Transients
SKA	The Square Kilometer Array radiotelescope
Superterp	LOFAR's central core consisting at LF of 6 x 48 LBA antennas
TBB	Transient Buffer Boards (LOFAR's waveform capture RAMs)
TLE	Transient Luminous Events
URAN	Ukrainian Radio Interferometer of NASU (National Academy of Sciences of Ukraine)
UTR-2	Ukrainian T-shape Radiotelescope, mark 2 (in Kharkov, Ukraine)

References

Armour, W., Karastergiou, A., Giles, M. et al. 2011, in proc. ADASS XXI, eds. P. Ballester and D.Egret (ASP Conf. Series)

Boischot, A., C. Rosolen, M. G. Aubier, G. Daigne, F. Genova, Y. Leblanc, A. Lecacheux, J. De La Noe, and B. M. Pedersen, A New High-Gain, Broadband, Steerable Array to Study Jovian Decametric Emission, Icarus, 43, 399-407, 1980.

Braude, S.Ya., A. V. Megn, B. P. Ryabov, N. K. Sharykin, and I. N. Zhouck, Decametric survey of discrete sources in the northern sky: I. the UTR–2 radiotelescope. Experimental techniques and data processing, Astrophys. Space Sci., 54, 1, 3–36, 1978.

Condon, J. J., Extragalactic Astronomy at Low Frequencies, ASP Conf. Ser. 345 "From Clark Lake to the Long Wavelength Array", N. E. Kassim, M. R. Pérez, W. Junor and P. A. Henning eds., 237-253, 2005.

Girard, J., Développement de la Super Station LOFAR & Observations planétaires avec LOFAR, Thèse de Doctorat, Observatoire de Paris, 2013.

Girard, J. N., P. Zarka, M. Tagger, L. Denis, D. Charrier, A. A. Konovalenko, F. Boone, Antenna design and distribution of the LOFAR Super Station, C.R. Phys. 13, « Les radiotélescopes du futur », p. 33-37, 2012a.

Hicks, B. C., Nagini Paravastu-Dalal, Kenneth P. Stewart, William C. Erickson, Paul S. Ray, Namir E. Kassim, Steve Burns, Tracy Clarke, Henrique Schmitt, Joe Craig, Jake Hartman and Kurt W. Weiler, A Wide-Band, Active Antenna System for Long Wavelength Radio Astronomy, Pub. Astron. Soc. of the Pacific, 124 (920), 1090-1104, 2012.

Moldon, J., et al., The LOFAR long baseline snapshot calibrator survey, Astron. Astrophys., submitted.

Prasad, P., and S. J. Wijnholds, AARTFAAC: Towards a 24x7, All-sky Monitor for LOFAR, in Proc. R. Soc. A « "New Windows on Transients across the Universe", Royal Society, London, 4. Pp, 2012.

Taylor, G. B., et al., First light for the first station of the Long Wavelength Array, J. Astronomical Instrumentation, 1(1), 1250004-1-1250004-20, 2012.

van Haarlem, M. P., LOFAR: The Low Frequency Array, Astron. Astrophys., 556, A2, 2013.

Zarka, P., J.N. Girard, M. Tagger, L. Denis, and the LSS team, LSS/NenuFAR: The LOFAR Super Station project in Nançay, SF2A-2012: Proc. Annual meeting of the French Society of Astronomy and Astrophysics, Eds.: S. Boissier, P. de Laverny, N. Nardetto, R. Samadi, D. Valls-Gabaud and H. Wozniak, pp.687-694, 2012.

NenuFAR as a pathfinder for SKA

Steve Torchinsky,

Philippe Zarka, Michel Tagger, Laurent Denis, Gilles Theureau, Stéphane Corbel et al.

The Phase I of SKA is expected to be operational by 2024. SKA for low frequencies will be built in Western Australia, and will initially consist of nearly 300000 antenna elements working in the frequency range 50 MHz to 350 MHz. NenuFAR at Nançay is a smaller instrument but with a number of architectural and operational considerations in common with SKA-low. Experience gained with the design, construction, characterization, and operation of NenuFAR can be useful to the SKA design process, possibly influencing important design decisions.

NenuFAR extends the frequency range down to 10 MHz which is lower than planned for SKA. This is primarily for the detection of cyclotron radiation from gas giant extra solar planets, but the lower frequency will also permit a pilot survey for the Epoch of Reionization Key Science projet, pushing the upper redshift limit of the survey beyond z=100. These surveys may produce important results which could influence the design decision for SKA related to its lowest frequency. More generally, scientific results from NenuFAR will help develop the observational strategies for SKA-Low, and detections/non-detections will inform technical requirements.

NenuFAR will be a complex instrument with a large number of antenna elements, operating not only as a standalone instrument, but also as part of a larger, continent-sized array. These are important similarities with SKA which will give practical experience with subarraying, with simultaneous multi-mode observing, and with calibration, to list a few examples. NenuFAR will also be a pathfinder for polarization, including the design considerations for polarization distribution of the dipoles and sub-stations, and the polarization calibration. These are all aspects of a complex system, similar to SKA, which requires a sophisticated monitoring and control system to take into account the multiple possibilities of observing modes, including simultaneous observing modes, and of course, the monitoring of the health of the instrument. Other practical areas may also prove important inputs to SKA design such as the layout and implementation of trenches for cabling and fibre optics. Thus, a number of design choices for SKA-Low should benefit from experience gained with NenuFAR including aspects of system architecture, installation, and operation.

Hardware Development

The NenuFAR project contains new technical elements that have not been tried before on the scale of a large telescope and which are part of the SKA Baseline Design. After extensive electromagnetic (NEC) modelling of several antenna geometries [*Girard et al., 2012 ; Girard, 2013*], the LWA antenna radiator [*Hicks et al., 2012*] was selected for NenuFAR. Three low-noise amplifier designs were considered. One was based on discrete components and two, designed and built in French laboratories, were based on ASICs. The design chosen (LonAmos) is an ASIC optimized for the 10-100 MHz band. This design will be further optimized for the 10-500 MHz band which is well adapted to SKA-Low. French laboratories have significant experience on the optimization of the hierarchical distribution of antennas within a large array, and also on the distribution of small arrays of antennas (≤25 elements) [*Girard, 2013 ; Girard and Zarka, 2014*]. For NenuFAR, phasing of these small arrays is done with analog systems built on discrete components, but use of analog ASICs is also under study.

All these studies serve to some extent for the optimization of SKA-Low. This is obvious concerning the high-frequency version of the LonAmos preamplifier, which may be a good alternative to the present LNA design for SKA-Low. The SKA-Low stations design consisting of 289 digital-phased SKALA antennas [*de Lera Acedo, 2012*] results from trade-offs between

sensitivity, cost, footprint, and field-of-view. For example, the dense/sparse transition at ~111 MHz leads to a sensitivity reduction by a factor ~5 at 50 MHz. If the SKA-Low scientific case turns out to be significantly driven by low-frequency objectives (e.g. EoR, dark ages, exoplanets…) and/or if the direct digitization of >260000 antennas raises technology or cost issues, then the experience gained on NenuFAR on the optimization of low-frequency antennas and the hierarchical distribution and phasing of sub-arrays will turn out to be very useful.

Software and Algorithm Development

The French community has provided very significant contributions to LOFAR imaging tools including the direction-dependent imager by *Tasse et al.* [*2013*], and advanced methods such as nonlinear Kalman filters [*Tasse, 2014*] and Sparse Image Reconstruction [*Dabbech et al., 2012; Garsden et al., 2014*]. Application of these new methods to real data (e.g. LOFAR) is well advanced. Further developments are being studied in the context of NenuFAR, such as image reconstruction algorithms (in particular spatio-spectral methods using sparsity [*thesis of A. Dabbech*], multiwavelength methods [*Rau and Cornwell, 2011*]), statistical description of the observation models (Bayesian statistics, non-standard inverse model), and ways to beat the confusion and reach high sensitivity with beamformed low-frequency observations by combining them with instantaneous coarse-resolution imaging and sky models.

Another path of research concerns dedispersion, which requires the processing of long series of samples across a broad bandwidth extending down to low-frequencies. Methods will be studied for optimizing blind searches of radio transients up to very large dispersion measures (~10^3) by combining channelization and coherent dedispersion, and/or by using machine learning techniques as alternatives to dedispersion.

Instrument Architecture

NenuFAR will carry out observational tests with results reported in time to have an impact on the design of SKA. These observational tests, including simulations, explore new capabilities at flux densities and dynamic range levels similar to, or scalable to, the full SKA.

NenuFAR antennas and mini-arrays are characterized via comparison of observations with simulations of their response to the low-frequency radio sky which is dominated by galactic background and A-team radio sources. Sky models are from *Polisensky* [*2007*], from de *Oliveira-Costa et al.,* [*2008*], and from the LOFAR MSSS-LBA sky model [*Heald et al., 2014*]. Observations of Jupiter and the Sun, compared to well-calibrated instruments, also provide quantitative information about the directional response of the instrument. NenuFAR antennas will also be characterized by a measurement campaign using a drone carrying an emitting system. Experience gained with all these methods will be important for the characterization of SKA-Low antennas and stations.

NenuFAR will have the unique capability of being operated simultaneously and near-independently both in Standalone mode and in LOFAR Super Station mode. The NenuFAR correlator will be designed based on the outcome of the evaluation of architectures based on FPGAs, GPUs and CPUs with the implementation of real-time imaging and filtering algorithms. For the "post-beamformer" (channelization + dedispersion + RFI mitigation + integration), architectures inspired by the LOFAR single-station backend ARTEMIS [*Armour et al., 2011*] are being evaluated.

Equipping one or more SKA-Low station with a similar receiver would open, for a limited cost, many possibilities for original science (e.g. transient searches such as those carried out with LOFAR-ARTEMIS [*Serylak et al., 2012*]). This also provides the possibility for student training and extensive testing in parallel with SKA operation (including possible calibration issues), in a

context very favourable to local efforts – e.g. based in a local research and/or teaching institute.

Science operation

A large part of the NenuFAR science, as discussed in the NenuFAR science case (following sections of this document), will be a precursor and a complement of SKA-Low, both in frequency range (10-85 MHz) and in sky coverage (Northern hemisphere). NenuFAR will test methods of scheduling and allocating time similar, or scalable, to those needed for the SKA. The Standalone mode of NenuFAR is constrained to observe within the wide analog station beam defined at a given time by its concurrent operation in LSS mode. Furthermore, at times when LOFAR doesn't use its international and remote stations (thus where the LSS mode is not used) NenuFAR can be used as a second core correlated with the unused stations. The sub-arrays formed by the core on one side, and NenuFAR/LSS + remote/international stations on another side, could be correlated by the same (Cobalt) or different (e.g. Cobalt + Jülich) correlators. This leads to issues concerning the planning as well as the Telescope Manager of the instrument, providing experience that will be applicable for the most versatile and efficient operation of SKA-Low.

For these reasons, on 27/08/2014, the SKA Organisation has granted to NenuFAR the formal status of SKA Pathfinder *(https://www.skatelescope.org/precursors-pathfinders-design-studies/).*

References

Armour, W., Karastergiou, A., Giles, M. et al., in proc. ADASS XXI, eds. P. Ballester and D.Egret (ASP Conf. Series), 2011.

Dabbech, A., D. Mary, and C. Ferrari, stronomical image deconvolution using sparse priors: an analysis-by-synthesis approach, ICASSP (IEEE) conference, 3665-3668, 2012.

Dabbech, A., Déconvolution d'images en radio-astronomie centimétrique pour l'exploitation de LOFAR et SKA : caractérisation du milieu non-thermique des amas de galaxies, PhD thesis, Univ. Nice, 2014.

Garsden, H., J. N. Girard, … and LOFAR builders list, LOFAR sSparse Image Reconstruction, Astron. Astrophys., submitted, 2014.

Girard, J. N., P. Zarka, M. Tagger, L. Denis, D. Charrier, A. A. Konovalenko, F. Boone, Antenna design and distribution of the LOFAR Super Station, C.R. Phys. 13, « Les radiotélescopes du futur », p. 33-37, 2012.

Girard, J., Développement de la Super Station LOFAR & Observations planétaires avec LOFAR, Thèse de Doctorat, Observatoire de Paris, 21/5/2013.
http://tel.archives-ouvertes.fr/index.php?halsid=s4sico0pmudj89ib8fabc5sfi1&view_this_doc=tel-00835834&version=1

Girard and Zarka, Optimization of a small 2D phased array layout synthesizing a wide-beam antenna pattern, Astron. Astrophys., to be re-submitted, 2014.

Heald, G. et al., LOFAR MSSS (Multifrequency Snapshot Sky Survey) : Status and early science, LOFAR science meeting, Amsterdam, 2014, http://www.astron.nl/lofarscience2014/

Hicks, B. C., N. Paravastu-Dalal, K. P. Stewart, W. C. Erickson, P. S. Ray, N. E. Kassim, S. Burns, T. Clarke, H. Schmitt, J. Craig, J. Hartman and K. W. Weiler, A Wide-Band, Active Antenna System for Long Wavelength Radio Astronomy, Pub. Astron. Soc. of the Pacific, 124 (920), 1090-1104, 2012.

de Lera Acedo, E., SKALA: A Log-periodic antenna for the SKA, ICEAA (IEEE) conference, 353-356, 2012.

de Oliveira-Costa, A., M. Tegmark, B. M. Gaensler, J. Jonas, T. L. Landecker, and P. Reich, A model of diffuse Galactic radio emission from 10 MHz to 100 GHz, MNRAS, 388, 247-260, 2008.

Polisensky, E., LFmap: A Low Frequency Sky Map Generating Program, LWA memo 111, 2007.

Rau, U., and T. J. Cornwell, A multi-scale multi-frequency deconvolution algorithm for synthesis imaging in radio interferometry, Astron. Astrophys., 532, A71, 2011.

Serylak, M., A. Karastergiou, C. Williams, W ; Armour, M. Giles, and the LOFAR pulsar WG, Observations of transients and pulsars with LOFAR international stations and the ARTEMIS backend, in Proc. IAU

Symposium 291, Neutron Stars and Pulsars: Challenges and Opportunities after 80 years, J. van Leeuwen ed., 2012.

Tasse, C., S. van der Tol, J. van Zwieten, G. van Diepen, and S. Bhatnagar, Applying full polarization A-Projection to very wide field of view instruments: An imager for LOFAR, Astron. Astrophys., 553, A105, 2013.

Tasse, C., Nonlinear Kalman filters for calibration in radio interferometry, Astron. Astrophys., 566, A127, 2014.

Zarka, P., J. N. Girard, M. Tagger, L. Denis, and the LSS team, LSS/NenuFAR: The LOFAR Super Station project in Nançay, SF2A-2012: Proc. Annual meeting of the French Society of Astronomy and Astrophysics, Eds.: S. Boissier, P. de Laverny, N. Nardetto, R. Samadi, D. Valls-Gabaud and H. Wozniak, pp.687-694, 2012.

Technical Specification of NenuFAR

J. N. Girard, P. Zarka, L. Denis, et al.

1. Introduction

LOFAR is the new European multi-scale low-frequency (LF) radio interferometer in the range 30-250 MHz with baselines from ~50 m to ~1000 km (van Haarlem et al. 2012). The constitutive elements of LOFAR are phased arrays or "stations" distributed in the Netherlands and surrounding European countries. One of these stations, FR606, is installed in the Nançay radio observatory (France). Each station consists of two arrays of antennas and a "back-end" that preprocesses antenna signals (filtering, digitization, spectral channelization and beamforming). Preprocessed digital data are then sent at ~3 Gbits/sec to the central computer (in Groningen, NL) that performs the correlations per interferometric baseline and/or final pencil beamforming. The Low-Band Antenna (LBA) array covers the range 30-80 MHz and consists of 96 elementary crossed dipoles in international stations such as FR606 (48 in Dutch stations). The High-Band Antenna (HBA) array covers the range 110-250 MHz and consists of 96 "tiles" of 16 analog-phased crossed dipoles (2x24 in Dutch stations). At any given time, the backend can be connected to either the LBA or the HBA (not both simultaneously). A third input to the backend exists, that was initially planned for an LBL (Low-Band Low, 10-50 MHz) array that never existed due to limited funding.

NenuFAR (formerly "LSS" for "LOFAR Super Station") exploits the availability of the third analog input of the LOFAR back-end to form a new LF phased array interferometer. No a priori constraints exist on its design and it will be fully compatible with LOFAR operations in the LBA band (i.e. that can be correlated with LBA arrays of other LOFAR stations, instead of the FR606 LBA array) and at the same time provide a considerably increased instantaneous sensitivity and frequency coverage.

2. Technical Description of NenuFAR

NenuFAR possesses a hierarchical design inspired of the HBA antenna field but adapted to a lower frequency band, which extend the LBA band (e.g. ~10-90 MHz). The NenuFAR "tile" is composed of adapted dual-polarization antennas which signal is locally combined as a small phased array. Each tile provides a large gain from 10-15 MHz to 85-87 MHz (i.e. a ratio fmax=fmin double of that of the LBA range). Their output is a pair (for the two linear polarizations) of analog signals that enters either the LBL analog inputs on the FR606 back-end or the analog input of a dedicated back-end installed close-by. The three main levels of the instrument drove three different design studies:

- The design of the antenna (feed and preamplifier)
- The distribution inside the LF "tile" or "mini-array" (the number, distribution of antennas and the phasing system)
- The distribution of these mini-arrays on the Nançay field (optimal for phased-array or interferometer performance vs. site constraints).

A lot of effort has also been put in the design of a prototype receiver for the three first prototypes of mini-arrays.

2.1 Antenna & preamplifier

The diagram of the antenna radiator was optimized via electromagnetic simulations with the NEC code and validated with tests on the sky; optimized parameters include a broad and smooth beam (nearly isotropic, albeit with extinction below 20° elevation) and maximum efficiency (related

to electrical and ground losses), over a large frequency bandwidth; this implies an antenna radiation resistance and (low) reactance as constant as possible over the band of interest and versus time; cost effectiveness and compatibility with LOFAR strongly favored linearly polarized crossed dipoles; the optimal compromise is a "thick" inverted-V dipole similar to the LWA Fork, with a metallic ground screen (see Figure 1 top & Girard et al. 2011, Girard & Zarka, 2012).

Three designs have been studied and realized for the antenna preamplifier, which is a key element for the antenna gain and its susceptibility to radio-frequency interference (RFI): (1) the "GURT2" design from the Kharkov Institute of Radio Astronomy,(2) the Subatech/Nançay design, and (3) the Nançay microelectronics laboratory design. (1) is based on discrete components, whereas (2) & (3) are based on ASIC circuits. All have good characteristics, with a noise ~10 dB below the sky noise level. For NenuFAR-1, the Subatech/Nançay design was selected.

2.2 The Mini-array

The number of antennas within each tile should be of the order of 16 (again as in HBA tiles) in order to provide at least an order of magnitude increase of the instantaneous sensitivity.

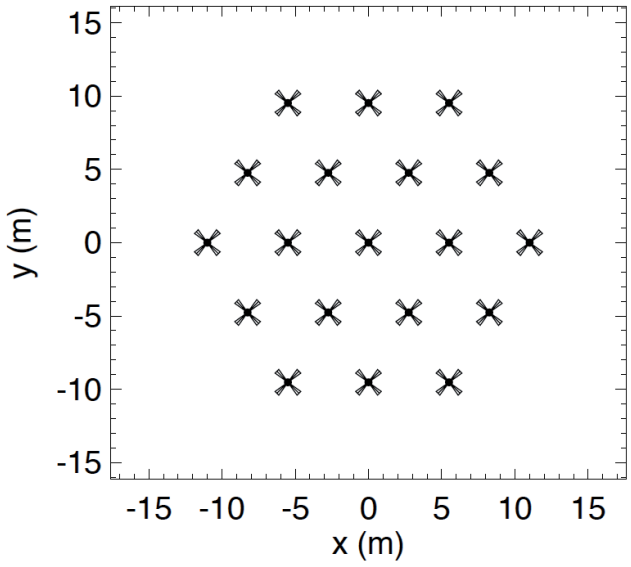

Figure 1. (Top) Picture of the prototype mini-array #1 (Bottom) Schematic layout of the mini-array showing the 19 inverted-V shape dual polarizations antennas. They are arranged in a 5.5 m triangular lattice forming a hexagon.

The antenna distribution within each LF tile was optimized for a low side lobe level and a large field of view symmetrical around the zenith; Girard & Zarka (2012) found that a distribution with a central antenna surrounded by two circular rings of antennas meets these requirements, especially if the rings have different (or no) symmetry axes, i.e. if the global distribution cannot be superposed to itself by a rotation $< 2\pi$. In parallel, we have calculated that analog phasing of each LF tile using 7-bit delay lines (cable lengths) allows to perform achromatic phasing over the whole NenuFAR band (10-87 MHz) with gain variations <10% across the beam, and provide one input per polarization to the backend. In order to be cost-effective, delay lines must be mutualized for groups of antennas, e.g. by arranging antennas with a regular spacing in two orthogonal directions. Taking into account this constraint we modified the above optimized antenna distributions to obtain an LF

tile of 19 antennas (a central one surrounded by an hexagon of 6 antennas and a second one of 12 antennas, or equivalently regular lines of 3 / 4 / 5 / 4 / 3 antennas with each line shifted by 1/2 inter-antenna spacing relative to its neighbours (Figure 1 Bottom). The absolute value of inter-antenna spacing was set to 5.5 m in order to maximize the effective area without overlap at LF, while keeping the NenuFAR extent compatible with its hosting at the Nançay station. The instantaneous LF tile beam will have an angular size of 10° to 50° over the NenuFAR spectral range (~25 at 30 MHz).

2.3 NenuFAR as an interferometer/phased array

The 96 tiles should be arranged in a relatively dense layout (within a few hundred meters diameter), providing a smooth overall beam with a low side lobe level and compatible with the available land in an observatory such as the Nançay station, and at the same time minimize the overlap between antennas effective areas in order to maximize the NenuFAR sensitivity.

The optimal distribution of the 96 LF tiles was computed using the Boone (2001) algorithm, taking into account a "site mask" of the Nançay station including its limits and forbidden areas (the station FR606 itself and other antennas of the site). It provides a smooth, Gaussian distribution of visibilities in the (u,v) plane, and thus a near-Gaussian NenuFAR beam pattern. The layout of trenches and cables connecting the LF tiles to the FR606 backend was optimized using a reasonable cost ratio per unit length of trench/cable in input to a specific optimization algorithm (Vasko et al. 2002). The obtained LF tiles distribution and layout is displayed in Figure 2. It implies a NenuFAR beam size of 0.5°-3° (~1.5° at 30 MHz). In order to reduce the side lobe level resulting from the regular antennas arrangement in the LF tiles, each tile will be rotated by a random amount with respect to each other, but all crossed dipoles within all tiles will be oriented along the same directions, at 45° from the meridian.

3. NenuFAR Performance & Observing modes

3.1 Observing capabilities and improvements brought by NenuFAR

NenuFAR by itself, is not a powerful imaging instrument, but its collecting area, and thus its sensitivity, will bring several significant improvements to LOFAR:

- The long LOFAR baselines including the NenuFAR will be ~19 times more sensitive than long baselines between two LBA arrays; as the available radio power corresponding to one angular details is generally weak, this increased sensitivity will give access to an increased number of calibrators (typically ~10) in the vicinity of the studied target; this will improve LOFAR's capabilities for high resolution imaging in the LBA range.
- By adding 96x19=1824 antennas to the present 2700 LOFAR LBA antennas, the NenuFAR will almost double LOFAR's sensitivity in the LBA imaging mode.
- When most of the "core" (closely-packed) LOFAR stations will be used for time-demanding projects such as observing the Epoch of Reionization (EoR), the NenuFAR will provide an alternative core and, by correlation with the "remote" LBA arrays, will preserve good imaging capability in parallel with the above projects; provided that the central correlator can handle two streams of data from two LOFAR sub-arrays (namely the core, and the NenuFAR+remote stations) the NenuFAR will improve LOFAR-LBA imaging capabilities for a significant fraction of the time.
- Correlation of signals from the LF tiles within the NenuFAR will provide sensitive baselines 2 to 3 times shorter than a LOFAR station diameter - the shortest baseline presently available - , permitting to image large-scale structures, larger than an instantaneous station beam (~10° at 30 MHz); short baselines are presently available by correlation of LBA antennas within a station, but with much lower sensitivity.
- The NenuFAR will also be a very large standalone instrument: it will have an effective area

(and thus sensitivity) ~19 times larger than the LBA array of an international station, i.e. <70% to 85% of all LOFAR-LBA arrays, but this area will be instantaneously and fully available during use, especially in coherent tied-array (or phased-array) beam mode (TAB); by contrast, the coherent phasing of LOFAR-LBA array signals is limited to the 24 core stations that share the same reference clock (and have the same ionosphere above them); thus, the instantaneous sensitivity of the NenuFAR in coherent TAB mode will be 1.6 times better than the LOFAR-LBA one (Figure 3).

- Finally, in standalone mode, the NenuFAR will extend the observation bandwidth to significantly lower frequencies than the LBA range.

The NenuFAR pointing will be controlled by a dedicated LCU (Local Command Unit) connected to 96 electronic modules, one in each LF tile, specifying the phasing scheme to be applied at any given time (different for each LF tile due to their random rotations); these modules are designed to be completely "radio-quiet" outside pointing time; pointing will occur at intervals from 20 to 60 sec, ensuring low gain variation in the main beam direction. The NenuFAR LCU will be connected to the LOFAR LCU of station FR606. When NenuFAR will be used jointly with other LOFAR LBA arrays (so-called "International" mode), pointing orders will come from the LOFAR operations center via the LOFAR LCU and be translated into LF tiles phasing commands by the NenuFAR LCU; data recorded by the LOFAR backend will be sent to the LOFAR central correlator. In "Standalone" mode, pointing orders will come from a local command computer, and the data will be recorded locally (see below).

More information about the "Super Station" mode and the "Stand-alone" mode can be found respectively in chapter §3 and §5.

3.2 Standalone use with a dedicated receiver

It is of importance to stress that a high duty-cycle of NenuFAR standalone mode and a dedicated receiver. The standard NenuFAR concept consists of the 96 additional LF tiles and their phasing and command system, that are connected to the LOFAR backend of FR606. The contract of any European station owner with the International LOFAR Telescope board includes the right to use that station in standalone mode for ~10% of the time. As the standard LOFAR station backend only allows to record low frequency-time resolutions observations (typically in 200 kHz in 1 sec bins), the full scientific exploitation of standalone NenuFAR observations requires either LOFAR's "Single Station" mode (cf. http://www.lofar.org/operations/doku.php?id=singlestation:start) or a dedicated post-backend (Serylak et al. 2012). The former consists of a sub-array formed by a single station, which high-resolution data are sent to the central correlator for processing as TAB data. The latter is for example the ARTEMIS (Advanced Radio Transient Event Monitor and Identification System) post-backend dedicated to transients detection and study, that ingests high resolution station data and locally computes high-resolution time-frequency planes including parametric dedispersion (Armour et al. 2011).

If one wants to compute locally more than time-frequency planes with NenuFAR standalone data (e.g. auto- and cross-correlations of tile signals), then a dedicated receiver is necessary. Such a dedicated receiver has been studied in the frame of the NenuFAR design study. It will consist of either a post-LOFAR-backend (ARTEMIS- like), or a fully independent backend. The LOFAR backend digitizes the LBA or NenuFAR tile signals, channelizes it in 200 kHz bands (called "subbands"), and computes beamforming within each subband. The beamformed signal of 244 subbands is sent to the LOFAR central correlator. The latter further channelizes (down to 0.76 kHz resolution) the signals of all subbands from all stations, and computes auto-/cross-correlations and/or incoherent or coherent (adequately time-shifted) summation in order to produced polarized images and/or TAB data (cf. http://www.astron.nl/radioobservatory/astronomers/technical-information/lofar-signal-path/lofar-signal-path/).

A post-LOFAR-backend dedicated receiver would ingest locally the station products (as

does ARTEMIS) and channelize, auto-/cross-correlate, and integrate them. A fully independent backend would perform the tasks of both the LOFAR backend and the central correlator, but in an optimized integrated way. A large computing power is required, but a preliminary design study suggests that this is within the scope of new generation FPGAs. Additional "intelligent" processing like RFI mitigation or parametric dedispersion could be included. Transient Buffer Board data will also be processed in all cases. A dedicated receiver is important not only because it allows local, flexible processing, but primarily because it will greatly increase the duty-cycle of the NenuFAR standalone use beyond the "guaranteed" 10% fraction of the time, albeit with some pointing constraints. With a post-LOFAR-backend receiver, usable in parallel to all NenuFAR observations (standalone or in correlation with LOFAR LBA), the standalone analysis of NenuFAR data will be possible 100% of the time during which the NenuFAR tiles are connected to the FR606 backend, but the target will necessarily be within the 0.5°-3° NenuFAR beam fixed by the current LOFAR observation program. Conversely, with a fully independent backend that would process NenuFAR data in parallel with the standard station backend, standalone mode becomes possible 100% of the time, whatever array (LBA, HBA or NenuFAR) is connected to the LOFAR backend. The only pointing constraint of this standalone NenuFAR mode is that the target must be located within the 10°-50° analog LF tile beam.

4. NenuFAR-1 & path to the full NenuFAR

The final distribution of the 96 mini-arrays was set by the positioning constraints around the FR606 station and the power distribution over the entire field. NenuFAR was divided in "petals" allowing a modular and flexible implantation of the instrument. Starting from the three prototype mini-arrays (Fig. 2, green) that were built during the design study, ~1/4 of the instrument (in fact 26 mini-arrays, defined as "NenuFAR phase 1" (or "NenuFAR-1") is planned to be built before early 2015. The chosen mini-arrays provide a decent instrument PSF that will improve gradually with the construction of additional petals of the array while keeping the best azimuthal symmetry of the mini-array distribution (and therefore, the azimuthal symmetry of the instrumental beam and interferometric coverage).

The expected performance of NenuFAR is compared to that of LOFAR in Fig. 3 and a summary table of the instrumental characteristics, compared to other classical radio instrument can be found in Table 1. The expected sensitivities (for a 8-hour time integration over the ~10-90 MHz) are 120-240 mJy for NenuFAR-1, 50-100 mJy for the whole NenuFAR.

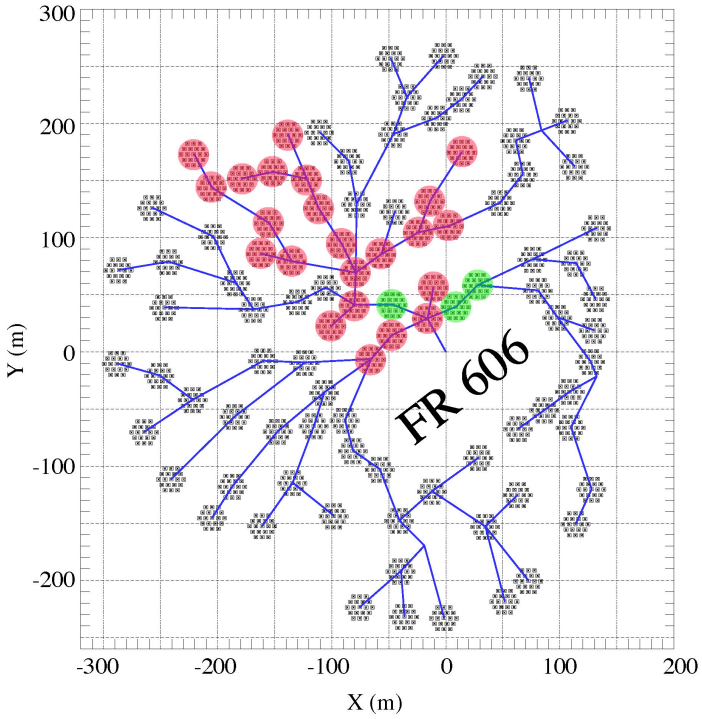

Figure 2. Distribution of the 96 mini-arrays around the LOFAR station FR606 in Nançay. Prototype mini-arrays (green) are included in NenuFAR-1 (pink) which account for ~1/4 of the total NenuFAR instrument.

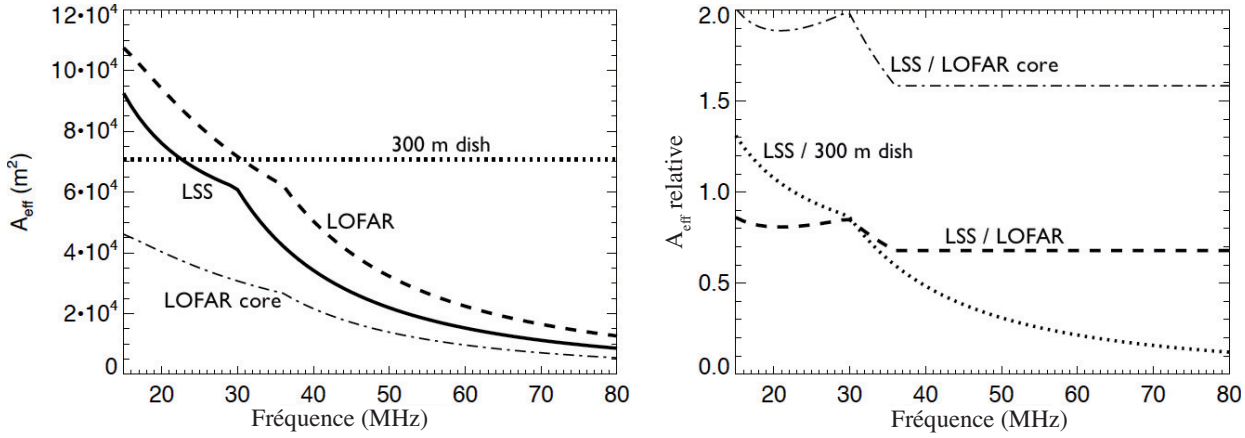

Figure 3. Theoretical effective collecting area of NenuFAR between 15 and 80 MHz for NenuFAR (NenuFAR), the full LOFAR-LBA, the LOFAR core only and a typical 300m-diameter dish radiotelescope (Arecibo).

Name	**$N_{antennas}$**	**Eff. Area (m^2)**	**Freq. Range (MHz)**	**Ang. Resol. (°)**	**N_{beams}**	**Pol. type**
NDA	144	4000 (a)	10-110	11° (a)	1b	2 circ
UTR-2	2040	143000	8-32	0.5°	5b	1 lin
VLA	27	~2000	73-74.5	0.5'	1b	2 circ
LWA	256	8000 (a)	10-88	9° (a)	4bx20 MHz	2 lin
MWA	2048	~2000 (c)	80-300	3' (c)	1bx30 MHz	2 lin
LOFAR-LBA	2688	72000	30-80	2" (b)	8b+nx4 MHz	2 lin
NenuFAR-1	494	~17000 (b)	15-80	~3° (b)	4bx65 MHz	2 lin
NenuFAR Stand-alone	1824	62000 (b)	15-80	1.5° (b)	4bx65 MHz	2 lin
NenuFAR +LOFAR	4512	134000 (b)	30-80	2" (b)	8b+nx4 MHz	2 lin
SKA	> 3000	1000000	0.07-10 GHz	<0.1"	Many	2 lin+circ

Table 1. Characteristics of NenuFAR and NenuFAR-1 compared to those of large LF radio instruments (observing below 100 MHz) existing or in project. (a) at 20 MHz, (b) at 30 MHz, (c) at 150 MHz.

5. Conclusion

The NenuFAR characteristics are compared to those of other existing international instruments in Table 1. In the European context, several instrumental projects are developed by LOFAR participants, such as ARTEMIS (from Oxford Univ., see above) or AARTFAAC (from

Univ. Amsterdam - it aims at cross-correlating the 288 LBA and HBA signals from the 6 central LOFAR stations to perform permanent all-sky monitoring (Prasad, 2012)).

NenuFAR is a LOFAR extension and a standalone instrument with emphasis on very high instantaneous sensitivity. We foresee it as an "Arecibo in Nançay". It is also a SKA precursor for the French community, both scientific and technical (for SKA-low).

References

Armour, W., Karastergiou, A., Giles, M. et al. 2011, in proc. ADASS XXI, eds. P.Ballester and D.Egret (ASP Conf. Series)

Boone, F. 2001, A&A, 377, 368

Girard, J. N., & Zarka, P. 2012, A&A, in revision

Girard, J. N., Zarka, P., Tagger, M. et al. 2011, in Planetary Radio Emissions VII, eds. H. O. Rucker et al. (Vienna: Austrian Acad. Sci. Press), p. 495

Girard, J. N., Zarka, P., Tagger, M. et al. 2012, C.R. Phys., 13, 33

Prasad, P. & Wijnholds, S. J. 2012, in proc. New Windows on Transients across the Universe (Royal Society, London, April 2012)

Serylak, M., Karastergiou, A., Williams, C. et al. 2012, in proc. Electromagnetic Radiation from Pulsars and Magnetars conference, Zielona Gora, 2012)

Van Haarlem, M. P. et al. 2013A&A, 556, id.A2,

Vasko, F. J., Barbieri, R. S., Rieksts, B. Q., Reitmeyer, K. L., & Stott Jr., K. L. 2002, Computers & Operations Res., 29, 441

NenuFar with LOFAR:
High resolution high sensitivity imaging

Frédéric Boone, Julien Girard, Philippe Zarka

July 1, 2014

A qualitative discussion of LOFAR+NenuFAR imaging properties

1 LOFAR without NenuFar

1.1 Configurations

The LOFAR configurations are described in detail by van Haarlem et al. (2013). The array is composed of 48 separate stations, of which 40 are in the Netherlands (Fig. 1), 5 in Germany, 1 in France, 1 in the UK and 1 in Sweden (Fig. 2).

1.2 Sensitivity distribution in the uv-plane

The distributions of sensitivity in the Fourier plane for a source at 60 deg elevation for a snapshot observation and for a 8h-integration are shown Figure 3 and 4, respectively.
As can be seen the distribution is extremely concentrated with ∼30% of the sensitivity within 0.3% of the largest baseline and ∼70% of the sensitivity within 10% of the largest baseline.
Such a concentrated distribution does not allow us to take the full advantage of the large baselines and make high resolution imaging. It is due to the very concentrated configuration optimized for observations with the Netherland stations. And because the LOFAR stations cannot be reconfigured (like ALMA for example) the distribution of sensitivity can not be adapted to the resolution.

1.3 Synthesized beam with high sidelobes

As sketched Figure 5, in principle, a perfect Gaussian distribution of FWHM equal to the largest baseline (∼1000 km) would allow us to obtain clean maps with a resolution of $0.2'' \times \lambda$[m]. But we are far from this situation and as illustrated Figure 6 the very high central peak and the low level extended

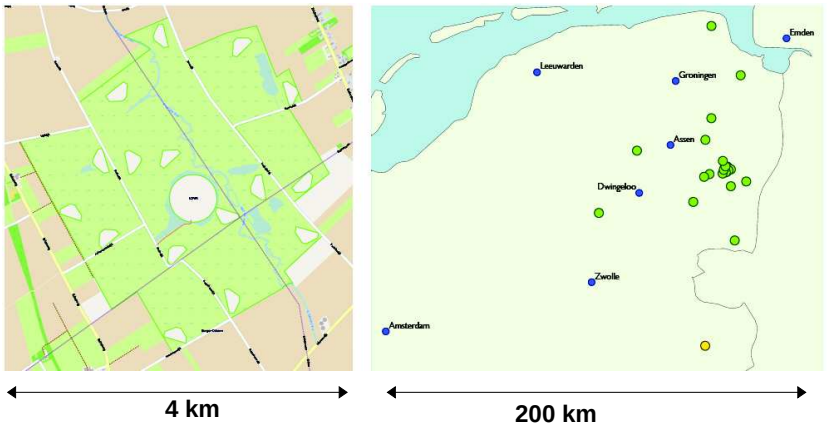

Figure 1: Netherland stations (from van Haarlem 2013)

Figure 2: Remote stations (from van Haarlem 2013)

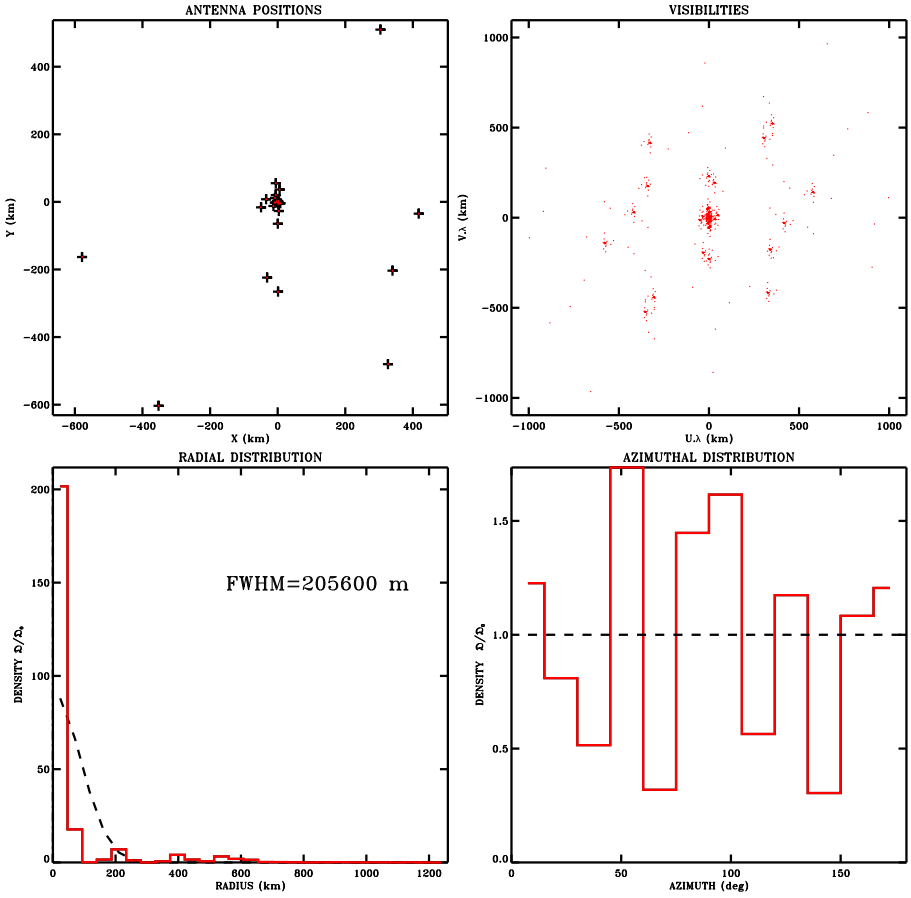

Figure 3: LOFAR uv-plane sensitivity distribution for a snapshot observation of a source at an elevation of 60 deg. The top-left panel shows the configuration, the top-right panel shows the *uv*-coverage. The bottom-left panel shows the radial distribution of the sensitivity in the *uv*-plane. The bottom-right panel shows the azimuthal distribution of the sensitivity in the *uv*-plane.

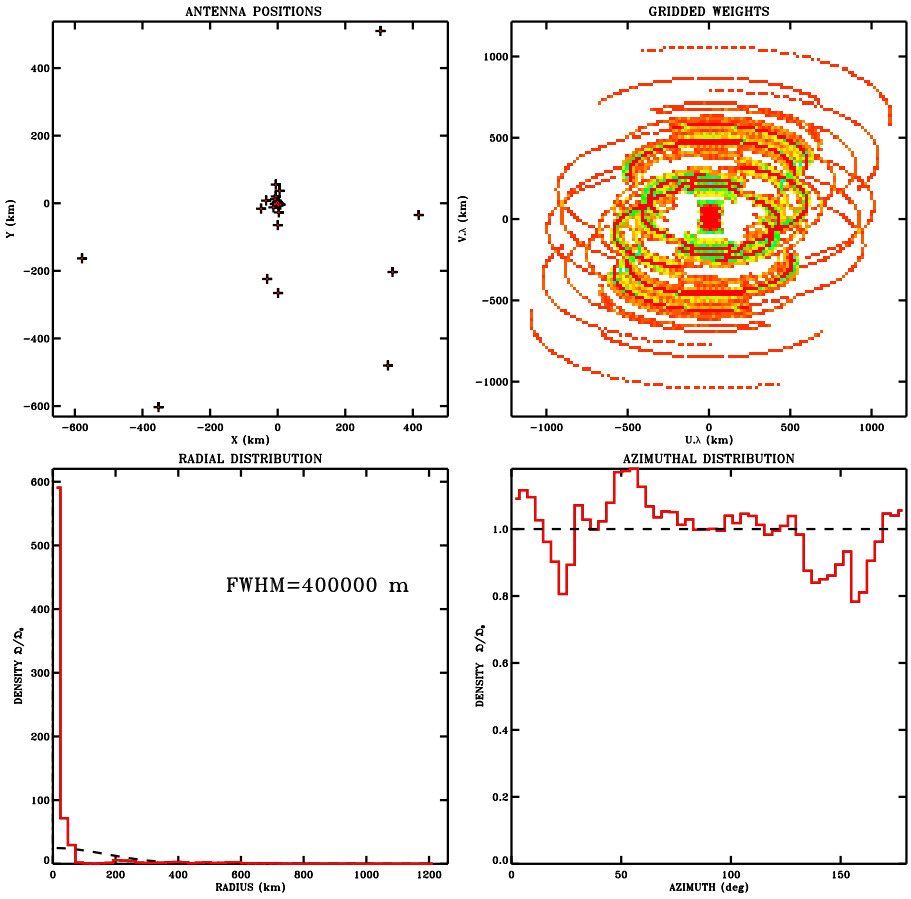

Figure 4: Same as Figure 3 for 8h of integration.

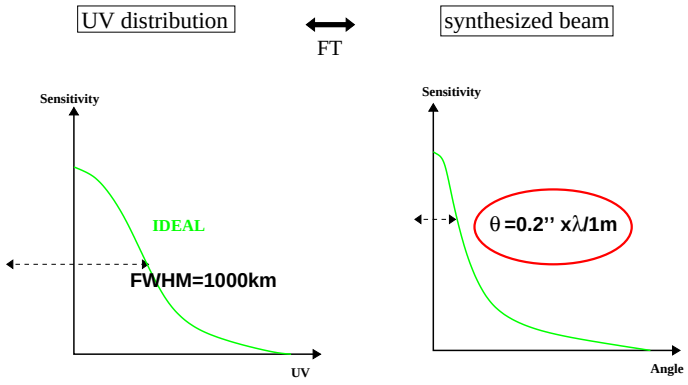

Figure 5: Sketch illustrating the Fourier transform relationship between the sensitivity distribution in the uv-plane and the synthesized beam or PSF. An ideal Gaussian distribution with a FWHM equal to the largest baseline ($\sim$1000 km) would give a Gaussian beam of FWHM=$0.2'' \times \lambda$[m]

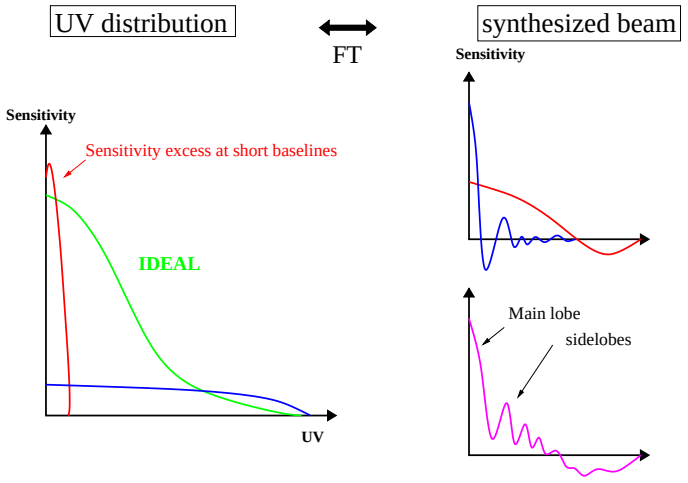

Figure 6: The central peak (red) in the uv-distribution gives a broad lobe in the image plane. And the extended low level distribution (blue) gives a narrow peak and high sidelobes. The addition of the two (purple) gives high sidelobes up to large distances from the main lobe.

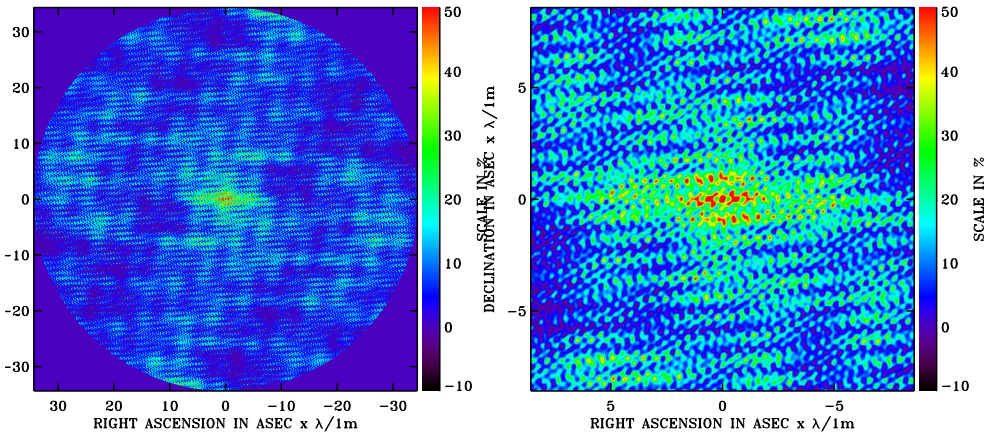

Figure 7: Synthesized beam obtained with the snapshot observation (Fig. 3)

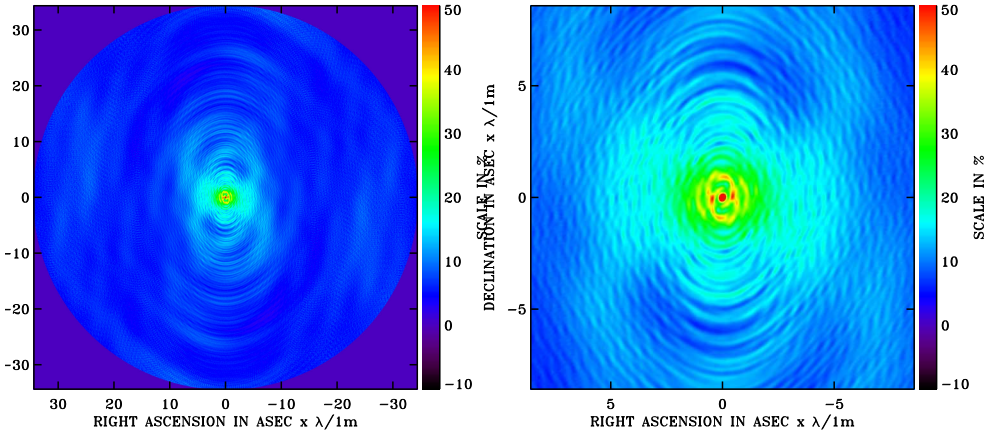

Figure 8: Synthesized beam obtained with the 8h observation (Fig. 4). The sidelobes still reach a level of 50%.

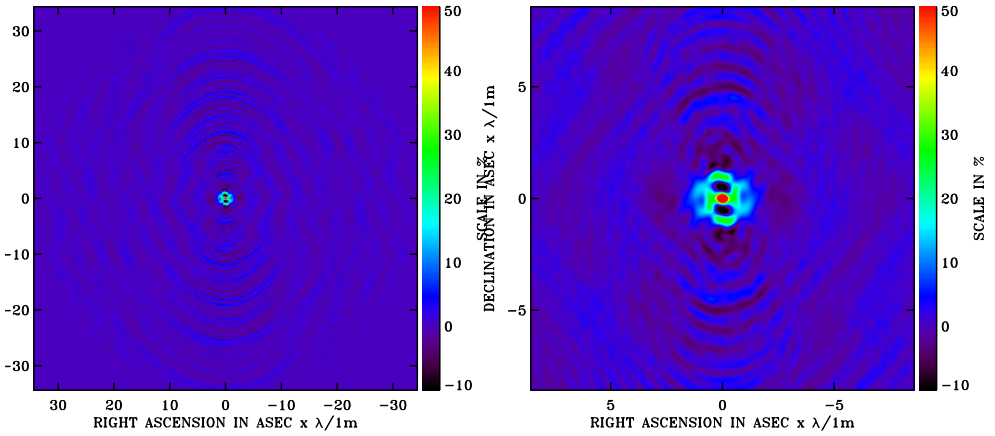

Figure 9: Synthesized beam for 8h integration and reweighting with sensitivity loss by a factor 2. The sidelobes are below 20%, i.e., twice lower than with natural weighting, (see Fig. 8).

distribution in the uv-plane result in a narrow main lobe with many high level sidelobes up to large angular distances from the main lobe.

The synthesized beams obtained with natural weighting in snapshot and in 8h are shown Figures 7 and 8. The level of sidelobes is at ∼20% up to 5″ away from the main lobe. We are far from the 0.2″ resolution.

2 Possible solutions

The configuration is similar to a very big central antenna (the 40 Netherland stations) correlated with 10× smaller antennas (the remote stations). There are two ways to improve LOFAR high resolution imaging capabilities: (*i*) software, by correcting the weights of the uv-samples and improve the distribution of sensitivity (downweight the short baselines); (*ii*) hardware, by increasing the size (and therefore the sensitivity) of the remote stations.

2.1 Reweighting

Whatever the reweighting scheme followed it necessarily results in a loss of sensitivity. We follow here a reweighting method that corrects for defects in the natural sensitivity distribution with respect to an ideal Gaussian distribution (Boone, 2013). With this method it is possible to reduce the sidelobes by a factor of 2 with a sensitivity loss by a factor 2 (Fig. 9). Or to to reduce the sidelobes by a factor of 4 with a sensitivity loss by a factor 4 (Fig. 10).

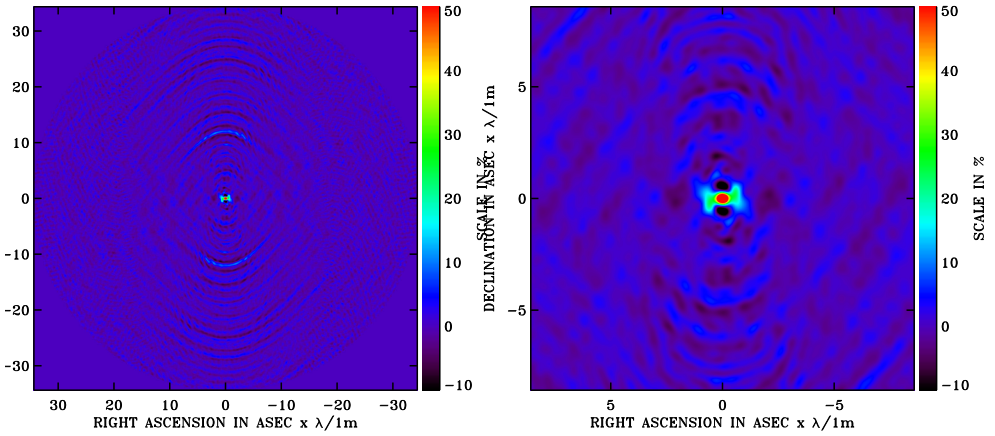

Figure 10: Synthesized beam for 8h integration and reweighting with sensitivity loss by a factor 4. The sidelobes are below 10%, i.e., 4 times lower than with natural weighting, (see Fig. 8).

2.2 NenuFAR

NenuFAR is 19 times more sensitive than the other remote stations, which is the right ratio to compensate for the lack of sensitivity over the largest baselines. The uv-distribution of sensitivity is significantly improved for the intermediate baselines and the central peak is significantly reduced (Fig.11). As consequence the synthesized beam obtained with natural weighting is better (Fig.12). And reweighting is much more efficient: it is possible to obtain sidelobe levels below 20% for a sensitivity loss factor of 1.5 only (Fig.13).

If all the remote stations were like NenuFar the high resolution imaging capabilities of LOFAR would be greatly enhanced (Figs 14 and 15).

3 Summary

- The NenuFAR station can improve the sensitivity balance between short and long baselines in LOFAR.
- Sensitivity increased by ∼2 and lower sidelobes.
- Would be even better if all international stations were like NenuFAR!

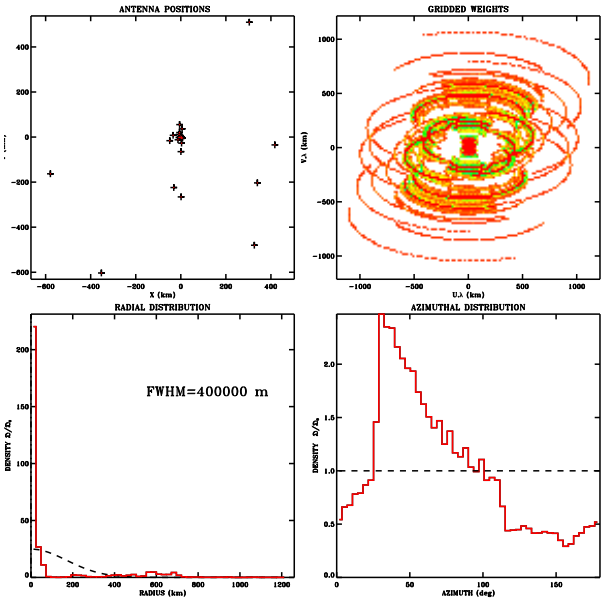

Figure 11: LOFAR+NenuFar with natural weights

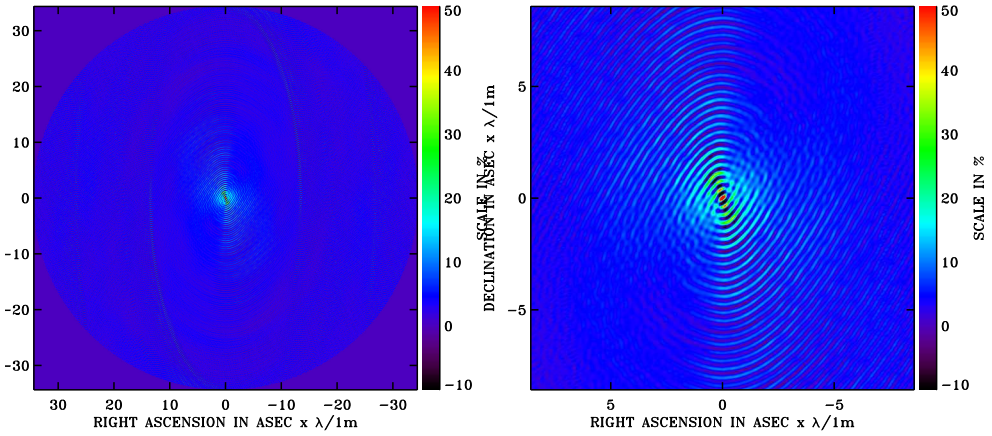

Figure 12: LOFAR+NenuFAR synthesized beam obtained with natural weights.

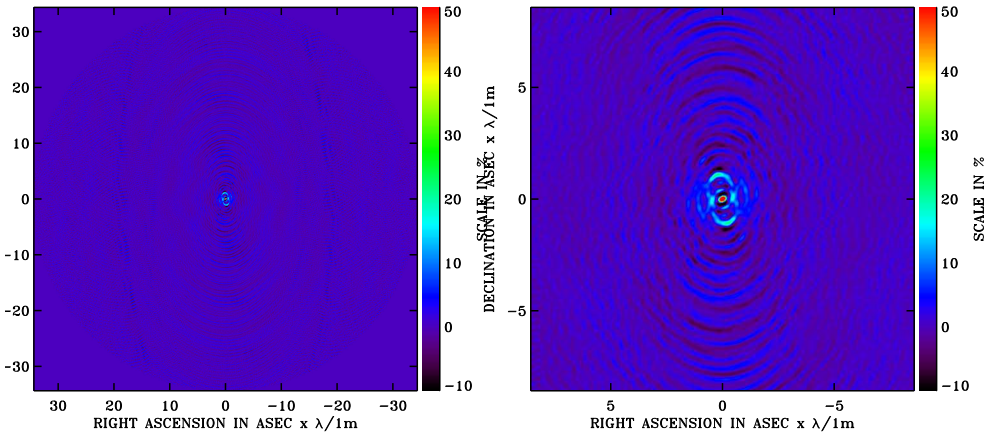

Figure 13: LOFAR+NenuFAR synthesized beam obtained after reweighting the data. The level of sidelobes is below 20% (i.e. 2x lower than with natural weighting) for a sensitivity loss by a factor 1.5 only.

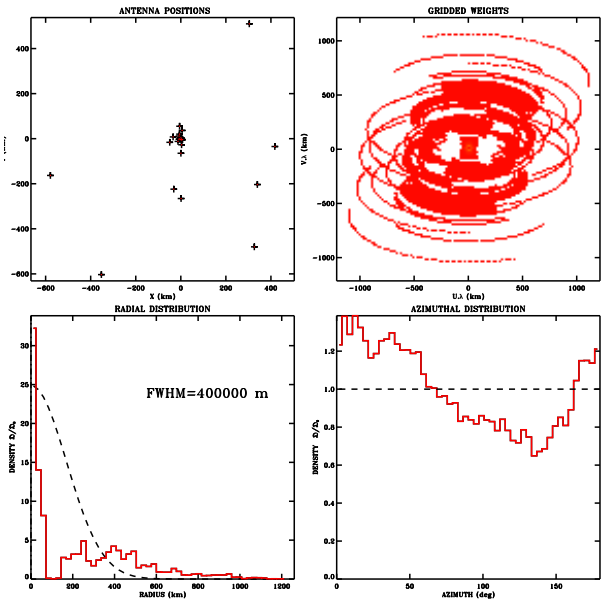

Figure 14: LOFAR *uv*-coverage with 8 NenuFAR international stations

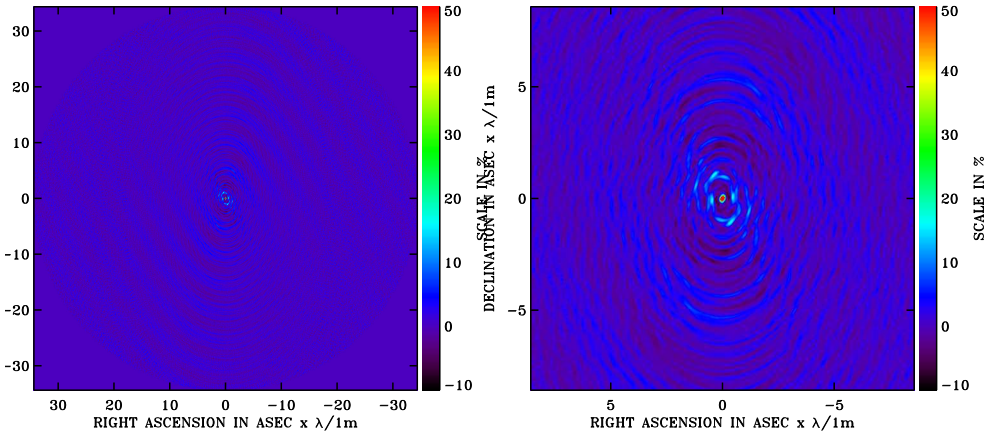

Figure 15: LOFAR beam with 8 NenuFAR international stations and natural weighting. The sidelobes are below 20%.

References

[1] Boone, F., 2013, Experimental Astronomy, 36, 77

[2] van Haarlem et al., 2013, A&A, 556, 2

NenuFAR in standalone mode: calibration, imaging, confusion, and decorrelation issues

Tasse C., Atemkeng M., Cecconi B., Girard J. N.,
Dumez-Viou C., Smirnov O., Zarka P.,
Larzabal P., El Korso M. N., Boyer, R.

Abstract: In this contribution, we discuss a number of important instrumental aspects of the NenuFAR array including decorrelation, fundamental confusion limit, and calibrability.

1 Introduction: NenuFAR and the radio interferometry measurement equation

Together with the the new generation of interferometers, NenuFAR is characterized by very wide fields of view, large fractional bandwidth, and high sensitivity. At these low frequency, the cross-correlation between voltages from pairs of antenna (the visibilities) are affected by complex baseline-time-frequency direction dependent effects (DDE) such as the complex mini-array beams, the ionosphere and its associated Faraday rotation, and the sky structure.

To model the direction-dependent effects (DDE - station beams, ionosphere, Faraday rotation, etc), we use the radio interferometry measurement equation (RIME) formalism, which provides a model of a generic interferometer (for extensive discussions on the validity and limitations of the measurement equation see Hamaker et al. 1996; Smirnov 2011). Each of the physical phenomena that transforms or converts the electric field before the correlation is modeled by linear transformations (2×2 matrices). If $\mathbf{s} = [l, m, n = \sqrt{1 - l^2 - m^2}]^T$ is a sky direction, and $\mathbf{M}^H$ stands for the Hermitian transpose operator of matrix $\mathbf{M}$, then the 2×2 correlation matrix $\mathbf{V}_{(pq)t\nu}$ between antennas p and q at time t and frequency ν can be written as

$$\mathbf{V}_{(pq)t\nu} = \mathbf{G}_{pt\nu} \left(\sum_{\mathbf{s}} \mathbf{V}^{\mathbf{s}}_{(pq)t\nu} k^{\mathbf{s}}_{(pq)t\nu} \right) \mathbf{G}^H_{qt\nu} \tag{1}$$

$$\mathbf{V}^{\mathbf{s}}_{(pq)t\nu} = \mathbf{D}_{p\mathbf{s}t\nu}(\mathbf{x}) \mathbf{X}_{\mathbf{s}} \, \mathbf{D}^H_{q\mathbf{s}t\nu}, \tag{2}$$

where $\mathbf{D}_{p\mathbf{s}t\nu}$ is the product of direction-dependent Jones matrices corresponding to antenna p (e.g., beam, ionosphere phase screen, and Faraday rotation), $\mathbf{G}_{pt\nu}$ is the product of direction-independent Jones matrices for antenna p (like electronic gain), and $\mathbf{X}_{\mathbf{s}}$ is referred as the sky term[1] in the direction $\mathbf{s}$, and is the true underlying source coherency matrix [[$\mathrm{X}_p\mathrm{X}^*_q$,$\mathrm{X}_p\mathrm{Y}^*_q$], [$\mathrm{Y}_p\mathrm{X}^*_q$, $\mathrm{Y}_p\mathrm{Y}^*_q$]]. The scalar term $k^{\mathbf{s}}_{(pq)t\nu}$ describes the effect of the array geometry and correlator

[1]For convenience, in this section and throughout the paper, we do not show the sky term $\sqrt{1 - l^2 - m^2}$ that usually divides the sky to account for the projection of the celestial sphere onto the plane, as this has no influence on the results.

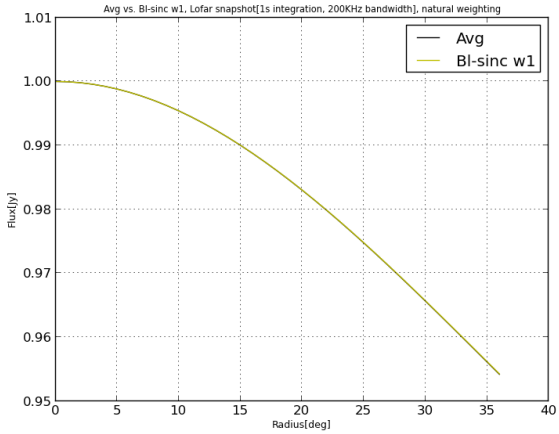

Figure 1: This figure shows how the time-frequency decorrelation effects lead to a loss of sensitivity as a function of distance from the phase center. In most observing setup, smearing should be limited to only a few percent in the NenuFAR primary beam.

on the observed phase shift of a coherent plane wave between antennas p and q. We have $k^{\mathbf{s}}_{(pq)t\nu} = \exp\left(-2i\pi\phi(u,v,w,\mathbf{s})\right)$ with $\mathbf{b}_{pqt\nu} = [u,v,w]^T$ as the baseline vector between antennas p and q in wavelength units and $\phi(u,v,w,\mathbf{s}) = ul + vm + w\left(\mathrm{n}-1\right)$.

2 Decorrelation issues

Decorrelation results in an effective loss of sensitivity (extensively discussed in Hamaker et al. 1996; Smirnov 2011, and references therein). It is partly due to the vector $\mathbf{b}_{pqt\nu}$ being defined in units of wavelength, making $k^{\mathbf{s}}_{(pq)t\nu}$ variable in frequency. Furthermore, the Earth's rotation causes $\mathbf{b}_{pqt\nu}$ to rotate in our coordinate frame, which also makes $k^{\mathbf{s}}_{(pq)t\nu}$ variable in time. To take this into account, the RIME can be rewritten as an integration over a time/frequency interval:

$$\left\langle \mathbf{V}_{(pq)t\nu} \right\rangle = \frac{1}{\Delta t \Delta\nu} \int_{t_0}^{t_1} \int_{\nu_0}^{\nu_1} \mathbf{V}_{(pq)t\nu} dt d\nu \tag{3}$$

For the general case of decoherence, a useful first-order approximation can be obtained by assuming that Δt and $\Delta\nu$ are small enough that the amplitude of $\mathbf{V}_{(pq)t\nu}$ remains constant, while the complex phase varies linearly. In that case, the decoherence is given in terms of the phase changes in time ($\Delta\Psi$) and frequency ($\Delta\Phi$):

$$\left\langle \mathbf{V}_{(pq)t\nu} \right\rangle \approx \mathrm{sinc}\left(\frac{\Delta\Psi}{2}\right) \mathrm{sinc}\left(\frac{\Delta\Phi}{2}\right) \mathbf{V}_{(pq)t_m\nu_m} \tag{4}$$

where (t_m, ν_m) are the time and frequency values at the center of the bin. Equation 4 is straightforward to apply numerically.

Each baseline and direction in the sky are affected by decorrelation at different level. In order to properly estimate the effect of smearing for NenuFAR, we simulate datasets based on the NenuFAR mini-array layout. The datasets are simulated according to Eq. 1, each containing a source having flux density of 1 Jy, and located at a variable distance from the phase center. Figure 1 shows the apparent flux density in the resulting synthesized dirty image

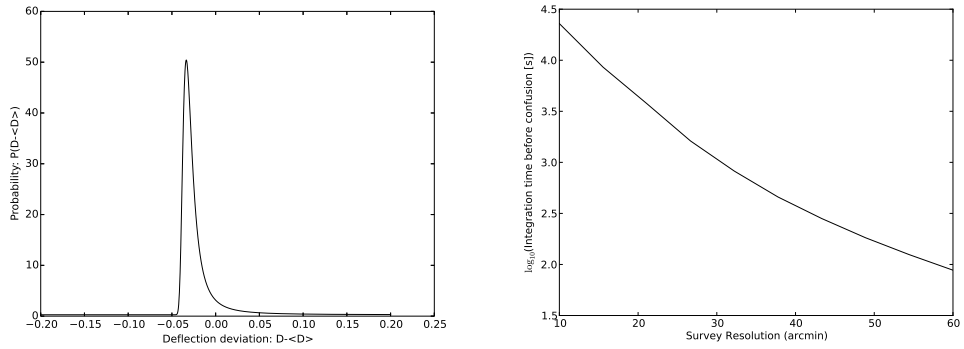

Figure 2: The left panel shows the deflection probability distribution for assumed $k = 5.10^{-3}$ and $\gamma = 2.1$ and primary beam width of 1 deg in diameter. Comparing the confusion noise standard deviation to the time-frequency integrated thermal noise, we can get an estimated integration time before reaching confusion as a function of NenuFAR resolution.

(using natural weighting), as a function of the source location with respect to the phase center. At a distance of 20 deg, the decorrelation factor is $\lesssim 2\%$ for $(\Delta t, \Delta\nu) = (1\text{ sec},\ 200\text{ kHz})$, and $\sim 0.6\%$ for $(\Delta t, \Delta\nu) = (1\text{ sec},\ 100\text{ kHz})$.

3 Confusion

The confusion limit is a fundamental number that can be computed for any astronomical instrument, and only depends on (i) the instrument's beam, and (ii) the number counts of the observed astronomical sources. Intuitively it is reached when it is often the case that more than one source contribute to a single resolution element.

The confusion noise is described in terms of the statistics of the *Deflection* (D) random variable, defined as the flux density observed in a beam formed in a random direction. The probability distribution $P(D)$ is given as an analytic expression by Condon (1974):

$$P(D) = 2\int_0^\infty \exp\left(-k\Omega_e\eta_1\omega^{\gamma-1}\right)\cos\left(k\Omega_e\eta_2\omega^{\gamma-1} + 2\pi\omega D\right)d\omega \tag{5}$$

$$\eta_1 = \frac{1}{2}\pi^{\gamma+0.5}\left(\Gamma\left[\frac{1}{2}\gamma\right]\Gamma\left[\frac{1}{2}(\gamma+1)\right]\sin((\gamma-1)\pi/2)\right)^{-1} \tag{6}$$

$$\eta_2 = \frac{1}{2}\pi^{\gamma-0.5}\Gamma\left[\frac{1}{2}(2-\gamma)\right]\Gamma\left[\frac{1}{2}(\gamma+1)\right]^{-1} \tag{7}$$

$$\Omega_e = \int f(\theta,\phi)^{\gamma-1}d\Omega \tag{8}$$

where k and γ parametrise the norm and slope of the radio source count $n(S) = k.S^{-\gamma}$ and $f(\theta,\phi)$ is the angular power pattern. Based on the VLA Low-frequency Sky Survey at 74 MHz source counts (VLSS, see Kassim et al. 2003), we can derive the expected deflection probability distribution corresponding to a NenuFAR primary beam (see Fig. 2). Assuming a Gaussian beam shape, the confusion noise can be compared to the thermal noise distribution to derive the confusion limit in terms of integration time, and number of detected sources before reaching the confusion noise. The thermal noise is computed at 50 MHz assuming (i) we are dominated by the galactic emission (~ 6000 K at 50 MHz), (ii) a bandpass of 60 MHz, and (iii) a 7 meters radius for the individual mini-array stations.

4 Standalone interferometric calibration

As explained in Sec. 1, in the low frequency observing regime of NenuFAR, the visibilities are affected by baseline-time-frequency DDE such as the complex mini-array beams, the cable length errors between the mini-arrays and the correlator, the ionosphere and its associated Faraday rotation, and the sky structure.

In order to properly estimate the sky term appearing in Eq. 1, these effects have to be estimated and corrected for in the imaging step. While the ionospheric effects is complex and hard to calibrate for extended arrays such as LOFAR (see Tasse 2014, and references therein), the problem is more simple for NenuFAR in standalone mode, because the station layout is compact. In that case at each frequency the ionosphere is reducible to a simple ionospheric phase screen. Source distortion is minimum and differential Faraday rotation does not occur. Calibrating for the cable delays should not cause problems thanks to the available large fractional bandwidth.

The field of view is large and the brightest radio sources (also referred as the A-team sources) will always contribute to the visibilities. All-sky models will therefore have to be used to calibrate NenuFAR in standalone mode. For this existing radio data can be used such as the multi-frequency all-sky LOFAR survey (Heald et al. 2014, in prep.) or the VLSS (Kassim et al. 2003). A difficulty however is that the Galactic extended emission may be resolved at a significant level. This issue might be addressed in the calibration step (i) by using only the longest baselines, or (ii) by taking into account the extended emission in the sky model.

5 Conclusion

We conclude that datasets will not suffer from strong decorrelation issues. The array conpactness coupled with the large collecting area leads a rather low confusion limit not suited for science requiring high angular resolution. Although ionosphere will be severe at those low frequency, the compact standalone mode simplifies calibration issues the more extended interferometers are facing. However the NenuFAR sensitivity to the polarised Galactic extended emission will require some effort in sky modeling or calibration strategy.

References

Condon, J. J. 1974, ApJ, 188, 279

Hamaker, J. P., Bregman, J. D., & Sault, R. J. 1996, A&AS, 117, 137

Heald, G., the MSSS survey team, & the LOFAR collaboration. 2014, A&A in prep.

Kassim, N. E., Lane, W. M., Cohen, A. S., et al. 2003, American Astronomical Society Meeting, 203,

Smirnov, O. M. 2011, A&A, 527, A106

Tasse, C. 2014, A&A

ALGORITHMS & OPTIMIZATIONS

Thierry LANZ, Chiara FERRARI, David MARY,
André FERRARI, Arwa DABBECH, Cédric RICHARD, Cédric FEVOTTE
Laboratoire J.-L. Lagrange, Observatoire de la Côte d'Azur

The signal processing team of the Lagrange Laboratory has expertise in image reconstruction using advanced models, in statistical detection, modeling and learning, and in optimization. Some members of the group have been working in the field of radioastronomical image reconstruction for several years.

This group is highly interested in being part of the NenuFAR project to offer and develop methodological tools in the framework of the SKA pathfinders. While it is not clear at this stage to which topic we would specifically contribute, we are broadly interested in :

- ***Image reconstruction algorithms, in particular spatio-spectral methods***

  In the framework of image reconstruction from radio interferometric data, we have developed a new algorithm (titled ``MORESANE'' for MOdel REconstruction by Synthesis-ANalysis Estimators, PhD thesis of Arwa Dabbech) that uses sparsity promoting restoration models based on highly redundant, shift invariant dictionaries. The proposed approach is aimed at efficiently restoring complex faint sources in high dynamic astrophysical maps.

  During the last, say, 7 years, innovations in radio image restoration methods have been based almost exclusively on the use of efficient sparse representations. Those can be expressed either in analysis or in synthesis. To cope with the notoriously difficult problem of restoring complex sources with a high dynamic, the proposed method is hybrid in its sparsity priors. On one hand, the image to be reconstructed is modeled as a sum of few elementary sources which, as opposed to classical synthesis-based sparsity priors, are let free and are learned from the data. On the other hand, these objects are iteratively estimated and deconvolved using analysis-based priors expressed in an Isotropic Undecimated Wavelet Transform (IUWT) dictionary.

  The algorithm has been tested on realistic simulations of observations performed with the SKA and its high-frequency pathfinders (ASKAP and MeerKAT; Dabbech et al. 2012, 2014). Refinements are required (e.g. taking into account the variations of the PSF within the field of view of the instrument; testing performances in presence of calibration errors) to fully allow the exploitation of the algorithm on low-frequency radio data.

  Beyond the problem of reconstructing images, the large bandwidths covered by current/next generation large radio arrays allow to reconstruct multi-wavelength images. In this case, spatio-spectral models must be injected in the algorithms to improve the restoration. In radio, the only existing multiwavelength imaging software is to our knowledge the MF-MS CLEAN algorithm (Multi-Scale Multi-Frequency deconvolution algorithm for wide-band Synthesis-imaging) of Rau et al. (2011). In optical interferometry, we have recently proposed an algorithm (named PAINTER, for sPAtIo-spectral Image recoNsTruction algorithm for optical intERferometry, Schutz et al, 2014), which is the first polychromatic restoration algorithm in optical interferometry. The method

may use different types of spatio-spectral regularizations and is based on dedicated optimization techniques. These principles could be used, for instance, to elaborate a multiwavelength version of the MORESANE algorithm.
Such progresses open an interesting path for multiwavelength imaging reconstruction algorithms, which will have to be elaborated for the SKA. Of course, the design of such methods will have to account for large scale and calibration error issues discussed below.

Rau, U. and T. J. Cornwell (2011). « Multi-scale Multi-frequency Deconvolution Algorithm for Synthesis Imaging in Radio Interferometry ». In : Astronomy and Astrophysics 532, p. 1–17.

Schutz, A. et al (2014), « A spatIo-spectral image reconstruction algorithm for optical interfermometry», submitted to JOSSA.

- ***Statistical description of the observation models***, in particular through the possibility of using data-driven Bayesian hierarchical models to model temporal and spatial variations of the ionosphere and of the receptors

The problem posed by radiointerferometric image reconstruction is a non-standard inverse problem, owing to the errors impacting the direct observation model. These errors include an imperfect knowledge of the receivers (temporal evolution of their responses, coupling effects) and random phases introduced by the ionosphere (which are critical for large fields-of-view observations). Accounting precisely for such errors is a major issue for improving image restoration methods. In terms of inverse problems, we face a semi-blind (or myopic) inversion problem.

The Bayesian inferential framework is particularly efficient in this setting since it allows to model relatively complex uncertainties on the data acquisition system through hierarchical graphical models. This technique was in particular recently used to compensate a posteriori for turbulence residuals of adaptive optics (Desidera et al. 2009, Prato et al. 2013). Bayesian models allow in particular to account for temporal evolution of calibration modeling errors. They also allow to treat the modeling error as a set of nuisance parameters and to reconstruct the probability distribution of the image conditioned to the observations, by conditionally integrating modeling errors. To our knowledge, such approaches remain however largely unexplored to describe and control modeling errors in radio interferometry. Efficient statistical sampling strategies allowing to reduce the computational cost exist in this framework. Their relevance (in optical imaging) is for instance well evidenced in Orieux et al., 2013, in the case where a parametric model of the imaging system is available.

We also note, on a fully unsupervised front, that the Bayesian approach does not necessarily have to rely on a physical model of the perturbations (for instance, we do not dispose of an accurate parametric model for the ionosphere). In this framework, techniques such as Gaussian processes have recently proved to track efficiently deviations with respect to nominal models, in particular in the framework of large data volumes (Hensman et al. 2013).

Desidera, G. and M. Carbillet (2009). « Strehl-constrained iterative blind deconvolution for post-adaptive-optics data », Astronomy & Astrophysics 507.3, p. 1759–1762.

Hensman, J., N. Fusi and N.D. Lawrence (2013). « Gaussian Processes for Big Data. » In : Proceedings of the 29th Conference on Uncertainty in Artificial Intelligence.

Orieux, F., et al. (2013). « Estimating hyperparameters and instrument parameters in regularized inversion Illustration for Herschel/SPIRE map making », Astronomy & Astrophysics 549.

Prato, M., et al. (2013). « A convergent blind deconvolution method for postadaptive-optics astronomical imaging ». In : Inverse Problems 29.6.

- ***Detection of transients, in particular using machine learning techniques***

The current approach for detecting fast transients (i.e. from microseconds to seconds) mostly rely on exhaustive de-dispersion of the time series based on known dispersion measures candidates. In this method, the time series are de-dispersed for a large set of possible dispersion models and then summed across all channels. The sum signal that has the highest maximum is used as a test statistic.

De-dispersion is an efficient method with a high power for low amplitude events. It is also able to reject efficiently braodband Radio Frequency Interferences (because the corresponding pulse arrives simultaneously at all frequencies), can be parallelized and be implemented for on-the-fly detection. Despite these benefits however, de-dispersion assumes that one of the dispersion models is the right one. While this is true for many fast transients, there may be exceptions (for instance the perytons, Burke-Spolaor et al 2011) and there may be other ``exotic'' events that remain undetected owing to the strongly supervised character of the de-disperison method.

It could therefore be useful to devise detection methods which offer more flexibility. Machine learning provides a large set of such methods. The large data volume generated by the radio arrays such as LOFAR - so large that the data can not even be stored for more than a few seconds- is particularly appropriate for statistical learning of target / nuisance subspaces or manifolds. Combination of supervised learning (accounting for our knowledge of the RFI for instance) with unsupervised methods (aimed at learning temporally varying background or structured noise for instance) can indeed be envisaged. The benefits of this kind of approaches was first demonstrated by Thompson et al. (2011). Fast transient detection, as the issues regarding calibration discussed above, is thus clearly a domain in radio where statistical modeling and learning could lead to efficient algorithms in the perspective of the SKA.

S. Burke-Spolaor, M. Bailes, R. Ekers, J. Macquart, and F. Crawford III. “Radio Bursts with Extra-galactic Spectral Characteristics Show Terrestrial Origins”, Astrophysical Journal, 727:18, 2011.

David R. Thompson, Walid A. Majid, Colorado J. Reed, Kiri L. Wagstaff, “Semi- supervised Novelty Detection with Adaptive Eigenbases, and Application to Radio Transients." Conference on Intelligent Data Understanding. October 2011.

- ***All related large scale optimization issues***

In practice, a strong limitation to the inversion - in particular for Bayesian approaches - is caused by the large volume of parameters to deal with (those concern both the data acquisition model and the image to restore). In such a setting, simply evaluating the likelihood associated to a parameter set may be problematic since this evaluation requires to compare the outputs of the direct model

with the data. Likelihood evaluation is however at the heart of all state-of-the-art restoration algorithms (for instance, the sparsity-based ones) and of course of the Bayesian approach as well. This problem has very recently generated a lot of attention in dedicated distributed algorithms, each working on a fraction of the full data samples and parameters (Blocker et al. 2014, Bardenet et al. 2014). The scientific goal is here to appropriately fusion these ``local'' informations by means of numerical methods that can be efficiently implemented in massively parallel architectures. This is a very active field of research today, as the efficiency of such methods directly conditions the success of large scale inversion in many application fields others than radioastronomy.

Bardenet, et al (2104). « Towards scaling up MCMC : an adaptive subsampling approach (2014). Accepted in Proceedings of the International Conference on Machine Learning (ICML) ». To appear in International Conference on Machine Learning (ICML).

Blocker, A., S.L. Scott and F. Bonnasi (2014). « Big data, big models, big problems : Consensus Monte Carlo methods for distributed Bayesian inference ». In : Joint Statistical Meetings.

Dedicated standalone receiver for transients detection

Cédric Viou, Andrée Coffre, Laurent Denis, Jean-Mathias Grießmeier

Summary: By design, the NenuFAR antenna fields will be used as an independent input stream for the LOFAR backend. Alternatively, or in parallel, the data from the NenuFAR arrays can be sent to a local backend, LANewBa. This backend will generate simultaneously two output streams: Subband data and beamlet data. The design of LANewBa is described, and the specifications and scientific use cases for the two types of output data for slow and fast transient detection are explained.

The planned data stream of the combination of the French LOFAR station FR606 and NenuFAR is shown in figure 1. By design, the NenuFAR antenna fields can be used as an independent input stream for the LOFAR backend. The LOFAR backend of FR606 can than be either set to accept data from the LBA field, the HBA field, or the NenuFAR antenna fields (using the former "LBL" connector in the RCUs). The LOFAR backend can then either send the collected data to LOFAR CEP in Groningen, or send the data to a local processor such as ARTEMIS. Alternatively, or in parallel, the data from the NenuFAR arrays can be sent to a local backend (LANewBa=LOFAR Advanced New Backend). As will be detailed below, this backend will generate (in parallel) two types of output: Subband data, which can be provided to a future correlator, and beamlet data, which can be sent to the existing ARTEMIS processor and/or a future super-ARTEMIS like machine.

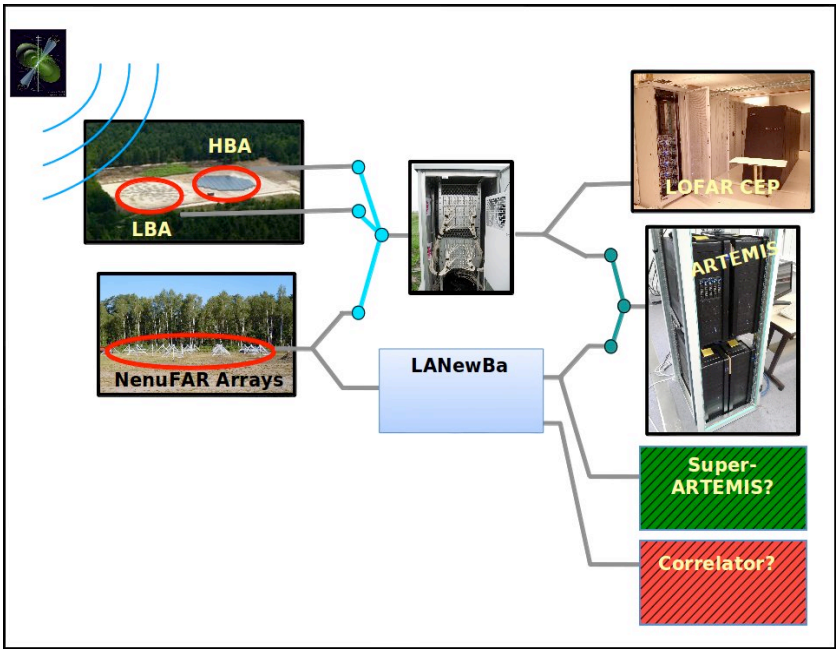

Figure 1: NenuFAR station setup.

The inclusion of a dedicated backend in the NenuFAR project offers a number of advantages:

- With a dedicated backend, NenuFAR will be able to observe continuously and without disrupting LOFAR observations. Using the connection to the LOFAR backend, NenuFAR can easily be integrated into the LOFAR network as a "super station" when required, but when LOFAR does not require the NenuFAR antenna field, it can be used separately as a stand-alone instrument.
- The LOFAR LBA antennae operate in the frequency range 10-90 MHz, and the LOFAR station backend is capable to correlate multiple beams. The total bandwidth of the station beamformer, however, defined as the sum of the bandwidth of the individual beams, is

limited to 48 MHz (96 MHz in 8 bit mode). Similar to LOFAR LBA, the NenuFAR antennae will be used over the frequency range 10-85 MHz (bandwidth of 75 MHz). The dedicated NenuFAR backend (LANewBa=LOFAR Advances New Backend) will make use of recent technical development, and will offer an increased processing bandwidth compares to LOFAR: It will provide 160 MHz of instantaneous bandwidth, enough for two beams covering the full antenna bandwidth (both beams have to fit in the same analog beam determined by the mini-array).

- LANewBa will feature a high dynamic range, using 14 bit digitization for improved RFI robustness (required at the lowest frequencies of the NenuFAR antenna band).
- Compared to an international LOFAR LBA field, the planned NenuFAR antenna field is larger (400m diameter). To assure the narrowband assumption for the beamforming process, LANewBa will offer the possibility to create beamlets of 97.65625 kHz. The standard 195.3125 kHz beamlets of LOFAR will remain possible, and switching the firmware between both versions will take a fraction of a second.
- In addition, LANewBa will offer a faster computation of cross-correlations for station calibration (for LOFAR, one correlation matrix per second; for NenuFAR, the number will be higher, but the final value will depend on available hardware resources).
- LANewBA will provide full Stokes polarization information for beamlet and crosslet statistics (for calibration and instrument diagnostic).
- The backend will include a hardwired port for external trigger messages (e.g. particle detectors).

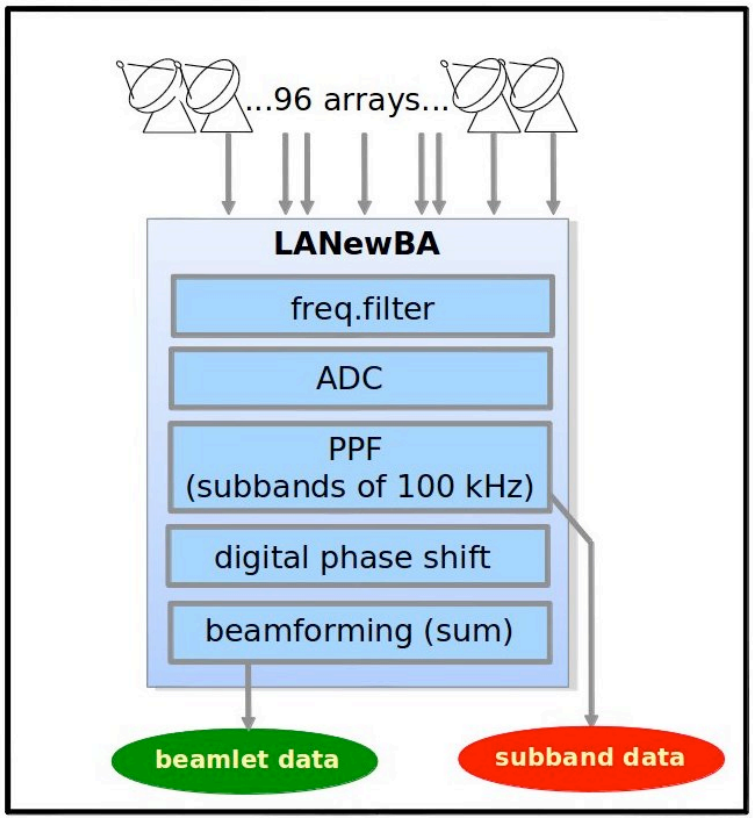

Figure 2: LANewBA receiver structure.

Figure 2 shows the planned design of the LANewBA receiver (equivalement to the RCUs+RSPs in the current LOFAR station). The data from the NenuFAR mini-arrays (up to 96 antenna groups with 19 antennae each) are input as complex voltages, with two polarization channels per mini-array. The data are frequency-filtered before analog-to-digital conversion. To be fully compatible with LOFAR, a clock frequency of 200 MHz is used. Subsequently, the data are channelized by a

polyphase filter bank. The width of the frequency channels is configurable, so that the channel width can either be 97.65625 kHz (to reduce phase errors due to the array size during the beamforming step), or 195.3125 kHz (to be compatible with LOFAR standards). The addition of a mode with a bandwidth of 48.828125 kHz (possible only for a reduced bandwidth) is under discussion. After the PPF, the data are sent to the first output port ("subband data port", see below). The same data are also phase shifted and summed in the beamformer (including gain correction), providing the data for the second output port ("beamlet data port"). Both output ports operate in parallel, and provide data for further processing (outside of LANewBA and requiring additional instrumentation), as detailed in the following.

Beamlet data for fast transient detection

Beamformed data will be output in "beamlet" format, fully compatible with the format used by LOFAR CEP. The planned output data rate is 2 x 5 Gb/s (for 2 beams of 80 MHz of bandwidth in dual polarization). The data can be sent either to the ARTEMIS processors, which accept 4*0.8 Gb/s (a total of 4*12 MHz in dual polarisation) or a new ARTEMIS-like, GPU-based processing facility ("Super-ARTEMIS", the details of which remain to be defined). This processing facility could handle data channelization, (incoherent or coherent) dedispersion, online RFI mitigation, transient detection, and/or S-burst detection.
Scientifically, such data are of interest for all fast (dynamic spectrum) transients at timescales of 1 millisecond or slower, including planetary radio emission (Jupiter, Saturn lightning, exoplanets), pulsars, RRATS (cf. next chapters).

Subband-data for slow transient detection

In parallel, LANewBA will output the sub-band data of all mini-arrays. This comprises 384 subbands (a total of 75 MHz of bandwidth); the maximum datavolume output on this channel is 480 Gb/s (2.5 Gb/s per mini-array and polarization). For this, LANewBA will have 2*24 10 Gb/s exits, connecting to a pair of 48 port 10 GbE-SFP+ switches. For a partial NenuFAR_1 with 24 mini-arrays, the datarate will be 75 Gb/s; for the full NenuFAR array (96 mini-arrays), it amounts to 480 Gb/s. These data can be input to a FPGA or GPU-based correlator (the details of which remain to be defined), which can use this for full-band spectro-polarimetric imaging (e.g. creating one image per second, correlating each of the mini-arrays and polarizations for a total of 192x192 points).
The resolution of the resulting images will be relatively low. The FWHM beamwidth of the a NenuFAR mini-array is 57° (15 MHz) and 11° (75 MHz). The longest baseline within NenuFAR will be of the order of 400m, giving access to structures between 3° (15 MHz) and 0.6° (75 MHz). The smallest resolvable structure is thus approximately 20 times smaller than the beamwidth. Still, this mode is useful, e.g. for surveys where a slow transient can be easily detected, which can e.g. be followed up using the beamlet data.
Scientifically, such data are of interest for all slow (image plane) transients at timescales of 1 second or slower (cf. next chapters).

Prospects for the Epoch of Reionization and Cosmic Dawn observations with NenuFAR

A. Fialkov, L. Koopmans, B. Semelin

Abstract

The redshifted 21-cm signal of neutral hydrogen from high redshifts ($6 < z < 1000$), which at every epoch is strongly correlated to the state of the intergalactic medium and the intensity of radiative backgrounds, is expected to be a unique probe of the Universe at early times. This important signal has not yet been observed, and its detection is the goal of many ongoing and designed experiments. In this section we discuss the prospects for observing neutral hydrogen signal with NenuFAR, a facility which has the potential to detect this signal from the early Universe ($z > 16$) for the very first time. NenuFAR will be capable of probing with high enough sensitivity redshifts ($16 < z < 45$) at which the signal from key cosmological epochs, such as the Dark Ages, Cosmic Dawn and the first half of the Epoch of Reionization, is expected to be found. If observed by this pioneering instrument, the cosmological signal of neutral hydrogen will provide novel information about the formation of the first stars, galaxies and black holes, constrain heating scenarios, probe the mechanism for reionization, and possibly even constrain properties of dark matter and dark energy at high redshifts. Importantly, NenuFAR will also help to pave the way for the Square Kilometer Array, allowing it to tighten the parameter space of the predicted signal of neutral hydrogen and to develop technical and observational aspects of this field.

Introduction

Neutral hydrogen (HI), being the most common element in nature, provides a unique way to probe the Universe at epochs that otherwise remain inaccessible, emitting a line at a rest-frame frequency of $\nu_0 = 1420$ MHz (corresponding to the wavelength of ~ 21 cm). This emission can be observed today and allows us to map the distribution of HI (and thus of most of the baryonic matter) from recombination to reionization, when the majority of the gas was neutral. Measuring the intensity of the redshifted HI signal at frequencies $\nu_0/(1+z)$, where z is the redshift at which the 21-cm line was emitted, provides the information needed to build a three-dimensional picture of the early Universe during the epochs of Reionization (the epoch during which intergalactic medium was photo-ionized by starlight produced in galaxies), Cosmic Dawn (when the first stars were formed) and the Dark Ages (the epoch before the first bright sources formed).

Theoretical modeling [7, 13] shows that the HI signal is sensitive to a plethora of astrophysical and cosmological phenomena, thus being a very useful probe for exploration of the cosmos. More specifically, the local strength of this signal depends on environmental aspects which include local density and temperature of the gas, intensity of Ly-α, X-rays, ionizing and Lyman-Werner radiative backgrounds contributed by the entire population of sources, as well as the rate of star formation (for the exact dependence of the 21-cm brightness temperature on the astrophysical and cosmological parameters see, for instance, eq. 1 in reference [13]). As a result, neutral hydrogen signal back illuminated by the diffused Cosmic Microwave Background (CMB) radiation, bears information about a wide list of physical processes and observables such as the initial conditions for structure

formation; the properties at various epochs of sources including stars, galaxies, black holes, etc.; the character of radiative backgrounds which build up in the course of cosmic history; the mechanism of reionizaton of the intergalactic medium. At the same time, the HI signal may also be sensitive to various exotic phenomena which, if observed, may revolutionize our understanding of the Universe. Some examples of these non-standard processes that can affect the redshifted 21-cm signal are the primordial heating of gas by dark matter annihilation or the suppression of star formation in light halos in Warm Dark Matter models, which would shed some light on properties of dark matter particles, the possible coupling of dark matter and dark energy at early times which may affect structure formation, the presence of primordial magnetic fields which may impact the thermal history, etc.

Unlike the CMB, which only probes the two-dimensional surface of last scattering, the redshifted 21-cm signal, produced by omnipresent neutral hydrogen at $6 < z < 1000$, provides information about a three-dimensional volume. Probing the line of sight direction while averaging over the two-dimensional sphere at every redshift yields the evolution of the "global" spectrum with time (redshift, frequency), which in turn provides information about key milestones in the history of the Universe. On the other hand, scanning two-dimensional surfaces perpendicular to the line of sight at specific redshifts gives information about spatial fluctuations in the intensity of the HI signal at each epoch. The power spectrum of these fluctuations, as well as higher order statistics, can teach us about the emissivity of the first sources of radiation in the UV and X-rays, about the masses of dark matter halos in which early stars were formed (a bit of information strongly linked to many astrophysical phenomena), etc. Using the information obtained from this tomographic scan of the high-redshift Universe it is also possible, for instance, to test for a redshift dependence of the properties of dark matter and dark energy.

Considerable observational effort is being made at present with the aim to constrain the parameter space of the 21-cm signal. The first experimental steps to detect the 21 cm global signal have been carried out by The Experiment to Detect the Global Epoch of Reionization Signature (EDGES) [3], which ruled out the models of rapid reionization that occur over a redshift interval shorter than $\Delta z < 0.06$ [4]. Many other experiments, including the Low-Frequency Array (LOFAR), the Murchison Widefield Array (WMA), the Precision Array for Probing the Epoch of Reionization (PAPER), are on the way to set limits on the 21-cm signal. Moreover, the ambitious Square Kilometer Array (SKA) which is currently being planned, will also explore among other radio signals the redshifted 21-cm with good sensitivity from a wide range of redshifts.

In this section we present the prospects for the observations of the Epoch of Reionization, Cosmic Dawn and Dark Ages with NenuFAR. We explain that, although the exact signal to noise for the 21-cm detection with NenuFAR depends on the intensity of the actual (still significantly unconstrained) signal as well as on the degree to which potential systematics and thermal noise can be mitigated, NenuFAR in stand-alone mode has all the chances to make the discovery and to be the first experiment to measure both the global signal and the power spectrum of the neutral hydrogen signal[1].

Prospects for the 21-cm signal observations with NenuFAR

The design of NenuFAR (in its stand-alone mode) allows for detection of both the global 21-cm

[1]Please note, that a similar experiment, Large-Aperture Experiment to Detect the Dark Ages (LEDA), is currently on its way, and it is expected to be as efficient as NenuFAR in detecting the global 21-cm signal. However, the detection of fluctuations in the neutral hydrogen signal is more likely to happen thanks to NenuFAR due to several improvements relatively to LEDA (e.g., larger collective area).

spectrum and its power spectrum from a key range of redshifts. In addition, it may be possible to produce images of the 21-cm signal from the early Universe, even though with coarse (degree-scale) resolution. For these measurements to succeed, however, it is essential to think carefully about noise characterization, calibration and removal of radio frequency interference and contaminating foregrounds.

Provided that the data obtained with NenuFAR can be cleaned to the desired level, the global 21-cm signal can (in principle) be detected within few days using auto-correlations of each individual station (while simultaneously using cross-correlations between different stations for calibration purposes). The field of view of NenuFAR (which is $8-60^{\circ}$) is sufficiently large to grasp a representative volume of the Universe (the observed surface area will contain several comoving Gpc at the high redshifts of interest). The low frequencies measurable by NenuFAR, namely 10-85 MHz (corresponding to wavelengths $\lambda = 3.5-30$ meters) should in principle allow the access to the global redshifted 21-cm signal from $z = 16-140$. However in practice, detecting the cosmological signal from $z > 45$ may be very hard due to the growing sky brightness and ionospheric effects at the relevant low frequencies. The observable range of redshifts includes the end of the Dark Ages, the Cosmic Dawn and the beginning of the Epoch of Reionization. Measurements of the global signal bring information on the instants in cosmic history which mark the beginning of star formation, the instant at which heating by the first sources overcame the adiabatic cooling of the gas caused by the expansion of the Universe. They also allow for a characterization of the efficiency of the heating sources and, finally, the beginning (but not the end) of the Epoch of Reionization. Remarkably, detection of, or even an upper bound on, the 21-cm signal from high redshifts would help to determine the real succession of events in cosmic history, which at present is only roughly constrained by numerical simulations. For instance, it is still not clear whether or not radiation emitted by first sources heated the intergalactic medium prior to ionizing it. An unexpected behavior of the global signal as a function of frequency (redshift) would hint to the presence of exotic phenomena such as non-standard heating inputs. Probing this signal with NenuFAR is certainly of great interest, both for the information content it may carry and for the fact that it has never been observed before. Moreover, a strong point of NenuFAR resides on the targeted high redshifts, given that most of the other current experiments aim for the HI signal from lower redshifts, $6 < z < 16$, probing the advanced stages of the Epoch of Reionization.

The power spectrum of the 21-cm signal may be easier to measure than its global behavior. In fact, the resolution of NenuFAR in stand-alone mode (e.g. $\sim 0.7^{\circ}$ at $z = 20$), together with its large field of view, allows one to probe fluctuations in the HI signal at very large scales (e.g. scales of $\sim 100-1000$ comoving Mpc at $z = 20$ corresponding to wavenumbers of $k \sim 0.006-0.06$ Mpc^{-1}). According to our estimates[2] (an example of the predicted power spectrum and sensitivity curves of NenuFAR at $z = 20$ are shown on figure 1) fluctuations from $z \sim 17-25$ can be measured with signal to noise larger than unity within 1000 hours of integration. The maximal signal to noise is of $\mathcal{O}(10)$ at wavenumbers $k \sim 0.03-0.05$ Mpc^{-1} and is expected to originate at $z \sim 20$. The redshift ranges and the exact values of signal to noise can vary within few tens of percents depending on model parameters for standard star formation scenarios. The power spectrum measurement contains

[2]The predictions are based on simulations of the 21-cm power spectrum at $k \sim 0.02-2$ Mpc^{-1} [17, 6, 8, 9] then extrapolated to larger scales. They also assume that first stars form via atomic cooling in halos heavier than $\sim 10^7$ M$_{\odot}$, with star formation efficiency $f_{\star} = 0.05$, and that the intergalactic medium is mainly heated by X-rays emitted by X-ray binaries of heating efficiency $f_X = 1$.

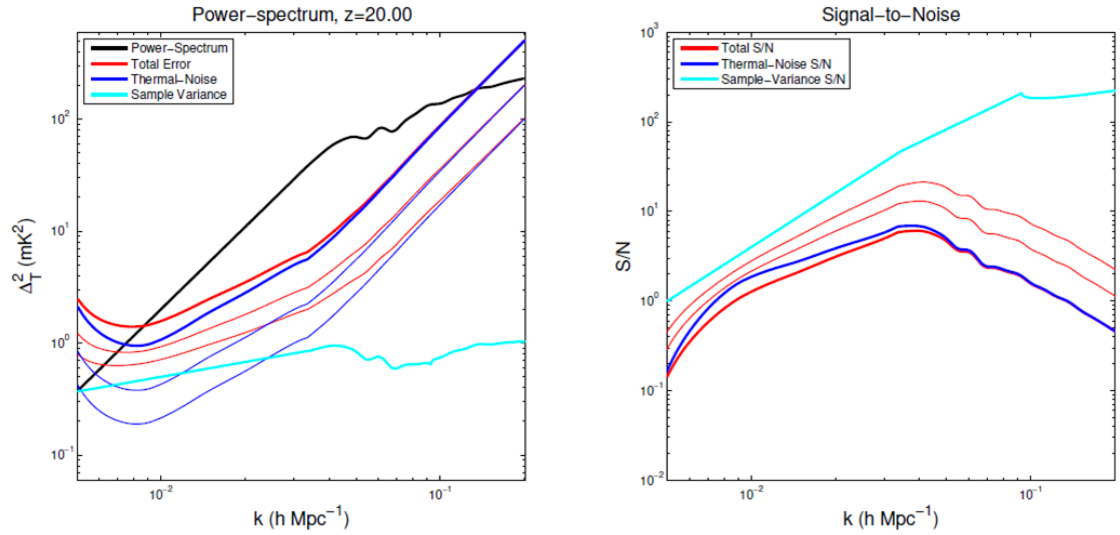

Figure 1: Prospects for detection of fluctuations in the 21-cm signal from $z = 20$ with NenuFAR. Left: We show an example of a typical spherically averaged 21-cm power spectrum ($k^3P(k)/2\pi^2$) at $z = 20$ (black line) together with sample variance (cyan), total error (red) and thermal noise (blue), which are shown for 1000 hours (thick lines), 2500 and 5000 hours of integration time, a 10 MHz bandwidth, 96 mini-arrays and the projected uv-density of NenuFAR. Right: The signal to noise at each wavenumber is demonstrated based on the data shown in the left panel of this figure. The predictions for the power spectrum are based on simulations of the 21-cm power spectrum from [17, 6, 8, 9].

information on the spatially varying star formation rate and Ly-α and X-ray radiative backgrounds. The effective mean-free path of Ly-α photons is 200-400 Mpc depending on redshift, and thus large-scale fluctuations imprinted in the HI signal via its coupling to the Ly-α background [18] are within the reach of NenuFAR. On the other hand, the mean-free path of X-ray photons, which heat the intergalactic medium at early times, depends on the details of their spectral energy distribution and can vary from 100 Mpc if the X-rays are soft to few Gpc in the case of hard X-rays. Measuring the level of fluctuations in the 21-cm signal at each observable wavenumber can constrain the effective mean-free path of X-rays, and thus their average energy. This information can further be used to pose constraints on the nature of heating sources. For instance, if the primordial gas was heated by X-ray binaries, the mean energy of X-ray photons is expected to be ~ 3 keV [10]. Finally, exotic mechanisms can also imprint large scale fluctuations in the 21-cm signal. In total, probing the large-scale end of the 21-cm power spectrum is very promising even with the projected resolution of NenuFAR in stand-alone mode, which tends to worsen at smaller scales (below 100 Mpc) at which the first ionizing bubbles are expected to be found.

Observational Challenges and Requirements:

The science-rich HI signal described above is very weak and hidden under thermal noise and foregrounds which are orders of magnitude stronger than the signal. The science discussed in the previous paragraphs can be done only if foreground removal, and ionospheric and RFI excision are done carefully enough, and astrophysical errors are mitigated to a sufficient level. Below we list the

essential criteria that are needed to lead to detection.

Integration time: Probing the global signal does not require a long integration time, and the necessary sensitivity for detection can be reached within a few days when looking for the signal from $z \sim 20$. The main difficulty in the global signal measurement resides in the calibration and noise and side-lobe mitigation, with detection becoming harder toward lower frequencies. Ideally, a properly made calibration would reduce all these errors to values below the expected signal level. Therefore, the calibration should be done with particular care.

As for the fluctuations in the redshifted HI signal, due to their extremely weak intensity, an integration time of 1000 hours or more is expected to be necessary in order to reach the detection threshold.

Sampling: One of the major sources of corruption of long wavelength radio-wave signals is caused by the Earth's ionosphere. Ionized gas causes both changes in phase and in amplitude of the radio-waves, which should be corrected for. Modulation of the signal by ionospheric distortions has periodicity of ~ 10 sec at these wavelengths; therefore the sampling time should be small enough to probe this periodicity. Since the sampling time is a trade-off between precision measurements and the amount of data needed to be stored and processed, a sampling time of order of 3 sec is recommended. At low frequencies the frequency resolution ought to be at least $\Delta\nu = 1$ kHz for sufficient RFI excision purposes. After a first lap of processing (done in semi-real time) the resolution can be reduced by an order of magnitude for further data analysis and storage.

Data rates: The data volume V collected during one night of observations is expected to be

$$V \approx 16 \left(\frac{B}{\Delta\nu}\right) \left(\frac{T_{int}}{\Delta t}\right) \left(\frac{N_{st}(N_{st}-1)}{2}\right) \times 10^{-12} \text{ [Tb]},$$

which accounts for both auto-correlations and cross-corrlations of N_{st} stations. Above, B and $\Delta\nu$ are the bandwidth and the frequency resolution in MHz respectively, T_{int} and Δt are the integration time and the temporal resolution given in hours. Assuming the number of stations to be $N_{st} = 20$ for the phase 1 of NenuFAR and $N_{st} = 96$ for the final configuration, and for $T_{int} = 12$ hours (one night of observations), $\Delta t = 3$ sec, $B = 75$ MHz and $\Delta\nu = 1$ kHz, the amount of data is expected to be few Tb in the first case and around 80 TB in the second (which can be reduced to few Tb after calibration). To handle this amount of data, one of the essential technical requirements is a fast correlator (e.g., Cobalt GPU correlator as used by the LOFAR team) and a fast processing cluster (also GPU based, as used by the LOFAR EoR KSP team).

Using noise loads: Experience with LOFAR has shown that long baselines can greatly assist calibration, modeling of the sky, ionospheric corrections, etc. Having some separate dipoles for calibration purposes, stationed far enough from NenuFAR (but not too far to ensure that they see the same ionospheric noise as the core of the instrument), might be necessary if ionosphere limits the total power experiments. However, one should note that NenuFAR is a rather compact (400 m) array over which ionospheric phases will be more coherent than over arrays of several km (e.g. the LOFAR core area).

Theoretical predictions: To better design the survey strategy and later on interpret the results, predicting the signal through theoretical, semi-analytical or numerical modelling is necessary. The signature of the integral signal as a function of redshift is rather straightforward and simple, thus theoretical models with few free parameters are a viable approach [14]. For power-spectrum measurement and imaging however, due to the complex non-linear physics involved, predictions are more reliably achieved with semi-analytic and numerical modelling. The signal measured by NenuFAR will have two very specific aspects: it will be at high redshift ($z > 16$) and on large scales only (> 100 comoving Mpc). At high redshift there is a good chance that the signal will be observed in absorption. During this early regime, along with the usual physics of ionization and heating of the IGM, three non-trivial processes influence in the local intensity of the signal, as was mentioned above: the Lyman-α flux sets the value of the spin temperature through non-saturated Wouthuysen-Field coupling (e.g. [2]), the Lyman-Werner flux regulates the formation of the first sources of light [1, 6], and the bulk drift velocity field between baryons and dark matter inhibits star formation in large patches of the intergalactic medium for a short period of time [16, 12, 17, 6, 8]. While the source formation regulation requires modelling on sub-kpc scales, the predicted 21-cm should cover a volume at least 2 comoving Gpc on a side to obtain any kind of sampling of the resolved scales. Semi-analytic simulations do cover those kinds of scales [15], while fully numerical simulations are currently limited to $500-600$ comoving Mpc [11, 19]. And of course, while an acceptable level of Lyman-α treatment is available, both semi-analytic and numerical approaches rely on sub-grid recipes to implement the sources formation regulation by Lyman-Wermer radiation and drift-velocities. Consequently we can identify three desirable developments in the modeling of the 21 cm in view of observations by NenuFAR:

1. Increase the volume of fully numerical simulation to > 2 comoving Gpc on a side, without sacrificing the resolution (too much), to check the preditions of semi-analytic models. This is doable considering that the simulations need not go further than $z = 16$.
2. Further investigate the regulation of the first source formation under the influence of an external Lyman-Werner irradation, and in the presence of drift velocities. Little has been done on those two aspects yet, and what has been done requires confirmation. This means small scale simulations where radiative transfer and dynamics are coupled.
3. Implement the lesson learned from the previous point in large scale semi-analytic and numerical simulations to achieve more robust predictions.

To summarize

In this section we have discussed the abilities of NenuFAR to observe the neutral hydrogen signal from Dark Ages, Cosmic Dawn and the first half of the Epoch of Reionization. NenuFAR has an excellent potential to be the first instrument to detect the global 21-cm signal and its power spectrum at $z > 16$ which covers the early phases of Reionization, the Cosmic Dawn and late phases of the Dark Ages. The science-rich HI signal is extremely weak and can be detected only if sufficient levels of calibration and noise mitigation are reached, the main requirements for which are listed above. Many issues related to data analysis and signal processing can only be understood and treated in the process of taking and cleaning data and cannot be anticipated. The experiences gained in observing at these low frequencies is unique and is essential to pave the road for future telescopes such as SKA.

References

[1] Ahn, K., Shapiro, P. R., Iliev, I. T., Mellema, G., Pen, U.-L., 2009, ApJ, 695, 1430

[2] Baek, S., Di Matteo, P., Semelin, B., Combes, F., Revaz, Y., 2009, A&A, 495, 389

[3] Bowman, J. D., Rogers, A. E. E., Hewitt, J.N., *ApJ*, 676 (2008) 1.

[4] Bowman, J. D., Rogers, A. E. E., *Nature*, 468 (2010) 796.

[5] Fialkov, A., Barkana, R., Tseliakhovich, D., Hirata, C. M., 2012, MNRAS, 424, 1335.

[6] Fialkov, A., Barkana, R., Visbal, E., Tseliakhovich, D., Hirata, C. M., MNRAS, 432 (2013) 2909.

[7] Furlanetto, S. R., Oh, S. P., Briggs, F. H., PhR, 433 (2006) 181; Pritchard, J. R., Loeb, A., RPP, 75 (2012) 6901.

[8] Fialkov, A., Barkana, R., Pinhas, A., Visbal, E., MNRAS, 437 (2014) 36.

[9] Fialkov, A., Barkana, R., Visbal. E., Nature, 506 (2014) 197;

[10] Fragos, T., et al., ApJ 764 (2013) 41.

[11] Iliev, I. T., Mellema, G., Ahn, K., Shapiro, P. R., Mao, Y., Pen, U.-L., 2014, MNRAS, 439, 725

[12] McQuinn, M., O'Leary, R. M., 2012, ApJ, 760, 4.

[13] Mellema, G., et al., ExA, 36 (2013) 235.

[14] Pritchard, J., Loeb, A., 2012, Rep. Prog. Phys. 75, 086901

[15] Santos, M. G., Silva, M. B., Pritchard, J. R., Cen, R., Cooray, A., 2011, A&A, 527, 93

[16] Tseliakhovich, D., Hirata, C., 2010, Phys Rev D, 82, 3520

[17] Visbal, E., Barkana, R., Fialkov, A., Tseliakhovich, D., Hirata, C. M., Nature, 487 (2012) 70.

[18] Wouthuysen, S. A., AJ, 57 (1952) 31; Field, G. B., *Proc. Institute Radio Energeers*, 46 (1958) 240.

[19] Zawada, K., Semelin, B., Vonlanthen, P., Baek, S., Revaz, Y., 2014, MNRAS,439, 1615

Radio follow-up of gravitational wave transient sources

Matteo Barsuglia, Marica Branchesi, Eric Chassande-Mottin,
Ismael Cognard, Chiara Ferrari, Susanna Vergani,
Antoine Petiteau, Michal Was, et al.

The gravitational-wave detectors LIGO and Virgo will soon resume observations in an advanced configuration leading to a ten-fold improvement of their sensitivity (i.e., an increase of the observable volume and hence in the number of accessible sources by a factor of 1000). The first science data are foreseen in 2015.

These detectors aim at observing the gravitational wave (GW) signature from cataclysmic astrophysical events such as merging binaries of compact objects (neutron star and/or black holes). The last minutes before the binary merges coincide ith the emission of an intense burst of GW. At design sensitivity, coalescing binaries of neutron star will be detectable up to 200 Mpc with advanced LIGO/Virgo. With this distance reach, tenth of such binary mergers can be expectedly detected per year. They are however large uncertainties on the rate of those events spanning almost three orders of magnitude.

Electromagnetic counterparts in all bands including radio are expected from GW transient sources. For instance, there are indications that short-hard gamma-ray bursts be associated with neutron star mergers. If this is true, the GW signal from such merger event may be followed by a radio afterglow as observed in the high frequency band (> 5 GHz) for GRB050724, GRB 051221A and GRB 130603B [Chandra & Frail, 2012]. Although the radio afterglow is expected to be dimmer at low frequency because of synchrotron self-absorption, it may still be observable with nenuFAR as detectable GW sources are relatively nearby.

Various scenarios predict the emission of an intense radio pulse promptly after the merger. Those include pulsar magnetosphere-like emission, as well as the excitation by GW of MHD modes with predicted radio fluxes that could reach several mJy to Jy in the low or intermediate frequency band [Moortgat & Kuijpers, 2004 ; Pshirkov & Postnov, 2010, Hansen and Lyutikov, 2001].

Another source of potential interest is superconducting cosmic strings. Cosmic strings are one-dimensional topological defects predicted in the grand unified theory and in the superstring theory. Oscillating superconducting strings act like antennas of cosmic size that emit electromagnetic radiation from radio to gamma-rays. This emission is enhanced at cups and kinks discontinuities, leading to intense (> Jy) short bursts in the radio band [Cai et al, 2012]. Bursts of GW are expected as well from the decay of cosmic string cusp and kinks [Aasi et al, 2014]. A joint GW radio coincident search may provide the tightest constraints on those objects.

LIGO and Virgo have recently initiated a collaborative program with the astronomy community for the follow-up of their candidate events. Alerts will be communicated to a network of partners that have signed a partnership agreement. The minute latency currently planned for the alert delivery is compatible with the delayed arrival of the radio transient due to dispersion (dozen of minutes). This allows to re-point the phased array to the source sky position before the arrival of the radio counterpart transient to Earth. GW alerts will include a position estimate for the source with a typical uncertainty of 100 square degrees. The coverage of such a large area is an issue for most wide-field optical telescopes. On the contrary, this is not a problem for the large field-of-view of phased dipole arrays. Thanks to the versatility offered by the optional switch to LOFAR, nenuFAR may be particularly well-suited in this context.

References

Chandra & Frail, 2012 *ApJ* 746:156
Moortgat & Kuijpers, 2004 *Phys. Rev.* D 70, 023001
Pshirkov & Postnov, 2010 *Astrophys. Space Sci.* 330:1, 13-18
Hansen and Lyutikov, 2001 MNRAS 322:4, 695-701.
Cai et al, 2012 *Phys. Rev.* D 86, 043521
Aasi et al, 2014 *Phys. Rev. Lett.* 112, 131101

Galaxy clusters and the large scale structures of the Universe

C. Ferrari[1], A. Bonafede[2], F. Vazza[2], G. Macario[1], C. Tasse[3]

Abstract – Low frequency observations are key to answer one of the open questions of extra-galactic astrophysics: the origin of diffuse radio emission from galaxy clusters. In this chapter, we will outline how the NenuFAR project can play a significant role in the study of non-thermal emission from the large-scale structures in the Universe.

1 – Introduction

Galaxy clusters are known to host a variety of diffuse and extended radio sources: tailed radio galaxies, whose shape is modeled by the interaction with the intra-cluster medium (ICM; e.g. Feretti & Venturi 2002); radio bubbles, filling holes in the ICM distribution and rising buoyantly through the thermal gas (e.g. de Gasperin et al. 2012); diffuse giant radio sources, (so called "halos" and "relics") revealing the presence of relativistic electrons and magnetic fields in the intra-cluster volume (e.g. Ferrari et al. 2008). It is currently debated how relativistic electrons can be accelerated over huge volumes (up to several Mpc-scales) and how the non-thermal components, that we observe at radio wavelengths, affect the physics and evolution of galaxy clusters (e.g. Vazza et al. 2012).

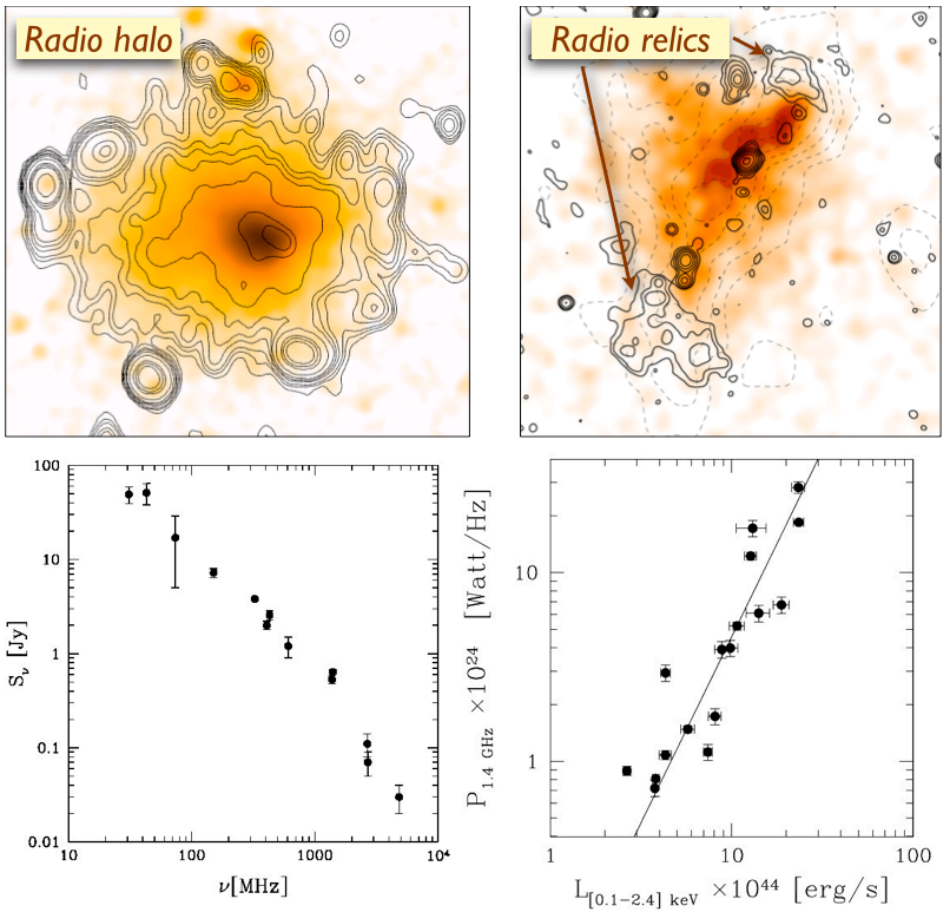

[1] Laboratoire Lagrange, UMR7293, Université de Nice Sophia-Antipolis, CNRS, Observatoire de la Côte d'Azur, 06300, Nice, France
[2] Hamburger Sternwarte, Universität Hamburg, Gojenbergsweg 112, D-21029 Hamburg, Germany
[3] GEPI, Observatoire de Paris, Meudon, France

Figure 1 Top: examples of diffuse radio sources in galaxy clusters (radio contours overlaid on X-ray images of the clusters). Bottom: radio spectrum of the halo in the Coma cluster (left) and 1.4 GHz vs. X-ray luminosity of clusters know to host diffuse radio halos (right) – [Extracted from Ferrari 2011 – see references therein]

Diffuse intracluster radio sources (called "halos" or "relics", depending on their observational properties) are generally characterized by steep synchrotron spectra (see bottom left panel of Fig. 1). This, together with their low-surface brightness and the possible spectral steepening at high radio frequencies due to electron ageing, makes them more easily detectable at long wavelengths. LOFAR and NenuFAR are opening the low-frequency part of the e.m. spectrum to high sensitivity and/or resolution observations, being therefore key instruments for the detection and study of diffuse radio emission from galaxy clusters. We expect in particular to have an enhanced statistics in the number of clusters known to host a non-thermal component (Cassano et al. 2010), the number of known "radio-loud clusters" being currently very limited (bottom right panel of Fig. 1).

2 – Radio emission from galaxy clusters : NenuFAR and the ILT

The LOFAR telescope is already showing its potential for the study of diffuse intracluster radio emission. The 58 MHz LOFAR image of the cluster MACSJ0717 reveals, for instance, a more extended diffuse radio source compared to the higher-frequency (610 MHz) GMRT map (see Fig. 2). Note however that the nature of this additional - very low-surface brightness - radio emission spotted by LOFAR needs to be confirmed. The first issue to control is related to potential ionospheric errors.

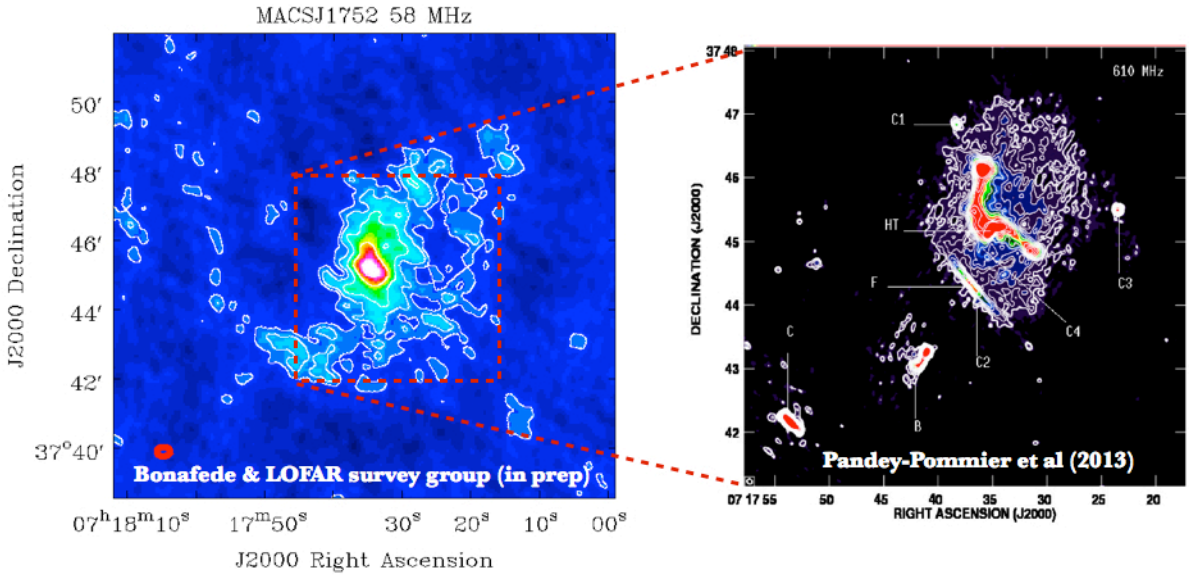

Figure 2: The cluster MACSJ0717+3745. Left: Preliminary LOFAR LBA image at 58 MHz, 6 MHz bandwidth (Bonafede and the LOFAR survey, in prep). The rms noise is 10 mJy/beam, the beam is 23"x16". Contours are drawn at (3,6,12) times the rms noise. The region within the dashed box corresponds to the size of the right panel. Right: recent image of the cluster obtained at 610 MHz by Pandey-Pommier et al (2013).

The ionosphere, whose electron content is varying on timescales of few seconds or below, adds a time, direction and position dependent varying phase to the geometric delays (see e.g Intema et al. 2009). Because of these effects, sources may appear to have shifted position or to be "blurred". The weakest sources could not be detected because of their shifted position from time to time, even if their surface brightness is above three or five times the rms noise in the radio mage. Ionospheric corrections depend on time, frequency, viewing direction, antenna location, and require accurate

calibrations. In particular, in order to track the ionospheric behavior with high precision, it is fundamental to have good sensitivity on the longest baselines, which provide the maximum resolution. The longest baseline of LOFAR is now the one formed by the French station in Nancay and the Swedish station in Onsala. It is about 1000 km long, and provides a sub-arcsecond resolution in the LOFAR HBA frequency range.
The addition of the French LOFAR Super Station (LSS) to the International LOFAR Telescopes (ILT) will provide a long $19^{1/2}$ more sensitive baseline and access to ~10 times more calibrators. These calibrators are fundamental to obtain a time and frequency dependent ionospheric screen. NenuFAR will therefore play a first important role for the study of weak and diffuse sources, since sensitive imaging at high-resolution is essential for a proper ionospheric fitting.

The fact of adding to the ILT a higher sensitivity short baseline (2x sensitive than the LOFAR core) will allow, in addition, the possibility of imaging large-scales (degrees) with a few arcsec resolution. Short baselines are crucial for the detection of large-scale radio emission from clusters, in particular for those at low-redshift ($z<0.1$). For instance, the radio halo and relic of the Coma cluster (very well imaged by LOFAR, together with a possible bridge of radio emission between them, Fig. 3) are filtered out by interferometers such as the VLA and the GMRT, due to a lack of very short baselines. On the other side, the excellent resolution provided by very sensitive long baselines of ILT+LSS is required not only for a good ionospheric calibration (see above), but also:

a) to have the capability to separately identify and study compact and diffuse radio sources that usually coexist in cluster fields (see e.g. Fig. 3),

b) to detect small-scale brightness variation of large scale synchrotron radio emission, that will identify the details of the physical mechanisms responsible for cosmic ray acceleration in clusters.

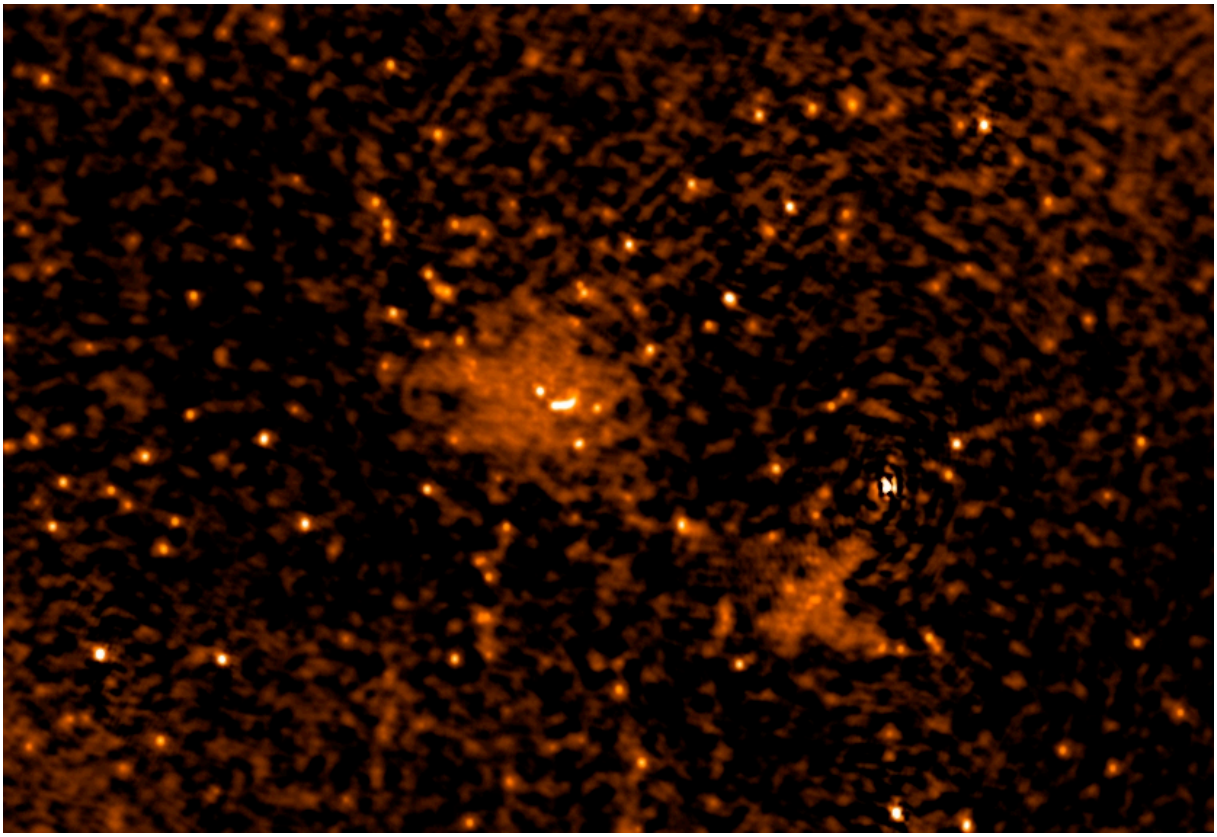

Figure 3: LOFAR HBA observations of the Coma galaxy clusters. The image is obtained using 6 MHz bandwidth centered of 137 MHz. The noise is 5 mJy/beam. The restoring beam is 2s"x30". The largest linear size of the radio halo, at the centre of the image, is about 1 degree (Bonafede and the LOFAR survey team, in prep).

3 – Radio emission from intra-cluster filaments : NenuFAR in standalone mode

The large-scale structure in the Universe is organized in a complex network of filaments connecting virialized structures and separated by voids. Their analysis can give important inputs to cosmological studies. The observational detection of the warm intergalactic medium associated to filaments is still challenging and only a few works claimed a detection of it through X-ray observations or - more recently - the Sunyaev'-Zeldovich effect (see e.g. Planck collaboration 2013, and references therein). We note, however, that these candidates still fall within the virial radii of the nearby galaxy clusters.
If filaments are magnetized, we can expect to detect the synchrotron emission related to accretion-shock accelerated particles along intergalactic filaments, well outside the cluster virial radii. This would be the first detection of the diffuse warm-hot gas component of the cosmic web.

We are currently studying the possibility to detect intra-cluster filaments at radio wavelengths with LOFAR (Vazza et al., in prep.). If the lack of arcsec/arcmin resolution of NenuFAR in standalone mode cannot allow detailed studies of diffuse emission in galaxy clusters (due to the impossibility to separate radio emission coming from the ICM or from compact sources), the French LSS could be the ideal instrument for a rapid low-resolution all-sky survey looking for candidates of intracluster filaments, extremely challenging to be detected in any other band of the e.m. spectrum. Further higher resolution ILT follow-up could then be programmed to study these candidates in detail.

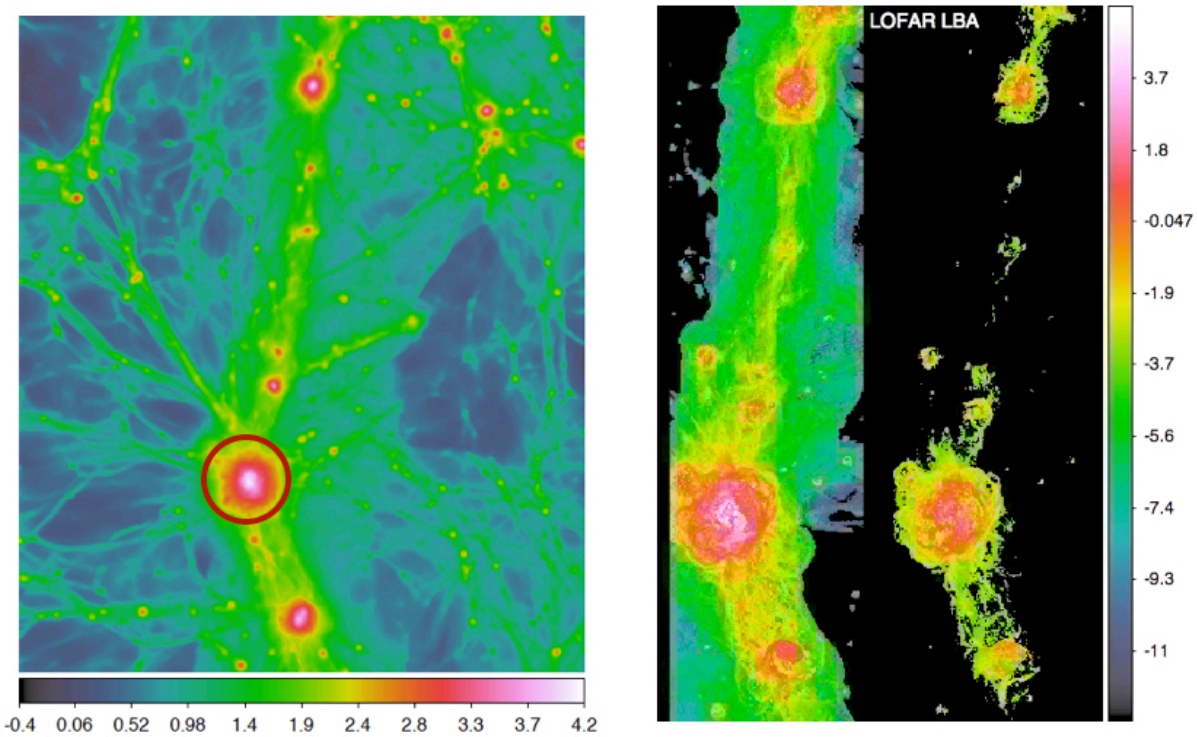

Figure 4 Left: Radio emission from intergalactic filaments, assuming a magnetic field whose energy is a few precent of the thermal one (Vazza et al in prep.). The red circle marks the approximate region within one virial radius of the most massive galaxy cluster along the filament. Right: on the left, the radio emission from the filament shown in the left panel is displayed. On the right, the expectation for LOFAR LBA detections is shown. The color scale is in logarithmic units of surface brightness (Jy/arcsec^2).

Note that the great advantage of having the full NenuFAR is the possibility to have a double core for the ILT. In such a way, extra-galactic studies (requiring both high sensitivity and high resolution, and thus the use of both core and the international stations) could be performed simultaneously to EoR observations, which require only the Dutch stations. To optimize the total uv-coverage, we would recommend to use the Dutch SuperTerp as core for the ILT and the NenuFAR station in standalone mode.

References

- R. Cassano et al., A&A 509, 68 (2010)
- L. Feretti and T. Venturi, Merging Processes in Galaxy Clusters. Edited by L. Feretti, I.M. Gioia, G. Giovannini. Astrophysics and Space Science Library, Vol. 272. Kluwer Academic Publishers, Dordrecht, 2002, p. 163-195 (2002)
- C. Ferrari et al., SSRv 134, 93 (2008)
- C. Ferrari, SF2A-2011: Proceedings of the Annual meeting of the French Society of Astronomy and Astrophysics Eds.: G. Alecian, K. Belkacem, R. Samadi and D. Valls-Gabaud, pp.111-114 (2011)
- F. de Gasperin et al., A&A 547, 56 (2012)
- H. T. Intema, A&A 501, 1185 (2009)
- M. Pandey-Pommier et al., A&A 557, 117 (2013)
- Planck collaboration, A&A 550, 134 (2013)
- F. Vazza et al., MNRAS 421, 1868 (2012)

Extragalactic projects with NENUFAR

F. Combes, C. Ferrari, M. Pandey-Pommier, P. Salomé, C. Tasse

Abstract : There are two main directions which are interesting to explore at very low frequencies at extragalactic scales : first at z=0 extend at low frequency the study of radio jets, lobes and other features to understand their time evolution, and second explore the radio jets and structures at high redshift (z=6-9, where the frequency is low-shifted by a factor 7-10), to compare with their local analogs at the same rest-frequency. Recent observations of jets or radio relics serve as examples to estimate the required sensitivity with NenuFAR.

1-Radio jets at low frequency

Radio lobes have different morphologies at low frequency. Since low-energy electrons are longer-lived, there can trace old extent of the previous jets. The goal is to investigate the history of the jets and AGN feedback.

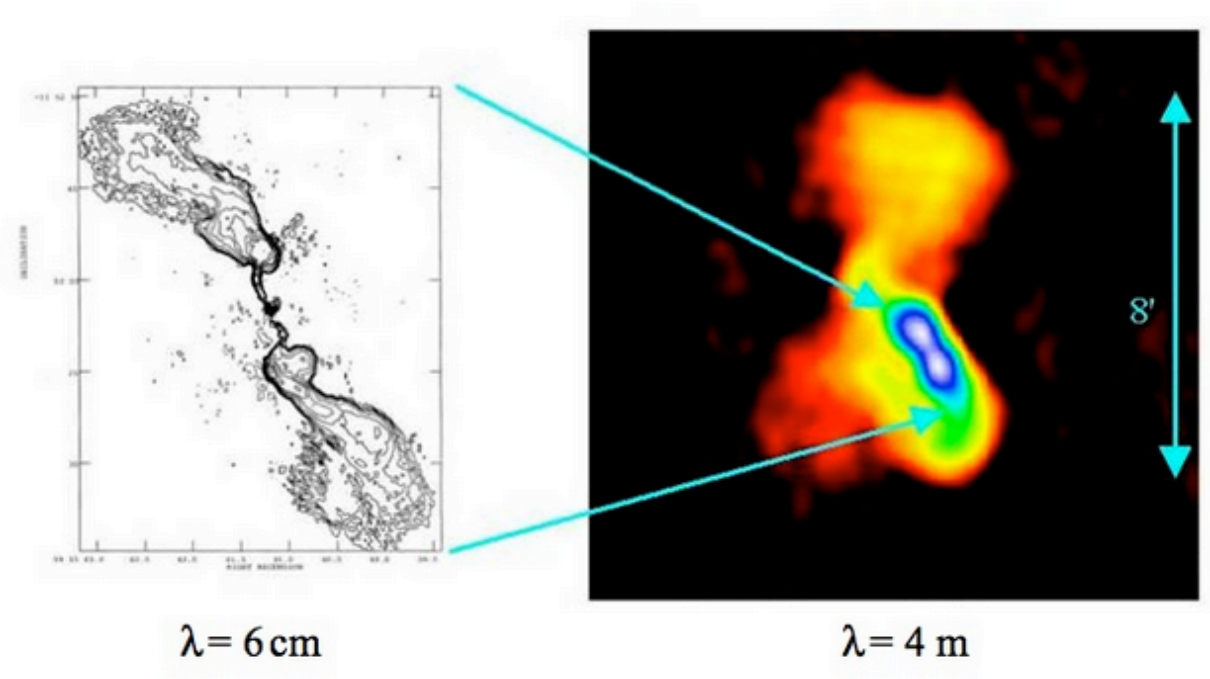

Figure 1 Hydra-A, at 74MHz (λ=4m), compared to at 5GHz (λ=6cm), from Lane et al. (2004). The observations have been done with the VLA, with 20'' resolution. At low frequency, the source appears much more complex and extended, over about 8' (530 kpc) in a north-south direction. The spectral slope is steeper in the South, where the source appears more confined. Aging of relativistic jets with time steepens their spectral slope.

One spectacular example is given in Figure 1, with Hydra A (the brightest galaxy at the center of its cluster). The shape and well-defined border of the northern lobe suggest that it is just filling a bubble in the X-ray gas (Simionescu et al. 2009), as are the buoyant structures in Perseus A (e.g. Salome et al. 2006).

Another well studied example is M87. Its LOFAR-HBA image at 140MHz, has been compared with many wavelengths by De Gasperin et al (2012). But no extension at low frequency could be found. The global age of the halo is 40 Myr, and the spectral index map does not reveal any aging.
FRII such as Cygnus A show different morphologies. They have hot spots, re-accelerating particles, and this is revealed in the spectral index map.

2-Radio-loud high-z quasars

There is a new phenomenon affecting the high redshift radio-loud quasars, which favors the use of very low frequency radio-telescopes: this is the surprising deficit in the radio detection of the high-z quasars in the Sloan survey. Out of the 106 000 quasars in the Shen et al (2011) catalog (SDSS-DR7), only 4 have been detected in radio at z>5. Already above z~3, there is a deficit of radio-jets or radio-lobes. This deficit contrasts with all the blazars detected optically or in X-rays.
This deficit is thought to be due to the interaction of the CMB with the emitting electrons. Indeed, the CMB energy is increasing as $(1+z)^4$ and can then exceeds the magnetic energy in the radio lobes of high-z AGN. Electrons then cool by scattering off CMB photons (inverse Compton emission), and not by synchrotron emission. This affects more the radio lobes, and not the relativistic jets in the center, where the magnetic energy remains much higher.

When the radio-lobe emission is modeled, two components can be separated, as seen in Figure 2. The two bumps, synchrotron and inverse Compton emission are seen at low and high frequency respectively. Simulations show how the change of the intensity of the magnetic field B from 10μG to 30μG can change the relative intensity of synchrotron and inverse Compton bumps (Ghisellini et al 2014). Radio knots concentrating B would also be easier to see in synchrotron, and will be less affected at high-z.

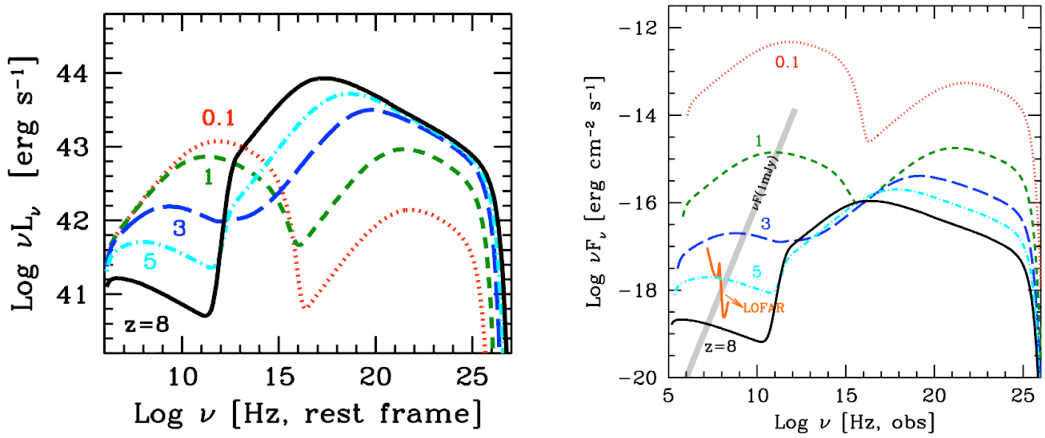

Figure 2 Modelisation of the spectral distribution of radio lobes (100kpc in size), in the rest-frame (left, luminosities) and the observer frame (right, fluxes), for different redshifts between z=0 and 8, from Ghisellini et al. (2014). The electrons are injected with a power-law distribution of slope 2.3, and the magnetic field id 10μG. In the right panel, are indicated the limit of F(ν) = 1mJy (sensitivity of FIRST at 14.4GHz), and in orange the LOFAR sensitivity.

This CMB interaction concerns only the high frequency, and therefore is a huge advantage for LOFAR and NenuFAR for radio sources at high z

3-Radio relics in merging clusters

Radio relics are emission features due to shocks triggered by cluster-cluster collision.
The magnetic field can be boosted (compressed) in the merger. These shocks can have 1 Mpc sizes (or more, see Figure 3), and they are in general in the outer parts, sometimes symmetrically located.

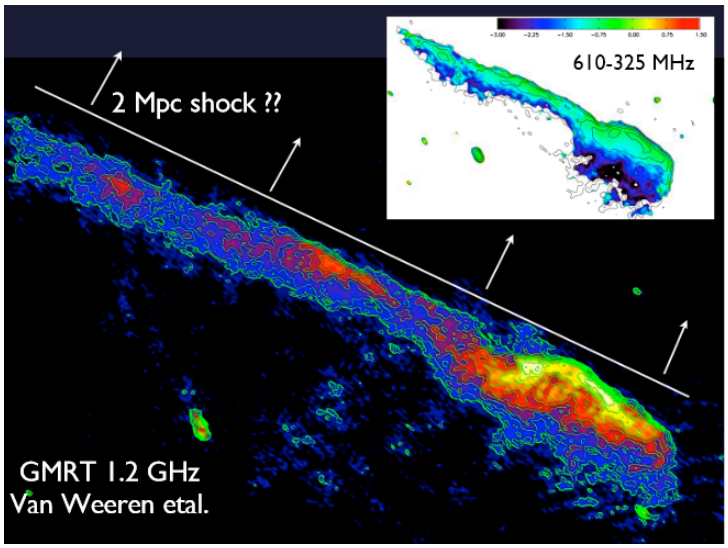

Figure 3 Observation of the tooth brush, a radio relic from Van Weeren et al. (2010). The insert shows the spectra index map, suggesting aging in the leading part of the shock, at low frequency.

The emission in the shocks is highly polarized. Certainly many more radio relics could be studied, in the karge number of low-z clusters discovered with Planck-SZ.
Some if these have been followed up with XMM, they are unrelaxed clusters, with radio halos.
The flux of detected relics lies between 5-10Jy, at z=0. The sensitivity of NenuFAR +LOFAR will allow to detect them until z=1 easily, according to the table below.

Table 1 Full NenuFAR: 96 mini-arrays of 19 antennas, First phase of NenuFAR= Nen-1= 1/4th of capabilities, i.e. 24 mini-arrays of 19 antennas

	Nen-1	NenuFAR	+ LOFAR
Spatial Resol	5°	1.5°	2''
Sensitivity (8h)	120-240mJy	50-100mJy	35-70mJy

References

De Gasperin F., Orrú, E., Murgia, M. et al. 2012, A&A 547, A56
Ghisellini G., Celotti, A., Tavecchio, F., Haardt, F., Sbarrato, T. 2014 MNRAS 438, 2694
Lane, W. M., Clarke, T. E., Taylor, G. B., Perley, R. A., Kassim, N. E. 2004 AJ 127, 48
Shen, Yue, Richards, Gordon T., Strauss, Michael A. et al. 2011 ApJS 194, 45
Salomé, P., Combes, F., Edge, A. C. et al. 2006 A&A 454, 437
Simionescu, A., Werner, N., Böhringer, H. et al. 2009 A&A 493, 409
Van Weeren, R. J., Röttgering, H. J. A., Brüggen, M., Hoeft, M. 2010 Science 330, 347

Extragalactic objects as Cosmological tools to study structure formation in LOFAR and SKA era

M. Pandey-Pommier[1], F. Combes[2], K. Ferrière[3], B. Guiderdoni[1]
(1-CRAL-l'Observatoire de Lyon, 2-LERMA-l'Observatoire de Paris, 3- IRAP, Toulouse)

Abstract – The non-thermal emission from extragalactic objects (like radio galaxies and clusters of galaxies) dominate the low frequency sky. Observations at meter-wavelength range serve as an important tool to study: the life cycle of radio galaxies (from youngest compact objects to giant radio galaxies with *relic* emission at their decay phase, the origin of non-thermal diffuse emission in the form of *relic, mini-halos* and *halos* from galaxy clusters. This chapter will highlight the capability of NenuFAR project to probe the extragalactic sky over a wide range of observing frequencies and demonstrate the significant role it can play in the study of extragalactic objects as well as cosmic magnetism.

1 – Introduction

The extragalactic sky is known to host a variety of compact and extended radio sources such as galaxies and clusters of galaxies, that play a key role in the study of galaxy evolution and in return large scale structure formation in the Universe. These studies help us to derive link between the evolving radio-loud Active Galactic Nuclei (AGNs, blazars, galaxies etc.) luminosity function and the evolution of galaxies, clusters and groups. However, the study of the radio-loud AGN evolution is non-trivial, as it involves longer timescales and needs statistically significant samples of radio galaxies at various stages of their life cycle (from the youngest compact sources (emission from core region like Compact Steep Spectrum (CSS) or Giga-Hertz Peak Spectrum (GPS)) to giant (Mpc-scale FRI and FRII galaxies with core-lobe morphology and high polarization) and fading (dying with extended relic emission), through to those with restarted activity). While the compact CSS/GPS and central core sources show inverted or flat spectra at MHz range, the emission from giant lobes and relic regions are brighter at MHz range (Alexander et al. 2000; Sirothia et al. 2013).

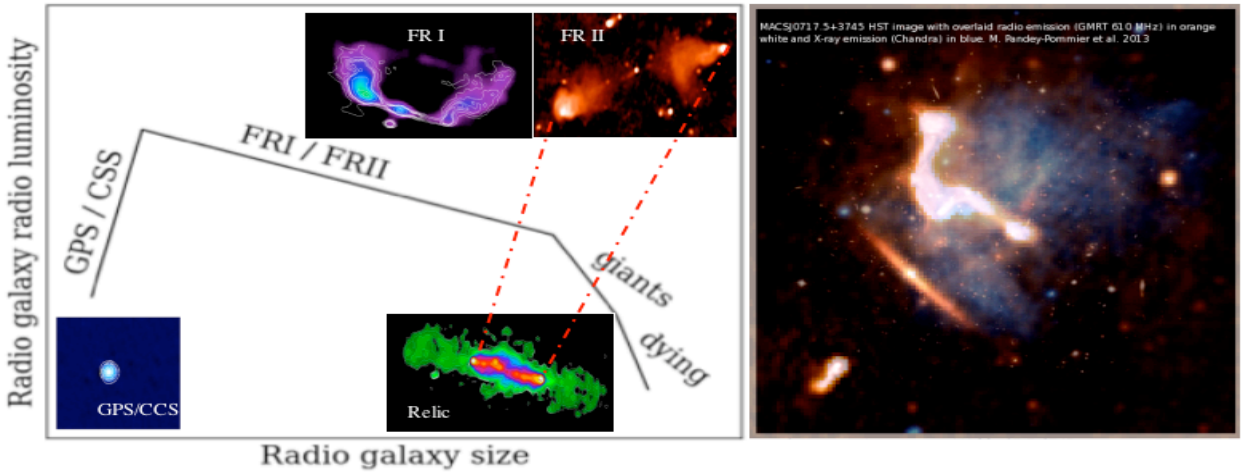

Figure 1. (*Panel I*) A schematic view of different stages (few kpc to Mpc-scale) of a radio galaxy life cycle. (*Panel II*) Galaxies in clusters with central Mpc-scale halo emission from GMRT (orange, refer observation parameters listed in table 1) overlaid on Chandra X-ray emission (blue) and HST optical emission (black-white) extracted from Pandey-Pommier et al. 2013.

Further, the ensemble of galaxies lying in over-dense Intra Cluster Medium (ICM), under the high gravitational pull, binds together to form clusters of galaxies. These clusters of galaxies are very luminous in X-rays and rich in optical properties. At radio wavelengths, in the presence of cosmic magnetic fields, galaxy clusters show diffuse non-thermal Mpc-scale emission (centrally placed non-polarized- *halos,*

mini-halos and peripheral highly polarized- *relics*) mapping the ICM, with very steep spectra that dominate at MHz-range (Cassano et al. 2014, Ferreti et al. 2012).

As these extragalactic diffuse sources are characterized by non-thermal emission with flat (core) or steep spectrum (diffuse extended lobes, halos, relics) that significantly emit at lower frequencies, hence deep images over wide frequency range with high sensitivity and resolution are highly desirable for their detection. As these non-thermal emission are highly polarised (synchrotron emission produced by relativistic electrons gyrating about magnetic field lines and Faraday rotation suffered by radio waves propagating through a magnetized plasma), they serve as best tools to study the evolution of cosmic magnetic field in the Universe. In fact, most of our present observational knowledge of cosmic magnetic fields comes from radio observations of synchrotron emission as well as Faraday rotation mesurements. Even the intercluster space could be threaded by a yet undetected magnetic field.

Critically, the wide frequency coverage along with high sensitivity and polarisation data offered from NenuFAR and cross identification from multi-wavelength data, will permit analysis of morphological, polarization and statistical radio properties in these extragalactic sources further revealing insights into the physical processes driving the evolution of these populations. These studies will also address the important problem of how relativistic electrons, in the presence of cosmic magnetic fields, give rise to non-thermal synchrotron emission, that can be accelerated over several Mpc-scales in extragalactic sources and increase their number counts at MHz range from few 10s known as of now to 1000s as expected via simulations (Cassano et al. 2014, Massaro et al. 2013). We also plan to conduct the study of polarization properties of the lobes and relics in these objects in order to study the evolution of magnetic field during large-scale structure formation over cosmic time scale as well as the interaction of jets/relics with the Intra Galactic Medium (IGM)

2- Non-thermal emission from galaxies and clusters using NenuFAR and LOFAR

As discussed in previous section, the non-thermal emission in radio galaxies and clusters dominate at lower frequencies and has low surface brightness, hence instrument with high sensitivity, resolution, polarization measurment and wide frequency coverage is needed to study the emission process in these objects. The LOFAR telescope is best suited for observations of such objects. Table 1 lists the system parameters of instruments proposed to be used for our survey.

Table 1: System parameters

Instrument	Frequency	Resolution	Sensitivity (mJy/beam) (8hrs observation)
NenuFAR-1	15-80MHz	3°	120-240
NenuFAR	15-80MHz	1.5°	50-100
LOFAR+NenuFAR	30-80MHz	2”	35-70
MSSS LBA	30-80MHz	1.7°	15
MSSS HBA	120-160MHz	2°	5
LOFAR LBA	30-80MHz	30”	18
GMRT	1400MHz	2”	0.03
GMRT	150MHz	20”	0.7
SKA Low	120MHz	10”	0.02
SKA Mid	1400MHz	15”	0.005
MWA	80-300MHz	3’	9

Towards the above discussed 2 science objectives (galaxies and clusters), we are already carrying out a GMRT survey on galaxy clusters and AGNs and have high resolution and frequency data available at the beginning of our project to compare with future data that will be available via NenuFAR project. We are also a part of LOFAR Magnetism and Continuum survey KSP groups and have access to polarization data available on these objects.

NenuFAR Standalone mode:

In recent years, the MSSS (Multi Source Sky Survey, roughly 1.5hrs on LBA fields and 14mins on HBA fields) and observations at low frequency band array (LBA) with LOFAR telescope has already given important results in the domain of large scale structure formation via discovery of diffuse Mpc-scale jet structure in giant radio galaxy UGC 9555 and detection of diffuse radio halo in Abell 2256 clusters of galaxies (Heald et al. 2013, van Weeren et al. 2012). These results being obtained with the LOFAR MSSS survey at roughly similar resolution to NenuFAR-1 and NenuFAR complete array (however 10 to 50 times better sensitivity) suggests that it will be possible to discover extended diffuse emission in such extragalactic objects by increasing observation time (data stacking).

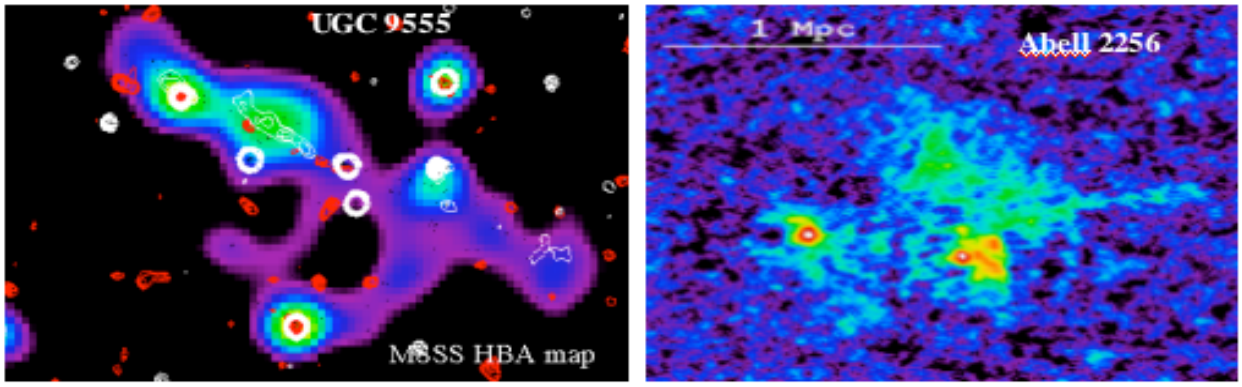

Figure 2. (*Panel 1*) Giant radio galaxy UGC 9555 discovered in MSSS data. (*Panel 2*) Abell 2256 halo emission imaged in LOFAR LBA and MSSS data (extracted from Pandey-Pommier et al. 2014, Heald et al. 2013, van Weeren et al. 2012)

Additionally, it is equally possible to study the MHz range emission from the selected bright compact AGNs (with flux density > rms noise of NenuFAR) and derive their spectral information (flat, steep) via wide frequency coverage offered with NenuFAR (NenuFAR-1) in standalone mode. This information when coupled with multi-frequency data (radio data at GHz-range, X-ray, Gamma-ray, optical) will allow us to identify their redshift and derive the correlation between radio power at MHz-range and high energy luminosity over cosmic time scale, showing its potential for the study of radio emission from compact AGNs and their evolution (Massaro et al. 2013).

NenuFAR+LOFAR:

1-Wide Frequency (MHz-GHz range) spectral study of compact AGNs and extended diffuse emission in galaxy and clusters- With combined LOFAR and NenuFAR array (LOFAR Super Station (LSS)), it will be possible to achieve arcsec scale resolution at MHz-range comparable to GMRT at 1.4 GHz, at better sensitivity compared to NenuFAR standalone array (and poorer sensitivity compared to GMRT data at 1.4 GHz)(refer Table 1). Thus, it will be possible to include fainter AGNs in the survey (by including AGNs with flux density > rms noise of NenuFAR+LOFAR) and provide better constraints to the correlation between radio power at MHz-range and high energy luminosity. The NenuFAR data at arcsec scale resolution will not only help us to identify the source morphology and detect more diffuse emission in clusters of galaxies (due twice more sensitive short baselines than LOFAR core as well as the

steep spectral nature of these sources), but will also provide multi-frequency spectral information to compare with the GMRT data at 1.4 GHz.

NenuFAR+LSS will also give access to short baselines, between the station-to-station baselines of LOFAR and the antenna-to-antenna baselines of a LOFAR station, which are needed to image large-scale structures in the synchrotron sky, both in total intensity and, if the absolute ionospheric Faraday rotation can be reliably calibrated, in polarized intensity. Such large-scale imaging observations will prove particularly valuable to study the large-scale interstellar magnetic field of our Galaxy. NenuFAR+LSS will also provide high-sensitivity long baselines, which will make it possible to reach high enough angular resolution to avoid beam depolarization and hence actually measure polarization. Such high-resolution polarization measurements will enable us to image and study magnetic fields not only in extragalactic sources but also in small-scale interstellar magnetic fields within our Galaxy, through Faraday rotation measures (again, under the condition that the absolute ionospheric Faraday rotation is reliably calibrated). Additionally, NenuFAR+LSS will be also able to accurately measure the dispersion measures and rotation measures of nearby pulsars, thereby placing new constraints on the structure of the interstellar magnetic field in the local ISM (see more details in the section on "NenuFAR pulsar science").

2- Search for Low Frequency Sky calibrators: Further, the high sensitivity data offered by French LOFAR Super Station (LSS) at long baseline (1000 km, sub arcsec scale resolution) will be very useful for differentiating the compact and extended sources, thus helping to carry out a search for low frequency sky calibrators. A compact calibrator sources is used to apply phase calibration to target sources during imaging, in order to correct for phase-changes due to ionospheric effects. As of now, the VLA catalog of phase calibrators at low frequency offers a limited choice. To identify such low frequency sky calibrators, a high sensitivity data with sub arcsec scale resolution is required, LSS data combined with LOFAR array offers important dataset to carry out the search and build a catalog for Phase calibrators in the low frequency sky.

Reference:

1- Alexander, P., *Evolutionary models for radio sources from compact sources to classical doubles*. *MNRAS* **319**, 8–16 (2000).
2- Cassano, R., Bernardi, G., Brunetti, G.,…Norris, R., Pandey-Pommier, M., Rottgering, H., et al. AASKA14, 'Advancing Astrophysics with the SKA' PoS, Sicily, 2014
3- Feretti, L., Giovannini, G., Govoni, F., & Murgia,M. 2012, A&A Rev.„ 20, 54
4- Heald, G. et al. 2013 , http://www.astronomy.com/news/2013/03/astronomers-discover-new-giant-galaxy-in-all-sky-survey-with-lofar-telescope
5- Massaro, F., D'Abrusco, R., Giroletti, M., Paggi, A.; Masetti, N.; et al. 2013, ApJS, 207, 4
6- Pandey-Pommier, M., et al., A&A 557, 117 (2013)
7-Pandey-Pommier, M., et al., presentation 'Giant Radio Galaxies' in LOFAR Science Week 2014, Amsterdam
8- Sirothia, S., Krishna, G., et al. 2013ApJ...765L..11S
9- van Weeren, R. J.; Röttgering, H. J. A.;…Pandey-Pommier et al. 2012, A&A...543A..43V

Nearby galaxies with NenuFAR

Albert Bosma (Laboratoire d'Astrophysique de Marseille)
Matt Lehnert (IAP) & Wim van Driel (GEPI, Observatoire de Paris}}

To study nearby galaxies, a first requirement is to have enough angular resolution and sensitivity to image individual galaxies adequately. For a single LOFAR station within the confines of the Nançay station, the angular resolution at LOFAR frequencies remains too low to resolve galaxies. Hence, the use of NenuFAR for nearby galaxies will be in the general contribution the LOFAR array can make, once there is a second core in addition to the initial core of LOFAR in Exloo.

The main radio continuum emission mechanisms in galaxies at radio frequencies is described in Figure 1a (cf. Condon 1992). At LOFAR frequencies, the dominant mechanism is synchrotron radiation. For spiral galaxies seen edge-on, free-free absorption can be important, and an early study by Israel & Mahoney (1990) at 57.5 MHz claims to have detected this, though the quality of their data is not optimum. With LOFAR, a statistical study of this effect can be easily undertaken.

The deepest images at radio frequencies so far is the work by Braun et al. (2007) using the Westerbork telescope with very broadbands at 18 and 22 cm. Their results show interesting faint emission around several galaxies, the origin of which is unclear. Heesen et al. (2014) analyse these data further, and try to relate the star formation rate derived from radiocontinuum data with that from other determinations in the infrared and at Hα.

For the LOFAR cosmic magnetism key programme (PI R. Beck), several preliminary results are already circulating, but only recently the first map of a nearby galaxy has been published (Mulcahy et al. 2014). The data look promising, and it can be expected that as LOFAR continues to operate, major results will become available. One of us (WvD) is working in collaboration with other members of the surveys key programme on data on the nearby galaxy M82. All these observations need high sensitivity at the required spatial resolution. Thus the addition of NenuFAR station to LOFAR will greatly enhance the capabilities to do this research.

To sum up, the impact on galaxy evolution of NenuFAR/LOFAR data will be:

i) an assessment of the importance of free-free absorption in spiral galaxies at low frequencies,
ii) finding interesting galaxies where the faint outer emission may indicate that 'something happened' to a galaxy,
iii) a statistical study of radio continuum emission as an indicator of star formation in spiral galaxies, and
iv) after much effort, the structure of the magnetic field can be assessed from polarization studies.

References

Israel, F.P. & Mahoney, M.J. 1990, ApJ, 352, 30

Condon, J.J. 1992, Ann. Rev A&A, 30, 575

Braun, R., Oosterloo, T.A., Morganti, R., Klein, U., Beck, R. 2007, A&A, 461, 455

Heesen, V., Brinks, E., Leroy, A.K., Heald, G., Braun, R., Bigiel, F. Beck, R. 2014, AJ, 147, id 103 - 49 pp.

Mulcahy, D.D., Horneffer, A., Beck, R. et al. 2014, A&A, 568, A74 - 18 pp.

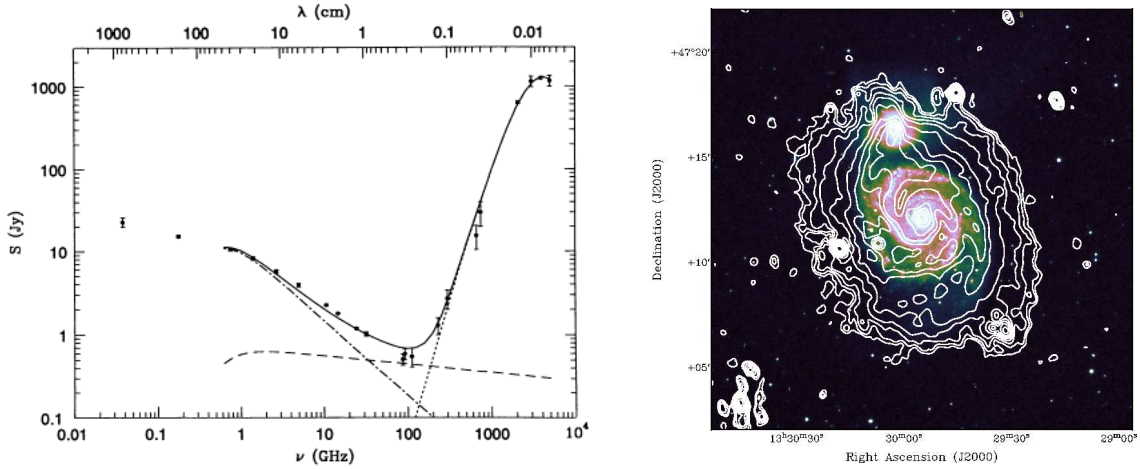

Figure 1: *Left*: The radio spectrum of M82 (Condon 1992) and most other spiral galaxies is the sum of contributions from steep-spectrum synchrotron radiation (dot-dash line), free-free emission (dashed line), and thermal radiation from dust (dotted line). Free-free absorption flattens the overall spectrum at low frequencies. *Right*: M51 at a central frequency of 151 MHz with a bandwidth of 47.7 MHz overlayed onto an optical DSS image using a cubehelix colour scheme. The resolution is 20 arcsec and a robust weighting of -0.5 was used. The extended disk is seen clearly. The contours start at 1 mJy/beam and increase by a factor 1.5.

NenuFAR pulsar science

J.-M. Griessmeier, I. Cognard, V. Kondratiev, G. Theureau, L. Guillemot,
J. W. T. Hessels, M. Serylak, B. W. Stappers

Abstract

Several pulsar applications have been identified which would greatly benefit from this instrument, including surveys and low-frequency observations. In particular, the instrument seems particularly well suited for the combination of both: Low-frequency pulsar survey observations (20-40 MHz), where NenuFAR has both a much larger field of view than UTR-2 and a higher sensitivity than LOFAR.

Introduction

The death of a massive star, through the so-called supernova explosion, leads to the formation of a condensed core almost only made of neutrons. Pulsars are magnetized neutrons stars producing beams of radio waves aligned with the magnetic axis and sweeping across the sky as the star rotates, as a lighthouse. Young pulsars are characterized by a period of 0.1-1 seconds, while older ones can be spun up during a mass transfer from a companion star, ending up with lower magnetic fields and very small rotational periods of the order of a few milliseconds. The main impact of the ionized interstellar medium is the dispersion of the radio waves proportional to the integrated electronic content: the Dispersion Measure (DM). Given the very small angular size of pulsars, low-frequency observations provide a unique probe of the distribution of the ionized interstellar medium via the strong scattering regime of the scintillation, a dominant phenomenon at low radio frequencies. With their steep power-law spectra, new pulsars are expected to be found in specific low-frequency searches along with other kinds of transient sources, such as the Rotating Radio Transients (RRATs), sporadically-emitting pulsars (McLaughlin, et al., Nature 439, 817, 2006), or Fast Radio Bursts (FRBs) described in this document by Corbel et al.

Surveys

Pulsars surveys

Finding new pulsars is important to put constrains on stellar evolution models. Some known pulsars also exhibit very peculiar emission characteristics, such as extreme nulling (a lot of missing pulses) or intermittency (oscillating between an ON and an OFF state over weeks-months timescales) for example. A survey with a large instantaneous field of view provides an efficient way to discover many more of those pulsars inherently difficult to find. Enlarging the ultra-stable pulsar dataset (Pulsar Timing Array) used to search for gravitational waves is also presently the main goal of pulsar searches.

For NenuFAR, the instantaneous field of view (FoV) of a phased 19 -antennas mini-array (MA_{19}) is 34° – 9° at 20 – 80 MHz, while the size of a pencil beam is 7° – 2° (refer to the technical section of this science case document). With this, NenuFAR will be an excellent survey instrument (both for pulsars and RRATs). For pulsar searches, the suitability of a telescope can be measured by a « figure of merit » (FoM). There are different ways to define this value:

1) According to Smits et al., A&A 493, 1161 (2009) and van Leeuwen et al., A&A 509, A7 (2010), the FoM is the speed of a survey for a given sensitivity. Is is given by:
   $FoM_1 = N_{beams} * FoV * (A / T)^2 \propto N_{beams} * A^2 / D^2$.
   Here, N_{beams} is the number of beams used, FoV is the field of view ($FoV \propto D^{-2}$, where D is

the diameter of the array), A is the effective area and T is the system temperature. When comparing different antenna configurations, T is constant and can be ignored.
FoM_1 gives the speed for **pulsar detection**, without precise localization of the source.

2) Stappers et al., A&A 530, A80 (2011) use a slightly different definition for the FoM:
$FoM_2 = N_{beams} * A^2 * FoV/Beamwidth \propto N_{beams} * A^2 / D$.
This combines **pulsar detection and precise measurement of the pulsar position.** For this reason, the value contains an additional factor of D (shifting beams until the pulsar is not seen anymore).

LOFAR being a sparse array ($A/D^2 << 1$), the FoM is relatively small. NenuFAR, however, will be filled in a much denser fashion, making it well suited for survey observations. In the following, we compare the FoM_1 and FoM_2 of different station configurations (normalized to the value of the coherently summed Dutch LOFAR core). We assume that the NenuFAR will have a correlator capable of forming 2 beams, while the LOFAR central processing is assumed to form 100 beams. Obviously, increasing the number of beams of NenuFAR beyond 2 could strongly increase its potential for pulsar surveys.

Setup	**Relative sensitivity**	**Relative sensitivity at 15 MHz**	**FoM_2**	**FoM_1**
LOFAR core	1	0.15	1	1
International LOFAR station	0.1	0.015	0.01	0.1
NenuFAR_1	0.3	0.12	0.1	0.4
Full NenuFAR	1.7	0.7	2	3

The table above shows that NenuFAR will be an excellent pulsar survey instrument, even if only 2 beams can be achieved. Even NenuFAR_1, the phase 1 of NenuFAR consisting of ~1/4th of the full instrument, is already close to the efficiency of the LOFAR core, while the full NenuFAR array would surpass it. Increasing the number of beams would increase the figures of merit proportionally.

Due to variable scattering, the number of potential sources for a low frequency pulsar survey is difficult to estimate. At 20 MHz, Zakharenko et al., MNRAS 431, 3624 (2013) detected 40 pulsars out of 74 already known. They expect to find 15 more pulsars in longer integrations, and 20 new, undiscovered pulsars that may not be observable at higher frequencies. At 10-90 MHz, a non-systematic LOFAR study (Kondratiev et al. 2014, submitted) already detected ~30 slow pulsars. As far as millisecond pulsars (MSPs) are concerned, (Kondratiev et al., 2014) detected 3 out of 9 observed MSPs in the LOFAR 10-90 MHz band. The non-detections can be explained by either a turnover of the pulsar spectrum, or scattering.

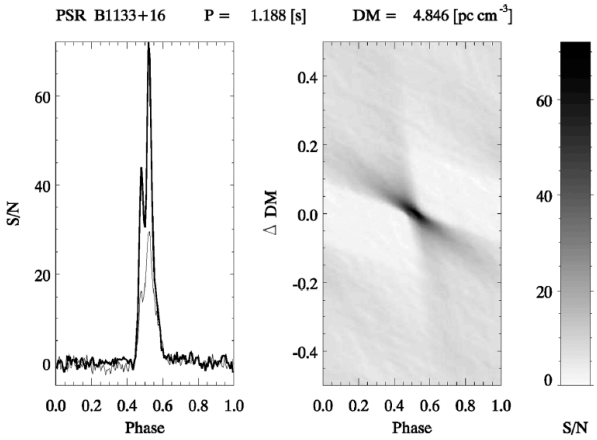

Figure 1: Detection of pulsar B1133+16 with UTR-2 between 23 and 27 MHz (bold curve), and between 18 and 22 MHz (thin curve) from Zakharenko et al., MNRAS 431, 3624 (2013).

In total, LOFAR is expected to find approximately 900 new pulsars (Leeuwen et al., A&A 509, A7, 2010), which will also increase the number of targets for low-frequency observations. More importantly, no instrument has done a high-time-resolution survey of the sky in the 10-40 MHz range, so that only a fraction of the potentially observable sources may be known. The systematic exploration of this parameter space will provide a wealth of information in a frequency domain where information is currently sparse. Also, while the spectra of most regular pulsars turn over at frequencies below ~100 MHz, there is a number of pulsars for which this is not the case, including some millisecond pulsars (Kuzmin and Losovsky, A&A 368, 230 2001). Pulsars from this population may thus be easier to find at low frequencies.
It should be noted that the effective time resolution of a low-frequency survey will be limited by scattering. For this reason, the survey volume will be somewhat limited, especially for observations within the galactic plane and fast-rotating pulsars. However, even the discovery of only a small number of additional sources would already shed light on the properties of low frequency radio pulsars.

Both NenuFAR_1 and NenuFAR are well suited for a blind pulsar survey.

Transient searches

In addition to pulsar searches, NenuFAR can be used for transient searches, such as RRATs. The Figures of Merit for such searches are the same as for blind pulsar searches; both NenuFAR_1 and NenuFAR are thus very well suited for transient searches. The number of targets is unknown, but LOFAR/ARTEMIS observations seem to indicate that the number of events is smaller than previously expected. However, even a single event would be highly valuable. With a dedicated receiver, the search for such events could be carried out in piggyback mode (similar to the ARTEMIS project on international LOFAR stations such as FR606), and the high FoM of NenuFAR would make it a prime instrument for this work. A systematic program to search for any kind of transient signal will be conducted with the decimetric Nançay Radio Telescope (NRT), mostly dedicated to the highly dispersed FRBs. Given the relatively large differential dispersive delay (a few minutes), a fast alert system is intended be used in order to detect the low-frequency part of the signal with NenuFAR. See the contribution by Corbel et al. in this document for another discussion on FRBs.

Anomalously intensive pulses (AIPs) are rare, bright events detected at UTR-2 (Ulyanov & Zakharenko, Astron. Reports 56, 417, 2012). They are usually defined as pulses 10 times brighter than the average emission, and have only been observed in narrow bands and at low frequency. Whether they are the same phenomena as the so-called Giant Pulses is still debated. NenuFAR will

surpass the capabilities of both UTR-2 and LOFAR for such observations: Its high sensitivity at low frequencies makes it more powerful than LOFAR, and its wide FoV (allowing for simultaneous observations of multiple targets) plus the full polarization information provided by NenuFAR makes it more adapted than UTR-2.

Both NenuFAR_1 and NenuFAR are well suited for a blind transient searches.

Low frequency studies

As shown in the table above, NenuFAR is optimized toward low frequencies, which translates in a sensitivity at 15 MHz comparable to that of the LOFAR core for NenuFAR_1, and a factor of 5 better for the full NenuFAR array.

This will give access to the low-frequency cutoff, propagation effects in the pulsar magnetosphere and in the interstellar medium. Currently only 40 of the ~2000 known pulsars have been observed at such low frequencies (Zakharenko et al., MNRAS 431, 3624, 2013). This is in part explained by the characteristic shape of pulsar spectra, but is also due to the lack of instruments adapted to those conditions. To this number of obvious targets for low-frequency studies, one should add the (unknown) number of detections from the low frequency pulsar survey (see above).

Pulse profile variation

The pulsar pulse profile varies with observing frequency. For example, Figure 15 of Stappers et al. (A&A 530, A80, 2011) shows that below 47 MHz, the pulse profile of PSR B0809+74 has an additional component, which below 41 MHz dominates over the component that is known from observations at higher frequencies (Fig.2). Similarly, Hassall (PhD, University of Manchester, 2011) shows that the width, the maximum, and the relative position and height of the different components are strongly frequency-dependent. This variation is due to the fact that radio emission at different frequencies is generated at different altitudes within the pulsar magnetosphere ("frequency to altitude mapping"). For this, however, it is preferable to record the information at the different frequencies simultaneously. With the large frequency span of NenuFAR, simultaneous frequency coverage will be possible over a wide frequency range and with high sensitivity. This can even be combined with HBA antennae from FR606 to reach a simultaneous frequency coverage ranging from 10 to 240 MHz for very wide-band studies of the pulses.

NenuFAR_1 is well suited for studies of pulse profile variations.
NenuFAR is very well suited for studies of pulse profile variations.

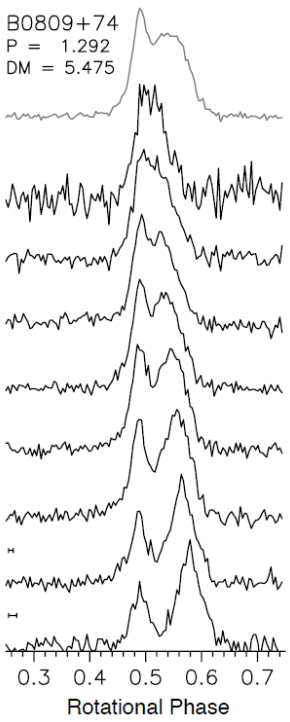

Figure 2: Profile evolution of PSR B0809+74, observed at 35, 41, 47, 53, 59, 65, 71 and 77 MHz (Stappers et al., A&A 53 A80, 2011).

Study of the interstellar medium

As the pulsar radio emission propagates through the interstellar medium, it is affected and modified by the interstellar medium ant its inhomogeneities. How severely the signal is affected mostly depends on the observing frequency (the effect being much more pronounced at low frequencies) and can usually be described by a power-law. For example, the dispersion depends on the frequency as ν^{-2}, temporal pulse broadening as ν^{-4} and scattering can vary with frequency as $\nu^{-4.4}$. At the same time, the importance of these effects at low frequencies provides the opportunity to study these effects with a much larger precision than at higher frequencies. This will allow us to put constraints on models of pulsar emission and to study the intervening interstellar medium. A good understanding of the interstellar medium is also essential to increase the precision of millisecond pulsar timing (e.g. Keith et al., MNRAS 429, 2161, 2013). The so-called Pulsar Timing Arrays (Foster & Backer, ApJ 361, 300, 1990) aim for a timing precision of 100 ns or less and aim at the detection of the stochastic gravitational waves background via variations of pulsar pulse arrival times.

Dispersion Measure (DM) monitoring is facilitated by access to low frequencies and by a good signal-to-noise ratio. With its limited sensitivity, NenuFAR_1 is probably not much better suited than the LOFAR core in the high band, where its sensitivity is at its highest. As a highly sensitive low-frequency instrument, however, NenuFAR will allow to measure variations in the dispersion measure (DM) with time, frequency, and intensity with an unprecedented precision. At low frequencies, it is also possible to measure the small rotation measure (RM) values of the nearby population of pulsars. This provides an unprecedented tool to study the local magnetic field structure (Stappers et al., A&A 53 A80, 2011). It will also be possible to search for deviations from the cold plasma dispersion and from the temporal broadening expected from the Kolmogorov turbulence law. Following the recent approach of 'interstellar holography' by Walker et al., MNRAS 388, (2008), this will allow the use of high dynamic range pulsar dynamic spectra to calculate so-called secondary spectra.

NenuFAR_1 is acceptable for the study of the interstellar medium (though LOFAR core HBA observations may be better).
NenuFAR is well suited for the study of the interstellar medium.

Millisecond pulsars

In the frequency range of LOFAR (low band) and NenuFAR, timing is less precise. Most millisecond pulsars (MSPs) have turned over (i.e. decrease in brightness at low frequency despite the usual strong inverse dependence with observing frequency), or are scattered out. Using empirical relationships, we estimate the amount of expected scattering for an MSP with a low Dispersion Measure DM=4:

DM ($pc.cm^{-3}$)	4	4	4	4
Frequency	80 MHz	60 MHz	40 MHz	20 MHz
$t_{scattering}$	18 μs	64 μs	380 μs	8000 μs

For these reasons, the number of observed MSPs is low. Kondratiev et al. (2014, submitted) detected 3 out of 9 observed MSPs in the LOFAR 10-90 MHz band, and there are no stand-alone observations of MSPs in the low band. Current LOFAR observations are taken for 60 minutes with the LOFAR core, i.e. 48*22=1056 antennas (Kondratiev et al., 2014, submitted). For NenuFAR_1 and NenuFAR, obtaining observing time may be less of an issue than for LOFAR. To simplify calculations, we assume an observing time of 9h. The NenuFAR_1 and NenuFAR bandwidth is larger than that of LOFAR, but the difference is less than a factor of 2, and it is probably more interesting to do this analysis in different frequency bands separately. For a NenuFAR_1 observation, the increase in SNR is at most 342/1056 * sqrt(9)=1.0. For NenuFAR, the increase in SNR is at most 1824/1056 * sqrt(9)=5.2. The ratio is even more favorable at low frequencies (below 30 MHz).

The number of observable MSPs is low, due to spectral turnover and scattering. However, for those MSPs that can be observed, NenuFAR_1 and NenuFAR can provide highly sensitive observations: The sensitivity of a NenuFAR_1 observation is comparable to a typical observation taken by that of the LOFAR core, while a long observation with NenuFAR is considerably more sensitive.

ISM turbulence with NENUFAR

François Levrier, Edith Falgarone, Marc-Antoine Miville-Deschenes

It is now widely recognized that the interstellar medium (ISM) is the siege of magnetized turbulence, where kinetic energy is injected at large scales by, e.g., differential rotation and supernovae explosions. This energy then cascades down until it is dissipated at small scales via various processes (viscous and ohmic dissipations, ion-neutral friction).

Our knowledge of the kinematic aspects of ISM turbulence has increased tremendously over the years, thanks to numerous line observations at large, intermediate and small scales (see e.g., Falgarone et al. 2009).

The magnetic aspects of ISM turbulence, on the other hand, are not so advanced, although progresses have been made, for instance via Zeeman splitting measurements (Crutcher et al. 2010) and studies of the polarization of thermal dust emission (Planck Collaboration XIX, 2014). Despite these progresses, many studies still rely on the simple Chandrasekhar and Fermi (1953) approach, which connects magnetic field strength, polarization angle dispersion and velocity dispersion, to gain insight on the structure of the field at small scales.

Only through the description of this structure over a broad range of scales will we achieve a better understanding of ISM turbulence as a whole, and constrain models that attempt to explain it. NENUFAR as a LOFAR Super Station (LSS) should be able to provide this :

The Galactic radio spectrum in the 10-85 MHz frequency range that will be accessible with NENUFAR is dominated by the synchrotron emission from cosmic ray electrons (CRE) in the magnetic field of the Milky Way (Peterson & Webber 2002). The energy of a CRE whose turnover frequency falls within the NENUFAR range is typically about 1 GeV (0.4 to 1.3 GeV), so these electrons are at the peak of the distribution in terms of energy spectrum (Casadei & Bindi 2004).

Also, above 10 MHz, free-free absorption of synchrotron emission by thermal electrons of the ISM is negligible, so it is reasonable to assume that, far from sources of CRE, the distribution of these low-energy CREs is rather uniform. Their synchrotron emission, as they interact with the Galactic magnetic field, will thus essentially probe the structure of the field, whose strength comes into play in the expression of the synchrotron emissivity.

The high angular resolution imaging (0.1'') that will be available with NENUFAR when used in conjunction with LOFAR, combined with the large field-of-view and the possibility to use short intra-NENUFAR baselines to probe larger scales, will make it a prime instrument to map the structure of the Galactic magnetic field over a broad range of scales. It will especially provide essential constraints on its small-scale structure, possibly addressing issues such as magnetic reconnection and ambipolar diffusion.

The transient radio sky and NenuFAR

S. Corbel and A. Loh
(University Paris Diderot & CEA Saclay)

The capability to study transient phenomena on time scales from milliseconds to years has recently increased and shown large discovery potential. Yet, the time domain of the sky has been sparsely explored. With the construction and exploitation of wide field imagers dedicated to sky surveys on a daily timescale in the radio (Lofar, ASKAP, MeerKAT), optical (Pan-STARRS, LSST), infrared (Akari), and X-ray (eRosita/SRG), and with the on-going surveillance in gamma rays from Fermi, there are new motivations to explore the transient sky. Discovering new classes of fast transients is one, as it could represent new exotic or explosive events out to cosmological distances, such as merging neutron stars or evaporating black holes.

Over the next decade, the combination of increased sensitivity, larger field of view, broader frequency range, and algorithmic developments will open up the time domain to a wide range of astronomical fields, from stellar flares and supernovae to neutron-star and black-hole births, quakes and instabilities. Near-coincidence searches with high-energy neutrino and gravitational wave signals will be actively pursued across the world. The dynamic and bursting events represent a new *terra incognita*. The synchrotron radio emission probes with unequalled angular resolution the cooling in the ambient magnetic field of the relativistic particles ejected by compact accretors or explosions. It also constrains the kinetic feedback of such events on their environment.

Transients can be divided in two groups based on their variability timescales. The incoherent synchrotron transients are usually varying slowly on timescale greater than few hours/days. They are typically associated with explosive events (gamma-ray burst, supernova explosion) with important energy injection in the environment resulting in bright synchrotron flares. They have a brightness temperature limitation of 10^{12} K and are detected from direct imaging analysis. NenuFAR observations will allow characterizing their radio spectra and their variability in the MHz regime, which to date remain poorly constrained. Constraining the electron distribution at low energy (e.g. low frequency) is crucial to constrain the jet energy budget of these systems, as well as measuring the synchrotron self-absorption frequency break and in fine the strength of the jet magnetic field. The accumulation of all observations for a given field would allow us to test the presence of radio relics due to the jet energy deposit on the ambient medium.

The other category is associated with very fast timescale variability (down to milliseconds) and those have no limit in term of brightness temperature. These coherent synchrotron events (e.g. pulsars) are detected from time series analysis. As an example, the recent discovery of Fast Radio Burst (FRB) represents one illustration of such new, exotic and fast radio phenomena (Lorimer et al. 2006, Thornton et al. 2013). This is, at some point, similar with

the fortuitous discovery of pulsars in the 60s. The FRBs are highly dispersed, short (few milliseconds) and bright (~1 Jy) radio bursts (Fig 1) and they are very likely located at cosmological distance (up to z ~1). They have been discovered around 1.4 GHz in beamformed surveys. The progenitor of these bursts are unknown, but likely points to physics in extreme environments. The extension of their radio spectra to low frequencies is unknown. With its large FOV and broadband low-frequency coverage, the NenuFAR array has the potential to discover up to several FRBs per day, either in beamformed data or even directly in imaging survey. Indeed, at low frequencies, the dispersion becomes so large that detection in direct imaging becomes feasible. In addition the large FOV allows a larger volume of space to be probed and compensates the decreasing amplitude of the signal (Hassall et al. 2013). Synergy with another local facility, such as the NRT, may also help to constrain the shape of their spectra in case of FRBs with very high dispersion measure.

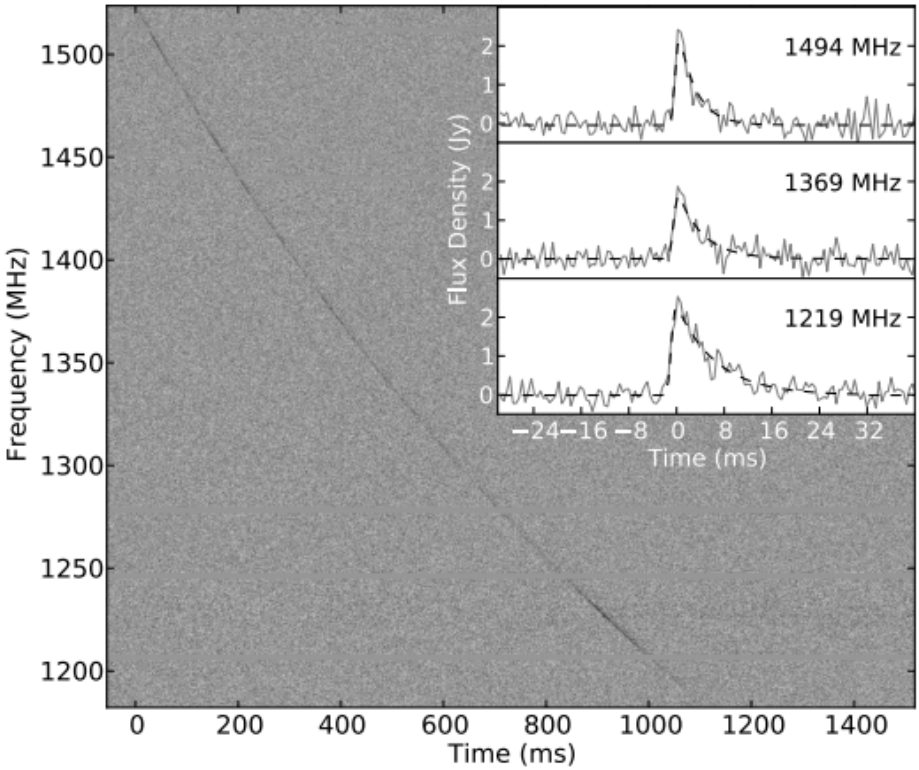

Figure 1: The spectrum (as a function of time) of one of the four FRBs recently discovered by Thornton et al. (2013). It illustrates that lower frequencies at later times.

New transients may be discovered either by dedicated surveys or by more clever strategies, such as performing commensal searches on all data coming from the

NenuFAR station. As the characterization of transients and their identification at other wavelengths represent another challenge, the synergies with forthcoming facilities would need to be explored. As an example, several groups in France are involved in the SVOM high-energy mission, which has the potential to reveal many transients in our Galaxy. With the increased sensitivity of the long baselines, NenuFAR (in LSS mode) could be a good opportunity to follow these transients in radio, but with some limitation due to self-absorption at low frequencies. Fermi is also mapping the whole sky every 3 hours, and has already revealed a few transients on daily timescale, for which no identification or explanation has been proposed.

References

Hassall et al. 2013, MNRAS, 436, 371
Lorimer et al. 2007, Science, 318, 777
Thornton et al. 2013, Science, 341, 53

Measurement of Cosmic Ray Extensive Air Showers with NenuFAR and CODALEMA: a SKA-EAS program pathfinder

R. Dallier[ab], L. Martin[ab], B. Revenu[a]

Abstract

We propose an additional use of the Nançay NenuFAR radio telescope as a cosmic ray radio detector. The presence of the cosmic ray detector CODALEMA, surrounding both NenuFAR and the FR606 LOFAR international station, offers a unique environment to test and improve techniques for cosmic ray radio detection, acting as a pathfinder for air shower detection with the SKA-Low in the future.

1. High-energy cosmic ray physics challenges

High-energy cosmic ray physics refers to the experimental study of cosmic rays above 10^{14} eV. Above this limit, direct measurements of cosmic rays with balloons or satellites are limited by their small area regarding the extremely low flux of particles. Instead, one has to detect the cascade of secondary particles, called extensive air shower (EAS), which follows the interaction of the cosmic rays with the Earth's atmosphere and spread at ground over very large areas. The primary particle characteristics are then inferred from the EAS measurements: the arrival direction of the primary particle coincides with the one of the EAS, its energy is deduced from the total number of charges created and the EAS longitudinal development is related to the mass of the primary. The experimental challenge stands in the ability to determine these 3 quantities with a sufficient level of accuracy.

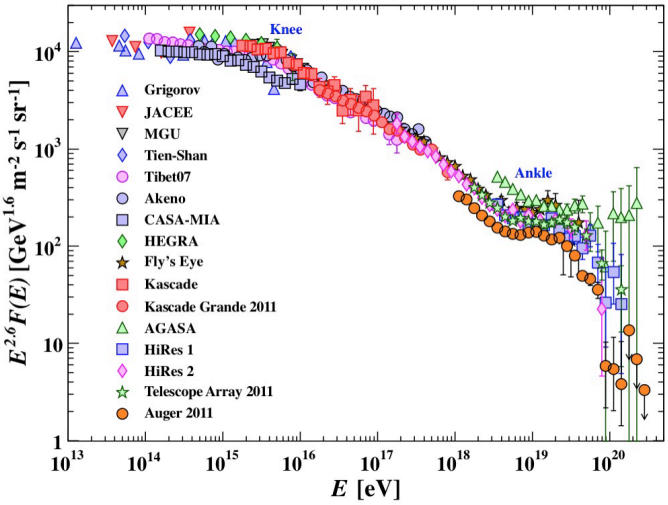

Figure 1: The all-particle spectrum from air shower measurements from several experiments [1]. The differential energy spectrum of cosmic rays has been multiplied by $E^{2.6}$ to make features easier to discern. The knee and ankle features are indicated.

Figure 1 shows the cosmic ray flux as a function of the incident particle energy. This spectrum can be described by a power law with 3 noticeable changes in the spectral index: the steepening of the spectrum at 10^{15} eV is called the knee, the second change in slope at 3×10^{18} eV is the ankle and the cut-off above 3×10^{19} eV marks the fall off of the spectrum. The latter feature is often attributed to the so-called Greisen- Zatsepin-Kuzmin (GZK) effect due to the interaction of ultra-high energy cosmic rays with the cosmic microwave background (CMB) radiation [2], but it could also be explained as an absolute limit of cosmic accelerators. This remaining uncertainty is due to the lack of statistics and the bad knowledge of the nature of the primary particles in this energy domain.

[a] *Subatech, Ecole des mines de Nantes - CNRS/IN2P3 - Université de Nantes, Nantes, France*

[b] *Station de radioastronomie de Nançay, Observatoire de Paris, CNRS/INSU, Nançay, France*

The interpretation of both the knee and the ankle is still also subject to debate. Particle physics explanations, such as the appearance of a new kind of hadronic interaction at high energy, are conceivable but most proposed interpretations call for astrophysical reasons. In these approaches, the knee could reflect the upper limit of galactic cosmic ray accelerators (supernova remnants, pulsars...) and then another but less pronounced knee, called second or iron knee, is expected around 5×10^{17} eV for heavier components of the primary spectrum. The ankle could be the region where the transition between cosmic rays from galactic and extra-galactic origin takes place. Another scenario interprets the ankle as an e^+/e^- pair production dip resulting from proton propagation over large distances in the CMB [3]. If this last interpretation is correct, then the end of the galactic cosmic ray origin would rather occur between the ankle and the knee. Changes in the observed composition of the primary spectrum between the ankle and the knee are then expected to sign this transition. Up to now, the mass composition in the range 10^{16} to 10^{18} eV has barely been studied and only few data above 10^{17} eV is available. Instead, most of the experimental efforts over the last decades have been dedicated to the higher energy part of the spectrum, above the ankle, where cosmic rays are expected to point directly toward their sources. The need for high quality data from the knee to the ankle is nonetheless patent as the composition in this part of the spectrum holds the key for discriminating between several theoretical viewpoints. As a cosmic ray detector, NenuFAR with CODALEMA would operate in this energy range.

2. The radio detection of cosmic rays

Two detection methods are commonly used in high-energy cosmic ray experiments, coming with their specific assets and drawbacks. First, ground arrays of particle detectors measure particle densities on the ground over large areas. This technique is robust and benefits from a high effective time of operation. However, it can only detect the very end of the EAS development and misses the rich information contained in its longitudinal development. As a consequence, estimators of the energy and mass are largely model dependent. The second technique uses fluorescence telescopes, which measure nitrogen fluorescence occurring in the atmosphere due to the interaction of charged particles in the shower with the air molecules. As fluorescence light is emitted isotropically, the shower development can be observed from the side and the fluorescence telescopes get access to the longitudinal development of the shower. Unfortunately, this detection method suffers from a critical duty cycle of the order of 14 % due to the clear and moonless nights needed for operating.

The last decade has seen the rebirth and development of a third detection method: the radio detection. It is based on the measurement of the electric field emitted by the air shower in the radio frequency domain. This electric field, generated at high altitude by the charged particles in the EAS, is an image of its longitudinal development. Therefore the shower history, corresponding to its evolution in time, is contained in the radio signal and can be retrieved. As the ground arrays, the radio detection does not suffer from limitation in its time of operation. Thus, it combines a high effective duty cycle with a sensitivity to the longitudinal development of the shower. This makes the radio technique a very promising tool for high-energy cosmic ray physics as both the mass and the energy of the primary particle should be accessible with a high degree of accuracy and enhanced statistics. The involvement of the cosmic ray community in radio detection has rapidly grown and numerous related programs have been created over the last few years. Besides pioneer experiments like CODALEMA [4] in Nançay and LOPES [5] in Karlsruhe (Germany), the radio technique is now also present in Argentina at the Pierre Auger Observatory with AERA [6] and earlier with its prototypes [7, 8], in Antarctica with RASTA on the IceCube neutrino detector [9], in China with TREND around the 21CMA radio telescope [10] and at last on LOFAR in the Netherlands [11]. LOPES, AERA, TREND, RASTA measure showers at frequencies below 80 MHz, while CODALEMA bandwidth extends up to 200 MHz. LOFAR has both a low frequency (30–80 MHz) and high frequency window (110–250 MHz), but these cannot operate simultaneously. France is involved in the major experiments that are AERA, CODALEMA and LOFAR. AERA is focused at scaling the detection technique up to much larger areas and thus energies and has by now instrumented an area of ~ 6 km^2 with a sparse array of autonomous antenna stations, like CODALEMA. One of its goals is to cross-check the mass sensitivity of the radio measurements directly with the Auger detectors. In contrast, LOFAR features a very dense core of radio antennas over an area of ~ 0.2 km^2 allowing us to study the electric field profile of individual air showers with very high precision.

In parallel with this flurry of experimental activities, sophisticated Monte Carlo simulation codes [12, 13] as well as macroscopic models [14, 15] have been developed to study the radio emission physics. Two mechanisms occurring in the shower have been identified as sources of the radio signal: a charge asymmetry building

up in the shower (charge excess, Askaryan effect) [16] and the systematic separation of charges due the Earth magnetic field [17]. Accordingly to all of the simulation codes, both sources should contribute to the creation of currents inside the shower but the emission should be dominated by the time derivative of the current induced by the geomagnetic deflection. Experimental observations from previous [18] and recent [19] work support this dominant mechanism. Today, we have a very good understanding of these emission mechanisms, down to the secondary contribution of the time-varying charge-excess radiation. The latter has been experimentally demonstrated with two independent types of observations [20, 21]. Building on this understanding, it has been demonstrated that all important properties of extensive air showers can be deduced from radio measurements, in particular the arrival direction, energy, and recently mass-sensitive observables for individual cosmic rays.

3. The NenuFAR cosmic ray program

The NenuFAR cosmic ray program aims to further develop the technique of radio detection and explore the mass composition of the $10^{16} – 10^{18}$ eV energy range of the cosmic ray spectrum. It will benefit from the proximity of the new setup of the CODALEMA experiment [22]. CODALEMA will surround NenuFAR with 57 standalone antennas and 43 particle detectors spread over an area of 1 km^2 across the Nançay radio astronomy observatory. The 1824 crossed dipoles of NenuFAR, operating in the 10 – 87 MHz frequency range are perfectly adapted for cosmic ray radio detection. Both instruments will operate jointly and will benefit from their complementary designs: NenuFAR will provide a high density antenna array and CODALEMA a large detection surface. Moreover, the LOFAR FR606 international station can also be used in a cosmic ray mode, as it is already done by the Superterp in the Netherlands. Associating the high antenna density of FR606, the medium antenna density of NenuFAR and the rather sparse array of CODALEMA will provide a unique opportunity worldwide to detect the same air shower events at different antenna density scales. In that respect, the future installation will combine the performances of LOFAR and AERA in the very intermediate energy domain of 10^{16} - 10^{18} eV: currently, LOFAR reaches these energies with a high density of antennas but few information on large distance electric field profile, while AERA does exactly the opposite. Figure 2 shows the map of the final setup that will be used in Nançay.

3.1. Technical implication and operating mode

There are differences in the way antennas are operated when they are used as radio telescopes or as radio cosmic ray detectors. These differences have to be kept in mind when aiming at an efficient coupling of both activities. On the one hand, radio telescopes dedicate a time slot to the observation of a given astrophysical object. Radio signals are continuously acquired during this time slot and the object is followed through the sky by phasing (beam-forming) the antennas toward the direction of the object. On the other hand, a cosmic ray detector does not acquire signals continuously but waits for a trigger condition to make a snap shot of radio signals when an EAS is present. No particular direction in the sky is favoured as cosmic rays are isotropically distributed. This could make analog beam-forming irrelevant for cosmic ray detection, but its effect on the EAS radio signal depends on the relative difference between the cosmic ray arrival direction (a priori unknown) and the direction of antenna phasing. Knowing the phased array response diagram, it is possible to correct this effect and retrieve the original EAS radio signal but, for particular incident directions of the cosmic rays, the antenna phasing might be destructive and the coverage map of the instrument then becomes difficult to handle. For NenuFAR, an analog beam-forming will be performed at the level of the mini-arrays of 19 antennas (MA_{19}). For the specific cosmic ray observation needs, the NenuFAR design has thus been adapted: on NenuFAR's dedicated backend, an acquisition channel will be implemented to extract signal from one single antenna of each of the 96 MA_{19} before the beam-forming. An external trigger input will also be available in order for NenuFAR to be triggered by the CODALEMA particle detector. This will allow a gradual convergence of the classical cosmic ray operating mode toward a procedure fully compatible with an operating radio telescope: first, the effect of the beam-forming on the cosmic ray detection capabilities will be quantified thanks the use of the CODALEMA particle detector and to the comparison between beam-formed and single antenna signals. The second step will be the elaboration of an EAS signal identification criterion based on radio signals only, so that NenuFAR could go without the particle detector. The final step will consist in the development of an analysis procedure to extract all cosmic ray information from the data acquired during astrophysical observation campaigns. This will constitute a milestone in the development of radio instruments as it will make both activities, radio telescope and cosmic ray detector, fully compatible for the very first time.

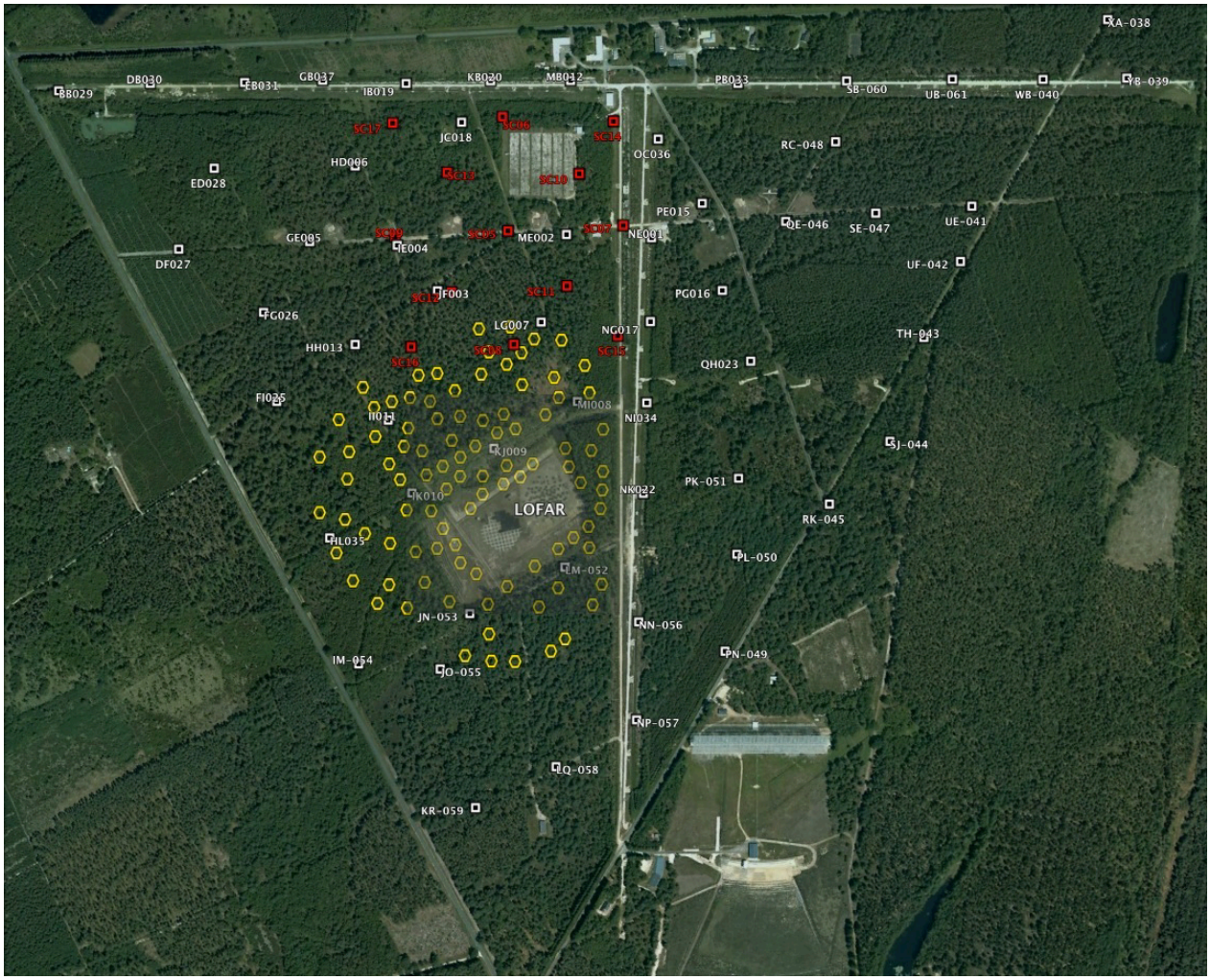

Figure 2: Aerial view of the Nançay observatory. White squares feature the 57 CODALEMA autonomous radio detection stations, red squares the current 13 scintillators (soon completed with 30 more associated with radio stations), and yellow hexagons the mini-arrays of NenuFAR. The LOFAR station is also mentioned.

Beside this operating mode prefiguring the regular operation of the telescope, NenuFAR can also be used as a standalone, dedicated instrument in a sizeable fraction of its time. During such periods, we intend to use NenuFAR in a "radio fly's eye" mode, by phasing each of the 96 MA_{19} in a different direction of the sky, thus covering the 2π sr with 96 beams. In that respect, NenuFAR will act as the LOFAR Superterp in cosmic ray mode, but with a sensitivity 19 times higher than the one reached with single antennas. We expect an observing gain on both sides of the energy range, with the ability to observe high energy showers falling far away from the center of the instrument. The quite large field of view of each MA_{19} (10 to 50° from 10 to 87 MHz) ensures an overlap between adjacent beams and makes possible the EAS detection by several MA_{19}. This would be the first time ever that such an operating mode will be tested.

3.2. Science objectives

The primary science objective of the NenuFAR cosmic ray program is to search for the transition region between galactic and extra-galactic cosmic rays in the spectrum. The NenuFAR setup is also particularly well designed to explore the low part of the frequency spectrum of the EAS radio signals thanks to its high frequency resolution and large frequency bandwidth. The frequency spectrum of the EAS radio signals is indeed expected to be maximum around 15 MHz or at even lower frequencies ([12] to [15]). Moreover, the low frequency components benefit from a lower attenuation with shower axis distance compared to higher frequencies, hence, the use of this part of the spectrum should enhance the detection performances of the radio technique at large distances. Among the last steps needed to validate radio detection as a mature probe for cosmic ray phys-

ics, the identification of the mass of the primary is of paramount importance. Several paths are currently followed to extract the primary mass from the radio signal: the measurement of the radius of curvature of the radio wavefront, the measurement of the ground profile of the electric field, its polarization or its frequency spectrum. It has recently been demonstrated that with its high-precision measurements of the profile, LOFAR is able to gather very accurate information on the mass of individual cosmic rays by fitting simulated two-dimensional radio power profiles to the data [23]. More advanced techniques that incorporate the polarization, spectrum and arrival time of the radio pulse will improve the reconstruction quality further and will be tested on the Nançay instrumental setup. It should then be possible to identify the different source components (protons and other nuclei) between the second knee and the ankle. A change observed in the average composition in this energy region is expected to sign the transition region between cosmic ray from galactic and extra-galactic origin.

4. Conclusion

Thanks to their proximity, NenuFAR, FR 606 and CODALEMA will be able to operate jointly to explore the primary composition of the cosmic ray spectrum from the knee up to the ankle. A signature of the transition between cosmic ray from galactic and extra-galactic origin will be searched for in this energy region. The full setup will constitute the cosmic ray radio detector with the highest antenna density. It is perfectly designed to study several features of the electric field emitted by EAS that have not been explored so far.

The whole setup will also constitute a pathfinder for existing and future large radio telescopes such as SKA-Low as it will, for the first time, define an operation mode able to couple both activities, cosmic ray studies and astrophysical surveys. A contribution to the future SKA design and programs has been submitted by the authors, associated to physicists from dutch and german groups. This proposal is based on the tests and operations that will be led with NenuFAR and CODALEMA.

References

[1] J. Beringer et al. (Particle Data Group), Phys. Rev. D86, 010001 (2012).
[2] K. Greisen, Phys. Rev. Let. (1966); G. T. Zatsepin and V. A. Kuzmin, Sov. Phys. JETP Let. (1966).
[3] V. S. Berezinsky, S. I. Grigorieva, and B. I. Hnatyk, Astropart. Phys. (2004).
[4] D. Ardouin et al., Nucl. Inst. & Meth., Section A, 555, 148163 (2005).
[5] H. Falcke et al. (LOPES Collaboration), Nature 435, 313 (2005).
[6] J. Maller, for the Pierre Auger collaboration, RICAP13, Roma, Italy (2013).
[7] Pierre Auger Coll. & Acounis S., Charrier D., Garçon T., Rivière C., Stassi P., JINST 7, P11023 (2012).
[8] B. Revenu, for the Pierre Auger collaboration, 32nd ICRC, Beijing, China (2011).
[9] M. Duvernois et al. (IceCube collaboration), 32nd ICRC, Beijing, China (2011).
[10] T. Saugrin et al. (TREND collaboration), 32nd ICRC, Beijing, China (2011).
[11] P. Schellart et al. (LOFAR Collaboration), A&A 560, A98 (2013).
[12] T. Huege, M. Ludwig and C.W. James, AIP Conference Proceedings 1535, 128 (2012).
[13] J. Alvarez-Muñiz, W.R. Carvalho and E. Zas, Astropart. Phys. 35, 325 (2012).
[14] O. Scholten, K. Werner and F. Rusydi, Astropart. Phys. 29, 94 (2008).
[15] V. Marin and B. Revenu, Astropart. Phys. 35, p. 733-741 (2012).
[16] G.A. Askaryan, Sov. Phys. JETP 14, 441 (1962).
[17] F. D. Kahn and I. Lerche, Proc. of the Royal Society of London, 289:206 (1966).
[18] H. R. Allan, Progr. in Elem. Part. & Cosmic Ray Phys. X, North-Holland and American Elsevier (1971).
[19] D. Ardouin et al. (CODALEMA collaboration), Astropart. Phys. 31, 192:200 (2009).
[20] V. Marin et al. (CODALEMA collaboration), 32nd ICRC, Beijing, China (2011).
[21] The Pierre Auger Collaboration, Phys. Rev. D, in press (2014).
[22] D. Torres-Machado et al. (CODALEMA Coll.), 33rd ICRC, Rio de Janeiro, Brazil (2013).
[23] S. Buitink et al. (LOFAR Coll.), 33rd ICRC, Rio de Janeiro, Brazil (2013).

From solar to solar-type stellar activity: what the decameter range can teach us

Carine Briand, Sophie Masson, et al.

Introduction

The activity of the Sun is known since several centuries. The proximity of our star provides us a wealth of details that serve to test numerous plasma fundamental processes, that lead to high resolution models of the atmosphere of our star and that may guide studies on other stellar systems. The solar activity is highly link to temporal evolution and spatial modification of the magnetic field topology. The magnetic activity of our star is revealed at every layer, from the photosphere to the high corona (see a review on Briand, 2003). Among the important issues raised by this activity we can mention two in particular: (1) the transfer of energy from large to small scales and the final dissipation into heat, process for which waves emissions take a central place, (2) the interaction of the energetic particles generated during eruptive phases with the objects of the solar system.

But the Sun is not the only star displaying flaring and interplanetary activity. The occurrence of flares in stars was revealed in the 50's. Rapidly, the importance of the flare activity in the evolution of dwarf stars was raised, which thus leads to the question of the place of the flare stars in the stellar evolution (Mirzoyan, 1984). In their interaction with their proto-planetary disc, young stars also generate flaring activity. A better understanding of the disc-star interactions requires the determination of the magnetic field strength (and ideally its vector components). The other category of flaring stars is the fully convective, low mass stars where dynamo process generates magnetic field that leads to numerous magnetic reconnection sites. Finally, when considering solar-type stellar activity, shock-producing system must be considered. Such system exist in high mass stars systems where strong, supersonic winds have already been detected in X-rays.

If the Quiet Sun radio spectrum is mostly of thermal origin (thermal bremsstrahlung, gyro-resonance), the strongest, sporadic emissions display brightness temperatures that highly exceed the thermal values, suggesting a non-thermal origin. Gyro-synchrotron emissions dominate at frequencies above 3GHz, while coherent plasma processes are mostly invoked to explain the emissions at lower frequencies, in particular in the kilo-decameter range.

The coherent emissions are triggered by plasma instabilities involving electrons (and to some less extend ion) dynamics. The source of free energy for the instabilities to develop comes from the distortion of the electron distribution function, either through the presence of an electron beam ("bump-on-tail", two streams) or a non-thermal plasma in a very dilute plasma, ideally in presence of a strong magnetic field (electron-cyclotron maser). The beam-plasma instability generates electrostatic waves at a frequency close to the plasma frequency ($f_p \sim 9\sqrt{N_e}$ kHz), waves that are then converted to electromagnetic waves at f_p or $2f_p$. The electron-cyclotron maser (ECM) generates waves at the electron cyclotron frequency ($f_{ce}(\mathrm{MHz}) \sim 2.8 B_G$). If the ECM process is largely invoked to explain the emission of the giant planets in the decameter range, beam-plasma instabilities are dominant in the world of the solar and interplanetary emissions since then $f_p >> f_{ce}$. Also, ECM emissions are invoked to explain the GHz down to some 325MHz emissions of cool dwarf stars. However, no detection of ECM emissions has never been attempted as it supposes very low magnetic field strength (below 50Gauss).

To understand the potential of observation to study the stellar activity in flaring stars and massive stars binary system, let's first understand how the decameter range provide information from our own star.

Solar activity

Radio emissions witness energy release in the high corona and interplanetary medium, sometimes without any counterpart in other wavelengths. In the low part of the radio spectrum (from 10MHz down to a 10kHz at Earth orbit), several characteristic features are observed (Fig 1): (1) slowly drifting emissions, signatures of the propagation of interplanetary shocks (also called Type II emissions), (2) intense, fast time-frequency drifting emissions, which trace the propagation of energetic electrons, accelerated during flares, in the interplanetary medium (called Type III bursts), (3) bursts of rapidly drifting emissions, lasting for days and related to the presence of opened magnetic field loops from solar active region (Type III storms). This range of frequency being below the ionospheric cut-off is accessible only from space instruments. Ulysses, WIND, STEREO have been providing us a large amount of radio data to study plasma processes from both remote instrument and *in-situ* measurement of electric (sometimes magnetic) waveforms, pushing the frequency limits towards very low frequencies (100 Hz).

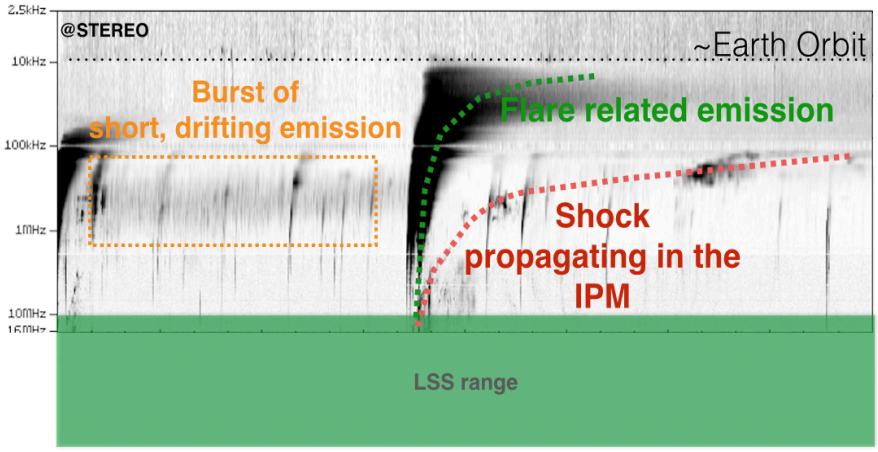

Figure 1: Solar time-frequency spectrum. Several typical radio emissions of the low frequency range are underlined: (1) shock propagating emission, (2) Flare related emission, (3) burst of short emissions. NenuFAR covers a frequency range complementary to the space instruments and provide data from regions closer to the Sun.

The higher part of the spectrum also provides a wealth of details that allows deducing numerous characteristics of the medium. The frequency range 10 to 80 MHz corresponds roughly to distances to the Sun between 1.2 to 2 solar radius. Being above the cut-off of the ionosphere, it is accessible to ground-based instruments.

As in the lower part, continuum and broadband emissions are also present above 10MHz. The large spectrum is difficult to interpret in term of beam plasma instability. Rather, electron maser cyclotron could be at the origin of the emission. In such case, they could provide a tool to diagnose the magnetic field direction.

Faint time-frequency drifting emissions are also characteristic of the high frequency range. They appear isolated, in time vicinity of very intense flare-related emissions, or in chain (see Melnik et al. 2014b, and reference therein). Following the hypothesis of beam-plasma instability for the mechanism at the origin of such emissions, the drift allows to deduce several characteristics of the interplanetary medium.

The sign of the drift indicates the direction of the electron beams propagation (inwards/positive -- or outwards/negative -- from the Sun). The velocity of the beams can be deduced from the drift value and a density model (Briand et al. 2008a). Sometimes, the drift changes its sign: this could reveal a local modification in the temperature of the corona (Melnik et al. 2014a). These faint emissions are not always related to CME or flare activity. As can be seen from the right panel of the figure 2, numerous faint emissions still occur at low frequencies (i.e. close to the cut-off frequency of the ionosphere). Recently Briand et al. (2007, 2008b) proposed a model based on a local heating of the

plasma. The interpretations of all these emissions are still under debate and some even are not supported by any explanation.

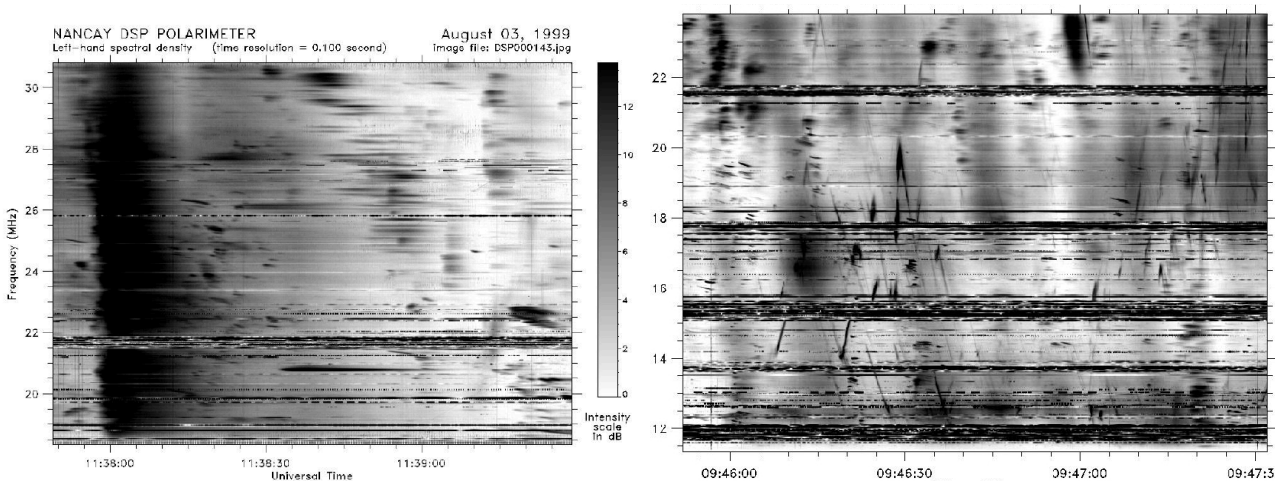

Figure 2: Two examples of solar emissions in the frequency range 18 – 30 MHz. On the left panel, the dark, rapidly drifting emission is the high frequency part of an intense flare-related emission (see Fig. 1). Next to this emission, and also clearly visible on the right panel, fainter drifting emission are present, either as isolated features or in chain (visible at about 09:46 on the right panel). The observations presented here were obtained with the Nançay Decameter array (left) and the UTR-2 Ukrainian radio-telescope (right)

How to be sure that the observed structures are of solar origin? Disturbances of the ionosphere can indeed produce similar features. Simultaneously observations with two distant radio telescopes are the most efficient way to disentangle ionospheric from solar emissions. With UTR-2 in Ukraine, NenuFAR provides an efficient second station of observation. Moreover, it will allow polarimetric measurements that UTR-2 cannot perform, succeeding to the decameter network, but with a larger frequency range and a higher sensitivity.

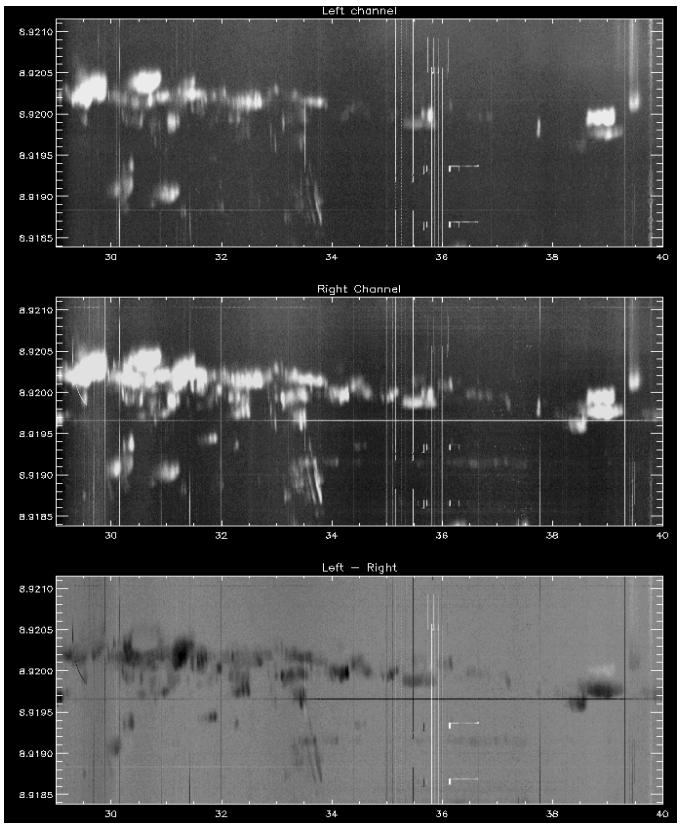

It is known that flare related emissions are up to 50% circularly polarized (when the emission is at the fundamental) or less than 15% (when it is on the harmonic). For shocks related emissions, the polarization is less than 5% polarized. The other narrow band, faint structures polarization is highly variable (from 0 to 100%!). Polarization is essential to determine the physical processes at play. In the beam plasma theory, the mode conversion from electrostatic to electromagnetic can produce polarization in presence of density gradient and/or magnetic field fluctuations.

Figure 3: Polarimetric observations obtained with the decameter network of Nançay. Left circular polarization is on the top panel, right polarization on the middle and the net polarization on the bottom (the frequency axis is horizontal, and expressed in MHz). Note the inversion of polarization of the emission between 30 and 40 MHz

In summary, the 10 – 80 MHz range of frequency is rich of emissions that can reveal local disturbances of the high solar corona. To understand such emissions, high spatial, spectral and time resolution are still necessary, together with polarimetric measurements and high sensitivity.

Stellar activity

Flares and (collisionless) shocks are among the main sources of intense decameter emissions at the Sun and in the interplanetary medium. Such activity also occurs at and close to other stars. Flares occur in young stars like Herbig Ae and T-Tauri from the interaction with the proto-planetary disc. Also fully convective red dwarfs present a strong activity. Magnetic field is generated by the convection process and leads to magnetic reconnection and flares.

Red dwarfs are in the lower part of the main sequence. They are cool (Teff~3500K), small ($R<R_{\odot}$), and faint ($L\sim0.01L_{\odot}$) stars. UV Ceti is the archetype of red dwarfs. In spite of these quite complicated conditions of observations, the interest for these stars resides in that they represent almost 75% of the stars of the Milky Way! However, less than 100 stars are indeed detected, and most within 10pc from the Sun. The first detections of radio emission (above 200MHz) simultaneously to optical flares were obtained in the 60's (Slee et al. 1963; Lovel 1969). Later on, it was also shown that radio activity could exist independently of optical counterpart.

Almost opposite to the dwarf stars, we find another kind of very interesting active system: the Colliding-Wind Binaries (CWB – Stevens 1992). They consist in systems of massive stars (without compact objects), like a Wolf-Rayet and an OB-type star, very luminous, with supersonic winds and large mass-rate lost. 70% of the O-type stars would belong to binary systems. They provide suitable environment for shocks to occur. The radiative cooling may be much longer than the flow time scale, leading to high temperature and high X-rays emissions. A topical issue is to understand if such shocks are also efficient particle accelerators to produce γ-rays. Colliding wind regions also produce radio continuum emissions due to accelerated electrons through Fermi mechanism. Several papers report non-thermal radio emissions from different sources (see for example Blomme & Volpi, 2014 and reference therein). But interesting characteristics of the shocks can also be deduced from the decameter observations. In particular, hydrodynamical simulations require details on the density, velocity structure of the colliding winds, information that could be extracted from radio observations.

However, very few observations have been reported in the decameter range. Leitzinger et al. (2010) present observations obtained with the UTR-2 Ukrainian radio telescope where some very faint time-frequency drifting emissions are noticeable. More recently, spectral profile of radio burst emissions AD Leonis and EV Lacertae display similar characteristic from the solar emission (Boiko et al., 2012). Also, frequency drifts seem to be present with both positive and negative slope. However, complementary observations are necessary – in particular with a better spectral coverage – to confirm the drift rates. The largest burst flux observed by the Boiko's group was 307 Jy, while a large number of bursts have flux of 10 to 50 Jy, which corresponds to brightness temperature of 10^{16}K, largely exceeding the thermal values.

Gershberg & Shakhovskaya (2003) compiled several results of optical observations performed by several groups between 1967 and 1973. In particular, they provide a time-energy distribution of several stars in the Pleiades and Orion clusters showing that energetic (10^{29} -10^{31} ergs) flares can be expected almost every day on several stars. Combined with higher frequency range observations, in particular in X rays, such observations can provide complementary information on the dynamics of the electrons.

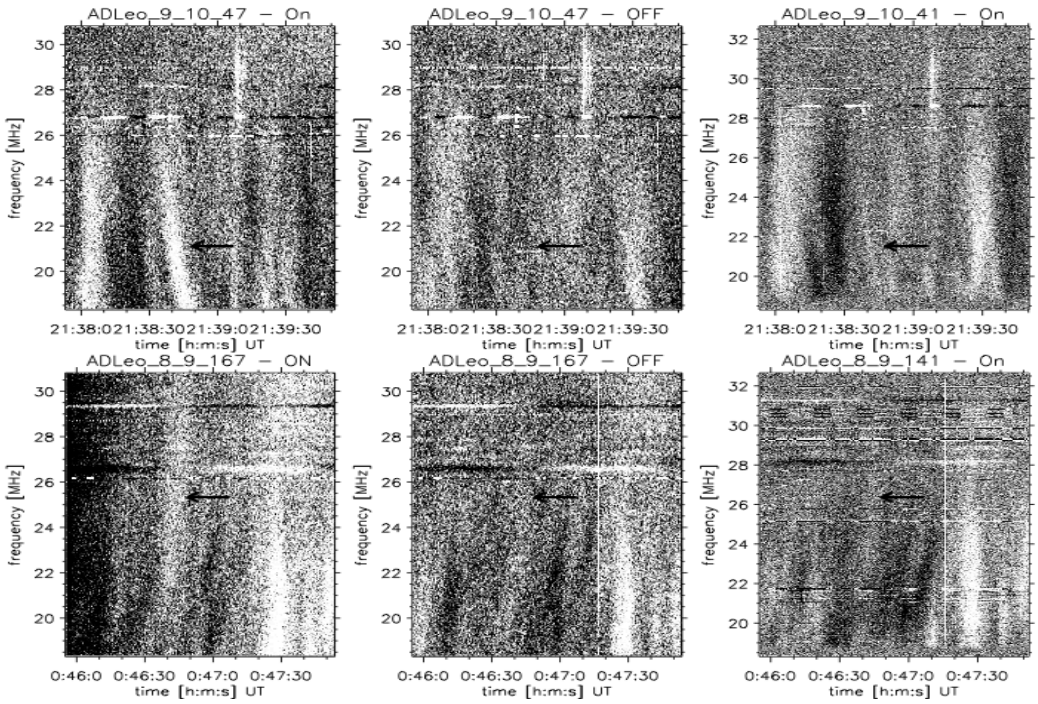

Figure 4: Time-frequency observations of AD Leonis observed with UTR-2 radio-telescope in 2010-2011 (@Leitzinger et al. 2008)

Conclusions

During the last decade, the observations of the Sun with decameter radio telescopes equipped with back-end facilities providing both high frequency and time resolution have revealed numerous faint, narrow banded emissions, tracing the propagation of electrons outward or inward the Sun. Such observations provide diagnostic tools of the density, the temperature and the magnetic structure of the corona, which is on the site of launch of the most energetic phenomena.

Our experience on the solar observations has prepared us to the study of other environments like flaring stars and binary stars. The decameter range of frequency provides a window to study the dynamics of the plasma around the stars, covering regions where the electron density spans between 1 and 100cm^{-3}. Surprisingly, this domain has almost not been considered up to now. Useful studies require observations with high sensitivity, polarimetric capabilities and survey mode to catch the shocks and flares from several stars. NenuFAR provides all these capabilities. It can thus play a central role in the innovative discoveries on the flaring stars and high mass binary systems.
Finally, it must be noted that this review was restricted to solar-type activity. But other kind of activity may also occur in stellar environments like in Algol or W Uma-type star, where strong inflows on the stars can produce other strong emissions. Could these flow also produce noticeable emission in the decameter domain must also be investigated.

Bibliography

Blomme R. & Volpi D. (2014), 'Non-thermal radio emission from O-type stars – V.9 Sagittarii*', A&A, 561, A18

Boiko et al. (2012), '*Search of the radio emission from flare stars at decameter wavelengths'*, Adv. in Astron. & Space Physics, 2, 121-124

Briand C. (2003), '*Solar activity I : aspect of magnetic activity'*, Astron. Nachr., 324(4), 357-361

Briand C., et al., (2008a), '*Faint solar radio structures from decametric observations*', A&A, 490(1), 339-344

Briand C. et al. (2008b), ' *Coherent electric structures: Vlasov-Ampère simulations and observational consequences*', JGR : Space Phys., 113(A7), CiteIDA07219

Briand C. et al. (2007), '*Electrostatic coherent structures generation by local heating in a collisionless plasma*', Phys. Letters A, 368(1-2), 82-86

Gershberg and Shakhovskaya (2003) *'Some results of international campaigns initiated by the Crimean Astrophysical Observatory for investigations of flare stars'*, Astronomical & Astrophysical Transactions, 22:4, 441 – 454

Leitzinger et al. (2008), '*Radio decameter observations of AD Leonis*', Central Europe Astrophysical Bulletin, 1, 157-163, ISSN 1845-8319

Lovel B., (1969), 'Observation of prolonged radio emission from red dwarf star', naure, 222, 1126-1129

Melnik V. et al. (2014a),' *Decameter Type III Bursts, Which Change Their Frequency Drift Rate Signs*', Solar Phys., accepted

Melnik et al. (2014b), '*Unusual Solar radio burst observed at decameter wavelengths*', Solar Phys. 289, 263-278

Mirzoyan L.V., (1984), '*Flare Stars*', Vistas in Astronomy, 27, 77-109

Slee O.B. et al. (1963), '*Radio emission from flare Star V371 Orionis'*, Nature, 199, 991-993

Stevens M.S. et al. (1992), '*Colliding winds from early-type stars in binary systems*', ApJ., 386, 265-287

Jupiter's decametric radio emission observed with NenuFAR

M. Panchenko[1], H.O. Rucker[1], A. Konovalenko[2], P. Zarka[3], L. Lamy[3], et al.

(1) Space Research Institute, Austrian Academy of Sciences, Graz, Austria;
(2) Institute of Radio Astronomy, Kharkov, Ukraine;
(3) LESIA-Observatoire de Paris, CNRS, Paris, France

Abstract

The large high sensitive ground-based telescope NenuFAR operated in the low frequency radio range (decameter and meter wavelengths) opens new perspectives to a better understanding of Jovian non-thermal decametric radio emission (DAM). The main research tasks on Jovian DAM which can be realized with NenuFAR are related to the observations of Jovian DAM with high spectral resolution. Moreover, the high angular resolution of the NenuFAR operated as LOFAR extension gives us an opportunity to study the sources of the DAM. There are also several advantages of the simultaneous observations of the DAM with NenuFAR and other ground-based decametric radio telescopes and space-born instruments.

1. Introduction

Jupiter with the largest planetary magnetosphere in the solar system is the complex source of a powerful coherent non-thermal radio emission attributed to the mechanism of the cyclotron maser instability [Wu and Lee, 1979]. This auroral emission is a result of a complicated interaction between the exceptionally dynamic Jovian magnetosphere and energetic particles supplying the free energy from planetary rotation and the interaction between Jupiter and the Galilean moons. Thus, auroral radio emission can be regarded as a very good tool to survey the energy dissipation in the auroral zones as well as to remotely monitor the activity and dynamics of the Jovian magnetosphere. The NenuFAR provides a serious advance in planetary science and opens new approaches to a better understanding of the Jovian Decametric Radio emission (DAM) - the strongest component of the auroral radio emission of Jupiter observed in a frequency range from few MHz up to 40 MHz. The main part of the DAM is accessible for observations from the ground in the frequency range between ~10 and 40 MHz.

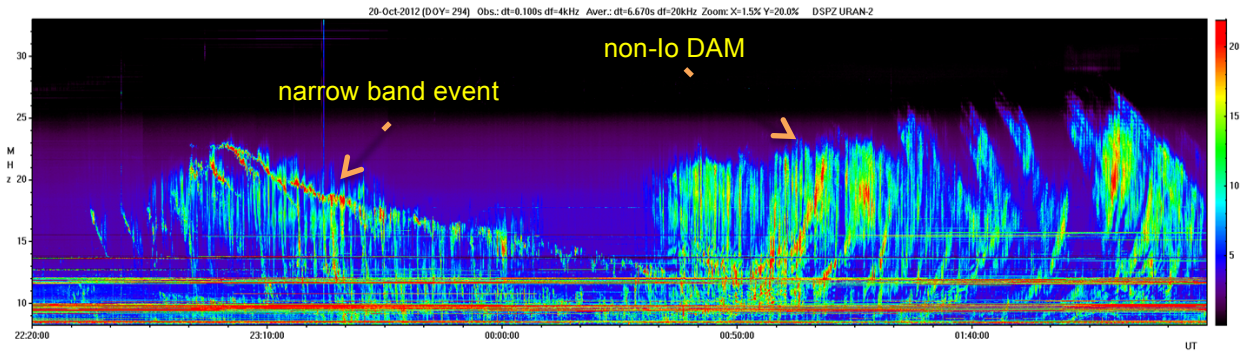

Figure 1. Jovian Io independent DAM and narrow-band radio emission observed by the URAN-2 radio telescope.

NenuFAR will consist of 1824 of dual-polarization antennas and will operate in the frequency range 10-85 MHz [Zarka et al., 2012]. The instruments will able to measure the full Stokes parameters and will have the high sensitivity (< 10 mJy). Moreover NenuFAR will be equipped with high-quality back-ends including wave form receivers and digital spectrometers. All these

make this instrument an ideal tool to study the Jovian DAM. NenuFAR project can play a significant role in the further understanding of the Jovian non-thermal radio emission.

2. *Objects of particular interest with NenuFAR as stand-alone station.*

As a stand-alone station NenuFAR will provide very high spectral resolution. Therefore the main research topic is studying of the fine spectral features in Jovian DAM such as S-bursts and quasi-continuous narrowband emission as well as analysis of the Faraday rotation and modulation lines in DAM.

Depending on the time scales the Jovian DAM emission exhibits different complex spectral structures. The „long " L- burst emission (e.g. Io and non-Io controlled DAM arcs) varies at the time scale of a few seconds, whereas „short" S-burts are characterized by millisecond duration and often have higher intensity than the L-burst. L-bursts of DAM are observed in a form of arc shaped radio bursts (in time–frequency domain on time scale of minutes) in a frequency range from a few MHz up to 40 MHz [Carr et al., 1983]. The S-bursts are detected as short impulsive spikes with fast drift in the time-frequency plane [Riihimaa, 1977; Leblanc, 1980]. The S-bursts are observed as single events or as groups of S-burst trains.

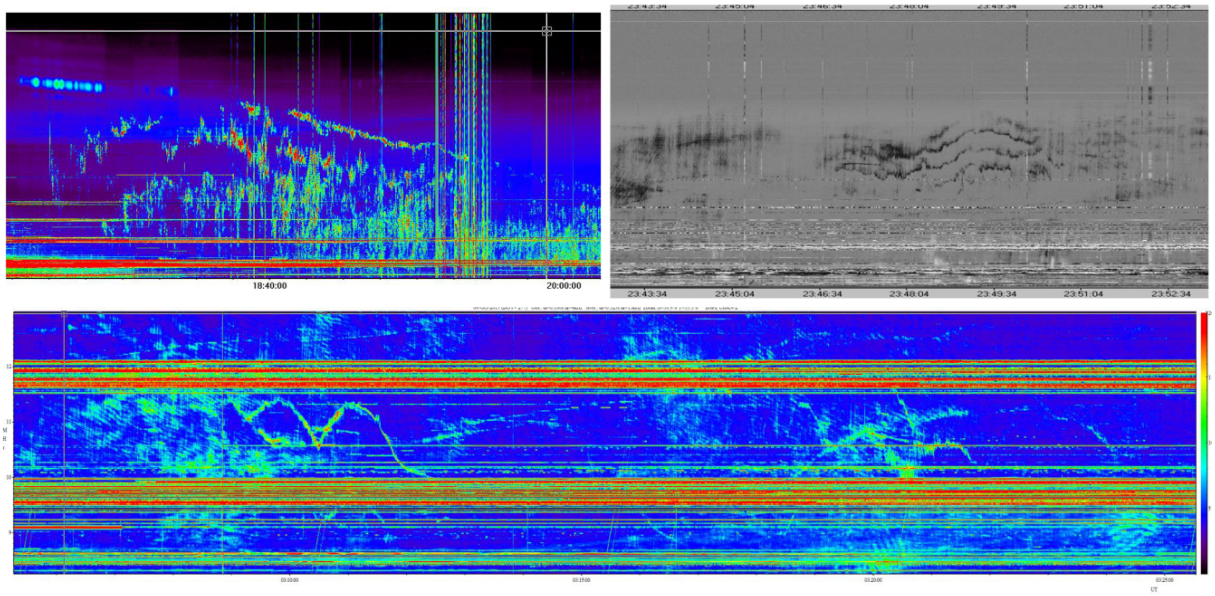

Figure 2. Examples of the fine spectral structures observed in Jovian DAM by the URAN-2 radio telescope. The temporal resolution was 0.1 sec and frequency resolution was 4 kHz.

Two types of DAM are distinguished: (1) Io independent or non-Io DAM is driven by the precipitating electrons accelerated by field-aligned currents caused, most probably, due to the breakdown of rigid corotation of the magnetosphere [Cowley et al., 2003] or reconnection in the magnetotail and the magnetopause; and (2) Io controlled or Io-DAM - satellite induced radiation caused by Jupiter-Io interaction [Saur et al., 2004]. The main part of the DAM is accessible for observations from the ground in the frequency range between ~10 and 40 MHz.

Narrowband emission and S-bursts. Very short impulsive S-bursts with fast drifting in the time-frequency plane are considered as the fundamental Jovian decameter radio emission. The narrow instantaneous bandwidth and fast frequency drift of S-bursts suggest that the source is relatively small (a few kilometers) and the electrons which produce this emission are traveling upward along the field line with a velocity on the order of 20000 km/s. The narrowband emission (NB) was

initially reported by Warwick [1963]. Sometimes NB transforms to a train of S-bursts, and vice versa. The so-called splitting events represent the NB emissions which appear on dynamic spectra as separated by 100-200 kHz narrow bands at the upper frequency limit of the Io controlled DAM emission at 21-23 MHz. Shaposhnikov and Zaitsev [1996] proposed the model in which the splitting events are generated due to conversion of the plasma waves, generated by the low frequency electrons near the upper hybrid resonance, into electromagnetic waves. According to this model, these events, being dependent on the plasma and cyclotron frequency in the source and being related to the propagation of the decametric radiation in the Jovian ionosphere, can be used as a probe of plasma parameters in the inner Jovian magnetosphere.

Faraday rotation. Highly elliptically polarized Jovian DAM [Dulk et al., 1994] observed by linearly polarized antenna exhibits Faraday fringes on the dynamic spectra due to the Faraday rotation - change in orientation of the polarization ellipse depending on wave frequency and the plasma density across the emission ray path [Ladreiter et al., 1995]. The main regions producing the Faraday rotation are Jupiter's magnetosphere, Io plasma torus, interplanetary medium and the terrestrial ionosphere. Only ~10-30% of the Faraday rotation is contributed by the Jovian magnetosphere and Io torus while the Earth's ionosphere introduce as large as about (70–90)% from the total amount of the Faraday rotation. There are methods which allow to calculate the amount of Faraday rotation [Shaposhnikov et al., 1999 and references therein] analyzing the Faraday fringes in the dynamic radio spectra. This yields an estimation of the Jovian magnetospheric plasma density and plasma inhomogeneity across the emission ray paths. The special interest is in the analysis of the Faraday rotation in the long-term observation. This can be used for the long term survey of the plasma density variation in the Jovian magnetosphere, mainly in the Io torus.

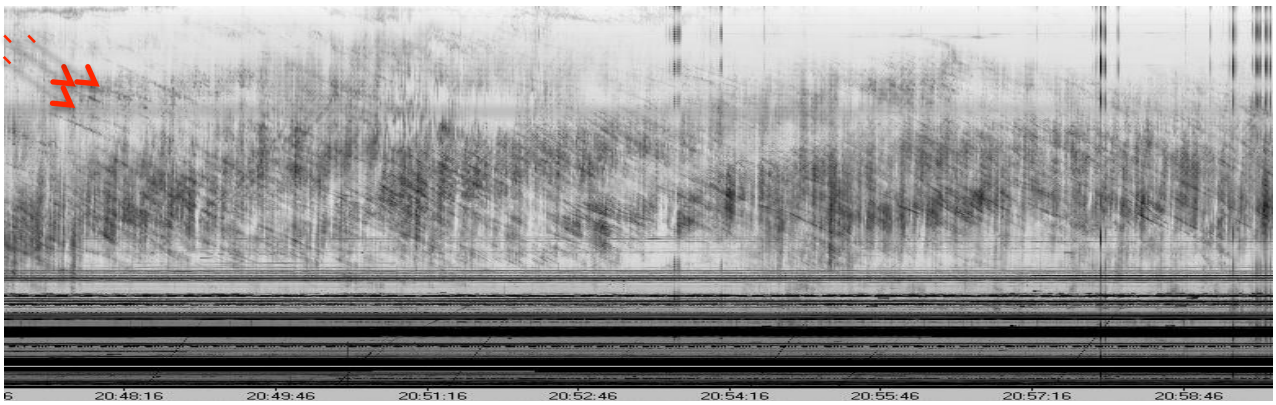

Figure 3. Modulation lines observed in Jonian DAM by URAN-2 telescope

Modulation lanes are other poorly-understood phenomena observed in the dynamic spectra with milliseconds time resolution. Modulation lanes are observed as lane structures drifting (positive and negative) in the time-frequency domain [Riihimaa, 1979]. The main explanation of this phenomenon is the radiation scattering on the regular field-aligned inhomogeneities [Imai et al., 2002] or on scattering the depleted field line tubes in the Jovian magnetosphere [Arkhypov and Rucker, 2013]. The proposed models of the modulation lanes origin generally fit the observation, but the origin of the diffracting structures is still unclear. Additionally the modulation lanes can be used for localization of magnetospheric inhomogeneities as well as of radio sources [Imai et al, 2002] and, therefore, can be regarded as a tool to probe the inner magnetosphere of Jupiter.

3. *Simultaneous observations of Jovian DAM with NenuFAR and other LF radio telescopes (e.g. UTR-2).*

Simultaneous multi-telescope observations represent the new perspective approach in the decametric radio astronomy. Contrary to stand alone observation, the multi-instrument approach has several advantages which yield detailed insight into properties of the radio emission. Simultaneous observations can also play a role of complimentary observations, when all involved telescopes operate at different frequencies record the radio phenomena in a broader frequency range, different time resolution or different modes e.g. polarization measurements, multi-beam observation. Additionally, the combination of the ground based and spacecraft observation allows us to cover the whole frequency range of DAM. Simultaneous observations provide also useful possibilities for testing the new methods of the observations and data processing.

The other useful application of the multi-telescope observations is the elimination or the decrease of the ionospheric scintillations and man-made interferences in the observed spectra. The influence of the terrestrial ionosphere is one of the major problems in the decametric radio astronomy. The partially ionized ionospheric plasma is not only an opaque barrier for the radio emission below 10 MHz, but it also produces the scintillation in the radio data due to variability and irregularities in electron density. These ionospheric scintillations, which are rapid fluctuations of phase and amplitude of the signal, strongly affects the low frequency radio signals decreasing the signal to noise ratio and distorting the signal phase. As a result the regular and irregular fluctuations of the signal are observed in the dynamic spectra. The other problem is the quasi-monochromatic interferences – the manmade radio signals from the broad-casting radio stations and other services. An effective method to identify the ionospheric scintillations and to prevent the interferences influence are the simultaneous observations of the same radio source by several spread telescopes operated under different radio interferences environment and ionospheric plasma conditions. Such multi-telescope observations allow to more reliable detection and recognition of the radio signal.

4. *Support of spacecraft missions and NenuFAR as a LOFAR extension.*

The Juno mission launched on Aug. 5, 2011 will enter a polar orbit around Jupiter. Waves instrument onboard Juno is dedicated to measuring the radio and plasma waves and will able to observe the Jovian DAM. JUICE (JUpiter ICy moons Explorer) - is the ESA's mission planned for launch in 2022 and arrival at Jupiter in 2030. The PWI (Radio & Plasma Wave Investigation) instrument onboard JUICE will use a set of sensors to detect the radio emission in the frequency range 80 kHz - 45 MHz. NeuFAR may play a significant role in observational support of these mission including simultaneous stereoscopic or supplementary observations.

NenuFAR as a LOFAR extension provides excellent angular resolution by very sensitive long baselines. High resolution imaging of the DAM sources can be used to study of the position and dynamics of the DAM sources and better understanding the relation between auroral particle precipitation processes and non-thermal radio emission.

References

Arkhypov & Rucker, *Icarus*, **226**, 1214, 2013.

Carr et al., *Physics of the Jovian Magnetosphere*, Cambridge Univ. Press, New York, 226, 1983.

Cowley et al., *J. Geophys. Res.,* **108**, 8002, 2003.

Dulk et al., *A&A.,* **286**, 683, 1994.

Imai et al., *J. Geophys. Res.,* **107,** A6, 12-1, 2002.

Ladreiter et al., *Planet. & Space Sci.* 43, 1595, 1995.

Leblanc et al., *A&A*, **86**, 3, 342, 1980.

Riihimaa, *Astrophys. & Space Sci.,* **51**, 2, 363, 1977.

Riihimaa, *A&A*, **78**, L21–L23, 1979.

Saur et al, *Jupiter: Planet, Satellites, and Magnetosph.*, Cambridge Univ. Press, 537, 2004.

Shaposhnikov and Zaitsev, *A&A,* 305, 352, 1996.

Shaposhnikov et al., *A&A,* 344, 709, 1999.

Warwick, *Astrophys. Journal*, **137**, 1317, 1963.

Wu and Lee, *Astrophys. J*., **230**, 621, 1979.

Zarka et al, P., *Proc. Annual meeting of the French Society of Astronomy and Astrophysics*, 687, 2012.

Search for exoplanetary radio emissions with NenuFAR

L. Lamy, J.-M. Griessmeier, P. Zarka, J. Girard, S. Hess, et al.

Abstract

Ongoing searches for exoplanets at low radio frequencies have not led to unambiguous detection so far. The radio emissions looked for are emitted by the magnetized circum-planetary plasmas of the solar system through a nonthermal coherent electron cyclotron emission. They are primarily driven by the interaction between planetary magnetospheres and the solar wind, or the planet's ionosphere or satellites. Radio detection will be information-rich, including the characterization of many planetary properties (as the magnetic field amplitude and tilt, rotation period, orbital period and inclination, nature and characteristics of the electrodynamic coupling at work) unachievable by other exoplanet observational means. The NenuFAR facility is well adapted to push this search ahead to the lowest frequency domain observable from the ground (extending that of LOFAR down to 10MHz) with high sensitivity, instantaeous measurements of all Stokes parameters, and long-term observations.

1. Introduction

Planets appear to be the most favourable cradle of life in the context of present astrobiology. With the growing number of exoplanets (>1800) detected by radial velocity or transits, which cover a broad range of sizes, masses, orbital parameters, it is increasingly desirable to determine the physical properties of exoplanetary systems to carry in-depth comparative studies. Topics of interest include planetary dynamos (large-scale planetary magnetic fields play an important role in protecting the planet's surface and atmosphere from the interplanetary medium), magnetospheric dynamics, energetics of star-planet interactions, planetary rotation, etc.

Experience from our solar system planets and theory tell us that the most intense electromagnetic emissions from magnetospheres result from coherent cyclotron radiation, through which keV electrons in strong magnetic fields generate intense, circularly polarized, sporadic emissions in the MHz to tens of MHz range (synchrotron emission is also produced at higher frequencies, but with a much lower intensity). Measuring the dynamic spectra in intensity and (circular) polarization of these cyclotron emissions can give access to the above physical parameters, as well as orbit inclination and the presence of satellites.

In section 2, we summarize our observational and theoretical knowledge of solar system magnetospheres and radio emissions, review the drivers for electron acceleration (star-planet or stellar wind-planet interactions, and magnetosphere-ionosphere or magnetosphere-satellite coupling), and extrapolate them to various exoplanetary conditions. In section 3, we summarize past and ongoing observations. Non detections put stringent limit on planetary emission above ~150 MHz, and hints of detections remain to be confirmed. In section 4, we examine the prospects for NenuFAR observations, including early science operations in Phase 1. In section 5, we give a special attention to synergies, both with other radio observations and with observations at other wavelengths.

2. Background and Motivation

2.1 Solar system magnetospheres and radio emissions

The Earth, Mercury, Ganymede, and the giant planets of the solar system all contain internal dynamo currents that generate planetary-scale magnetic fields. These internal dynamo currents arise from differential rotation, convection, compositional dynamics, or a combination of these in objects' interiors.

Interaction of these planetary-scale magnetic fields with the solar wind creates a magnetosphere, a cavity in the wind dominated by the planet's magnetic field. Inside the cavity, charged particles are accelerated to keV-MeV energies by various processes (magnetic reconnection at the boundaries, interaction with embedded moons, waves…).

Accelerated charged particles in a magnetic field generate radio emissions. The most intense ones are produced at high magnetic latitudes (so-called auroral, circumpolar regions) by a nonthermal coherent process

well-identified today, that involves keV electrons: the Cyclotron Maser Instability (CMI) *[Treumann, 2006]*. This process widely operates at all magnetized planets, which are thus strong radio emitters *[Zarka, 1998]*.

Emitted frequencies are local cyclotron frequencies met by energetic electrons moving along magnetic field lines. Their range extend from very low values (a few kHz) far from the planet, up to the maximum surface cyclotron frequency (f_{ce} [MHz] = 2.8 B [G] ; 1 G = 10^{-4} T). For most solar system planets, planetary surface field magnitude is ≤1 G, thus emitted frequencies lie below ~2 MHz. They are reflected off by the Earth's ionosphere and thus cannot be detected from the ground. Jupiter, having a stronger dynamo and surface field (up to 14 G), emits CMI radiation up to 40 MHz, which consists of bursts of duration from sub-millisecond to several tens of minutes. These bursts are easily detected by ground-based radiotelescopes.

MeV electrons also produce synchrotron emission in Jupiter's inner magnetosphere (so-called radiation belts) *[de Pater, 2004]*. Its spectrum extends over high harmonics of the cyclotron frequencies, up to several GHz. The synchrotron process is a nonthermal incoherent mechanism, much less efficient than the CMI, so that this emission is 10^5 times weaker than the CMI. It is also much more stable in time, showing variations at timescales longer than days/weeks.

2.2 Predictions for radio emissions from exoplanets

Due to the high efficiency of the CMI, Jupiter's auroral radio emissions are extremely intense (brightness temperature ≥10^{19} K, flux density ≥10^7 Jy at Earth *[Zarka, 2004]*), as intense as solar ones (which are mostly due to plasma radiation), as shown on Figure 1.

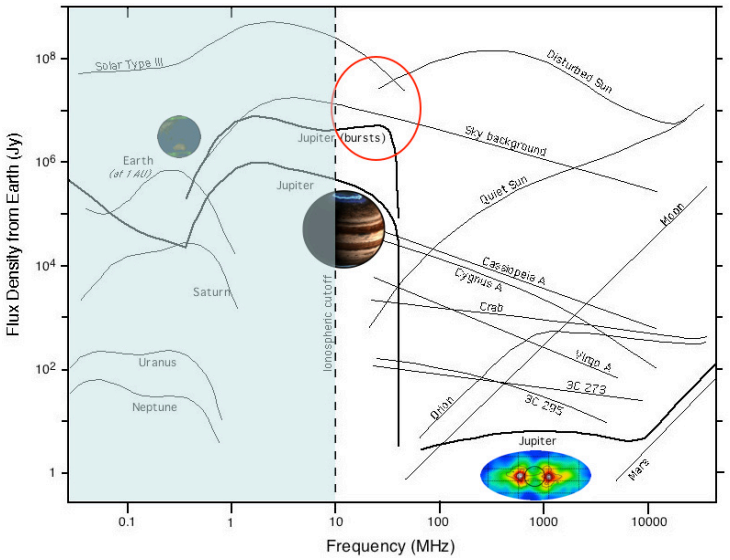

Figure 1 : Spectra of astronomical radiosources detected from the Earth's vicinity. Auroral planetary spectra lie below the Earth's ionospheric cutoff, except Jupiter's decametric (CMI, auroral and Io-induced) and metric-decimetric (synchrotron) emissions. Normalized to the same observer distance of 1 AU, Jupiter's spectrum must be upscaled by ×20, Saturn's by ×100, Uranus' by ×400, and Neptune's by ×900, so that all are grouped within 2–3 orders of magnitude.

Considering this favourable planet-star contrast ~1, much larger than in the visible (~10^{-9}) or infrared (~10^{-6}) ranges, observational searches for low frequency radio emission from exoplanets started even before the confirmed discovery of any exoplanet *[Zarka, 2011, and references therein]*. It proved to be a difficult task and no unambiguous detection has been obtained yet (see below). But the discovery of many exoplanets by radial velocities and transit methods has motivated both theoretical and observational work on magnetospheric emissions from exoplanets.

It was soon realized that due to the high brightness of the galactic radio background, Jupiter's decametric CMI emission cannot be detected at stellar distances (several pc) even with the largest existing instruments. The search for more intense planetary emissions followed two complementary directions: (i) establishing empirical scaling laws for radio emissions from solar system planets and extrapolating them to exoplanets, and (ii) identifying the primary engine of planetary radio emissions and the regime of parameters which allow this engine to produce more powerful emissions.

A scaling law was first found to relate the magnetospheric radio output with the total solar wind power input (dominated by the solar wind ram pressure) on the magnetospheric cross section *[Farrell et al., 1999]*, with a proportionality constant ~10^{-5}. The specific case of coronal mass ejections (CME) impacting a magnetosphere was also considered *[Griessmeier et al., 2007]*. A second scaling law was found to relate the

magnetospheric radio output with the incident Poynting flux convected by the solar wind on the magnetospheric cross section *[Zarka et al., 2001 ; Griessmeier et al., 2007]*, with a proportionality constant ~a few × 10^{-3}, as illustrated in Figure 2. The latter results were obtained by considering average planetary emissions, but these are intrinsically highly variable and the 10% (1% resp.) most intense events were found to display intensities larger by 1 (2 resp.) orders of magnitude, hence shifting the Y-intercept of Figure 2 toward higher values. This scaling law was found to apply more generally to any plasma flow-obstacle interaction, including Io-Jupiter and Ganymede-Jupiter interactions, and at least to one documented example of magnetized binary star (the RS CVn system V711τ) *[Zarka, 2010]*.

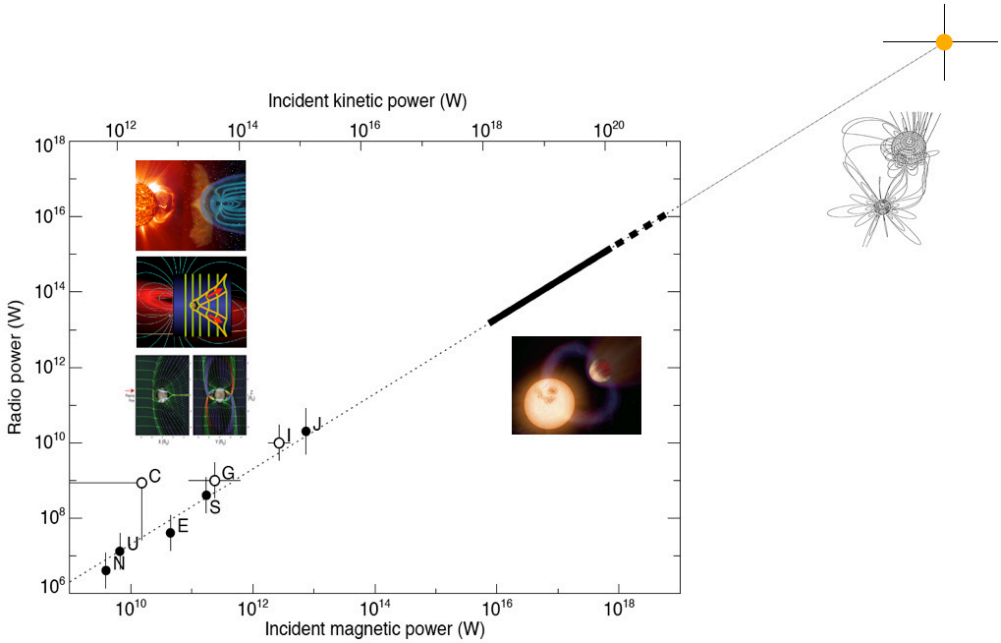

Figure 2 : Scaling law relating magnetospheric (Earth, Jupiter, Saturn, Uranus and Neptune) and satellite-induced (Io, Ganymede, Callisto) radio power to incident Poynting flux of the plasma flow on the obstacle. Dashed line has slope 1, emphasizing the proportionality between ordinates and abscissae, with a coefficient 2×10^{-3}. The thick bar extrapolates to hot jupiters the magnetospheric interaction (solid) and satellite-planet electrodynamic interactions (dashed). The orange dot illustrates the case of the RS CVn magnetic binary V711 τ (cf. text). Insets sketch the types of interaction.

The physical mechanisms underlying these scaling laws include magnetospheric compressions by the solar wind or CME and associated shocks, magnetic reconnection between the magnetic fields of the flow and of the obstacle, and Alfvén waves produced by the so-called "unipolar inductor" interaction of a conducting non-magnetized body (the moon Io) moving across magnetic field lines (of Jupiter). All these mechanisms lead to the acceleration of electrons that in turn emit radio waves. *Jardine and Cameron [2008]* proposed direct electron acceleration at the magnetosphere's nose through a runaway mechanism. *Nichols [2011]* estimated the power dissipated by magnetosphere-ionosphere coupling, independent of the solar wind.

For exoplanets orbiting very close to their parent star, especially hot jupiters, it was found that star-planet magnetic/plasma interactions (SPI - incl. magnetospheric compression, magnetic reconnection, and unipolar inductor) involve a power 10^3 to 10^6 times larger than that of the solar wind-Jupiter interaction *[Zarka, 2007]*. In the unipolar inductor case, the star needs to be strongly magnetized (surface field $\geq10^{1\text{-}2}$ G), the exoplanet plays the role of Io and its parent star that of Jupiter. Extrapolating the above scaling laws, their radio output should accordingly be 10^3 to 10^6 times that of Jupiter. *Willes and Wu [2005]* studied the particular case of terrestrial planets in close orbits around magnetic white dwarf stars, acting as a unipolar inductor, and generating CMI radio emission with large flux densities. These systems could be remnants of main sequence stars with a planet surviving the stellar expansion phase and back in stable orbit.

For exoplanetary magnetospheres governed by internal processes (magnetosphere-ionosphere coupling), it was found that for giant planets orbiting at a few AU from their parent star, the auroral radio output may reach

10^4 to 10^5 times that of Jupiter if the star has a strong X-UV output and the planet has a fast rotation (P=1-3 hours).

All theoretical predictions thus suggest that exoplanetary magnetospheric radio emissions much stronger than Jupiter's are likely to exist, and thus be detectable at stellar distances with large enough instruments. Sporadic further amplifications may occur e.g. due to scintillations. CMI radio emission generated within the exoplanet's magnetosphere is likely to be restricted to low frequencies (10s of MHz, depending on the planetary field strength), whereas unipolar inductor driven CMI emission, being excited by the exoplanet in the stellar magnetic field, may reach higher frequencies (100s MHz to a few GHz).

Finally, it must be noted that CMI radiation is strongly circularly/elliptically polarized (synchrotron emission from Jupiter's radiation belts is linearly polarized), and beamed anisotropically so that it is generally strongly modulated by the planetary rotation and revolution around its host star. Conversely, solar/stellar plasma radiation is essentially unpolarized and sporadic. Even in the absence of sufficient angular resolution (known exoplanets orbit at <<1" from their parent star), polarization and temporal modulations should allow to discriminate stellar and exoplanetary radio emissions.

Theoretical predictions thus suggest that detection and identification of CMI radio emission from exoplanets is possible, so that it is worth observing. But what do we have to learn through radio emission detection ?

2.3 Motivations for the search for exoplanet's radio emissions

Planetary magnetic fields are a window to a planet's interior, and magnetospheric radio emissions are a probe of planetary magnetic fields. Ground-based detection of Jupiter's decametric radio emission *[Burke and Franklin, 1955]* provided the first proof of existence and the first measurement of the Jovian magnetic field. Its monitoring allowed us to define accurately the rotation of its interior, and to discover the existence of a strong interaction between the moon Io and the Jovian magnetosphere *[Bigg, 1964]*. Maps of the synchrotron emission revealed the tilt of the magnetic field relative to the rotation axis (~10°) *[Berge and Gulkis, 1976]*. Magnetospheric radio emissions are thus a unique tool for probing exoplanet's interior structure (composition, thermal state) and dynamics (including the effect of spin-orbit locking for hot jupiters), leading to an improved understanding of the planetary dynamo process.

Each planetary magnetosphere - in our solar system - is a space plasma physics laboratory. In-situ spacecraft exploration and remote electromagnetic (Radio, UV, IR, X) observations permitted to infer their general properties, but also revealed numerous specificities related to the magnetic field amplitude, tilt, distance to Sun, presence of embedded moons and rings, atmospheric composition …

The CMI theory provides a well-understood, quantitative framework for studying magnetospheric radio emissions properties and using them as a diagnostic tool of planetary plasma environments and processes. Recent exhaustive simulations in that framework *[Hess and Zarka, 2011]* showed that the measurement of the radio dynamic spectrum - in intensity and polarization - of an exoplanetary system would bring the following informations (difficult or impossible to determine by other means) about these objects, as illustrated in Figure 3 : in addition to the exoplanet's magnetic field intensity and tilt, one will be able to measure the planetary rotation and revolution periods (effectively testing tidal spin-orbit synchronization), the orbit inclination (resolving the ambiguity on the planet's mass), and identify the primary engine of the electromagnetic output of the system: SPI (magnetospheric compression, stellar wind-magnetosphere magnetic reconnection, or "unipolar inductor" interaction if the exoplanet is weakly magnetized and the star strongly magnetized), or internal magnetospheric processes (magnetosphere-ionosphere or magnetosphere-moon coupling). Temporal modulations different from the planetary rotation and orbital periods could additionally reveal the presence of moons and/or the signature of stellar wind activity.

Similar to the question of solar system formation, which requires comparison of numerous systems to infer general properties, the recent field of comparative magnetospheric physics (which relies on a corpus of 6 planetary magnetospheres so far) will considerably expand with the detection of exoplanetary radio emissions, that will permit to explore a large range of parameters (star-planet distance, stellar magnetic field and wind strength, stellar X-UV flux, planetary magnetic field, rotation, orbit inclination …). We will be able to study interactions between plasma flows (magnetized or not) and obstacles (magnetized or not) in various regimes, and to infer the energy dissipation involved in SPI. Furthermore, the above scaling laws will be confirmed and/or modified or refined, expanding their range of application and their predicting capability.

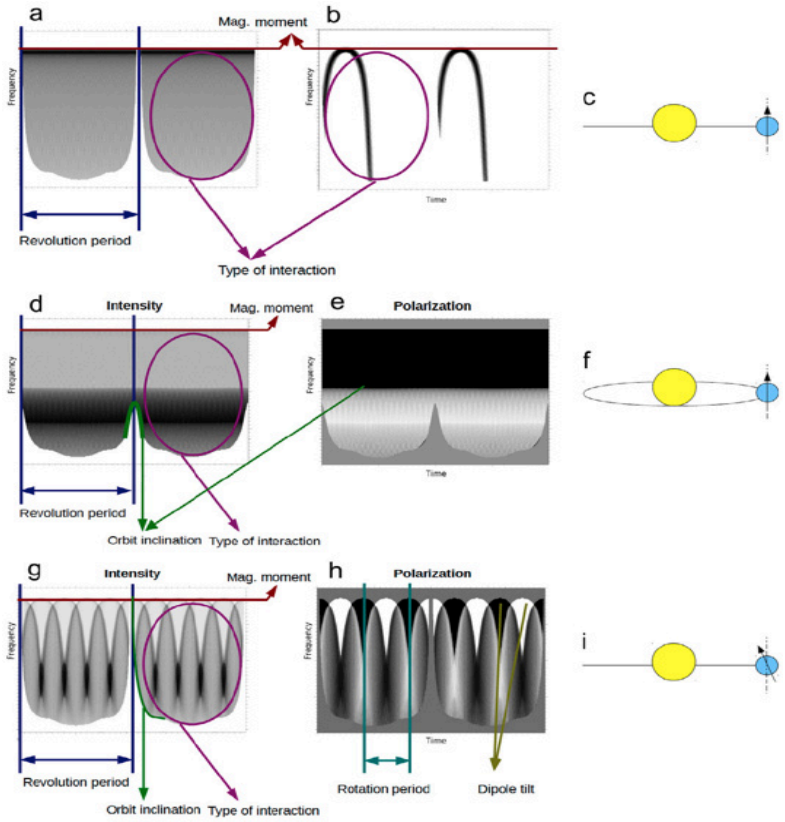

Figure 3 : Simulated dynamic spectra in intensity (a,b,d,g) and circular polarization (e,h) and associated parameters of the system that can be determined: (a,b,c) exoplanetary magnetic field aligned with the rotation axis and 0◦ orbit inclination, for emission (a) of a full exoplanet's auroral oval and (b) an auroral active sector fixed in local time. (d,e,f) aligned exoplanetary magnetic field and 15◦ orbit inclination, for emission of a full auroral oval. (g,h,i) exoplanetary magnetic field tilted by 15◦ and 0◦ orbit inclination, for emission of a full auroral oval. From *[Hess and Zarka, 2011]*.

Existence of a magnetosphere is also an essential ingredient in favour of the possibility to develop life: it ensures shielding of the planet's atmosphere and surface, preventing O_3 destruction by cosmic rays bombardment as well as atmospheric erosion by the stellar wind. It also limits atmospheric escape, as ionized material following dipolar field lines returns to the atmosphere *[Griessmeier et al., 2004, 2005]*.

Finally, radio detection may evolve as an independent discovery tool, complementary to radial velocities or transit measurements because it is more adapted to finding planets (giant or terrestrial) around active, magnetic or variable stars.

3. Past and ongoing observations and results

Most of the searches focussed on known exoplanetary systems discovered by radial velocity or transits measurements. Application of scaling laws to the exoplanet census (e.g. from *www.exoplanet.eu*) guided target selection *[e.g. Lazio et al., 2004; Griessmeier et al., 2007, 2011]*, with promising candidates such as τ Boo, υ And or 55 Cnc. A review of past and ongoing observations has been given by [*Zarka et al., 2014*] and will not be duplicated here. We will only remind that first, encouraging, hints of detection have recently been achieved at high frequencies : GMRT observations of 153 MHz identified a signal in the range 4-30 mJy from 5 planetary systems which remain to be confirmed though*[Lecavelier et al., 2013 ; Sirothia et al., 2014]*, while no positive result has been obtained at lower frequencies, especially in the 10-100MHz range. This may be due to intrinsically low intensities and/or relatively rare strong emitters and/or intrinsically bursty emissions (*e.g.* intense arc-shaped radio emissions of Jupiter/Saturn typically last for a few h, as illustrated in Figure 3b) with respect to a low duty cycle *[Zarka, 1998 ; Zarka et al., 2004a]*. In addition, less than a few % of presently known exoplanets (http://exoplanet.eu/) have been observed, for no more than a few hours each, thus the parameter space is still largely unexplored. We are thus in a situation where efforts intensify, both for targeted observations (still at a modest level with large instruments) and systematic searches in sky surveys (that become available for the first time at low enough frequencies).

4.Science outcome enabled by NenuFAR-1/NenuFAR

4.1 An instrument adequate to track exoplanetary signals

The result of past searches suggest that magnetospheric radio emissions much stronger than Jupiter's and at frequencies ≥150 MHz is rare (see Figure 4). Jupiter bursts in the 30-40 MHz range can exceed 10^7 Jy at Earth, i.e. ~20 mJy at 1 pc range, the average flux density of the emission at hour timescale being about one order of magnitude lower. It is thus needed to explore a large sample of targets with highest possible continuum sensitivity, preferably at low frequencies (although unipolar inductor driven CMI emission may reach hundreds of MHz). In this frame, NenuFAR will ideally complement the capabilities of existing radiotelescopes by extending the LOFAR-LBA and UTR-2 frequency range to 10-85MHz, with a high sensitivity and instantaneous measurements of all the Stokes parameters. Indeed, the final NenuFAR effective area (~60000m^2@30MHz) achieved with its 96 mini-arrays, each made of 17 crossed-dipoles, will by twice that of the LOFAR-LBA core or ~75% of the total LOFAR-LBA effective area, hence comparable to LOFAR sensitivity displayed in Figure 4. NenuFAR-1 will already reach a fair effective area (~15000m^2@30MHz) over the same frequency range with ~24 mini-arrays out of 96.

When a signal is detected attributing it to the exoplanet's magnetosphere, to an exoplanet-induced signal into the star's magnetic field, or to exoplanet-independent stellar activity should be relatively easy on the basis of polarization and temporal modulations of the signal. Thus measurements in circular (V-Stokes) or full polarization (4-Stokes) are required, over long or repeated observations for each target. Confusion will also be lower in V-Stokes measurements, and long observations will allow to search for Jupiter-like bursts from exoplanets with less limitation by confusion (provided that the beam shape remains smooth and stable with time).

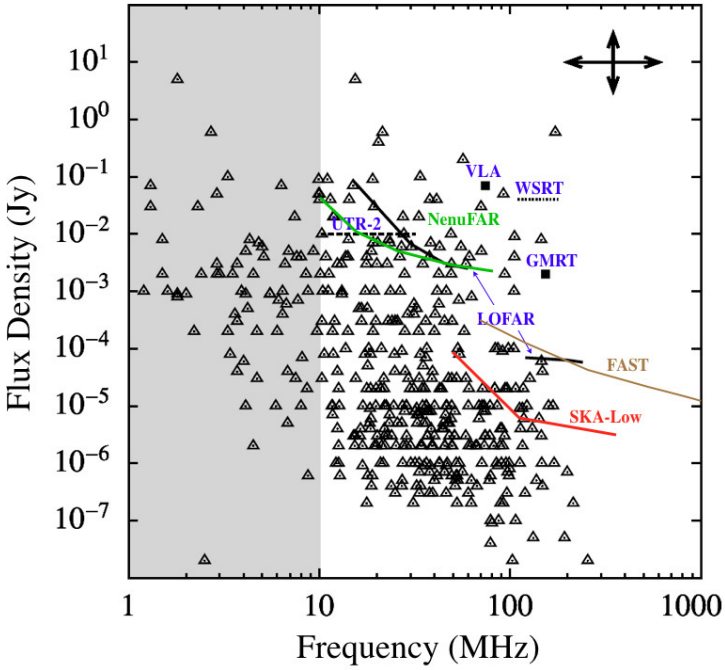

Figure 4 : Predicted maximum emission frequency and expected radio flux for known exoplanets (in 2011, indicated by triangle symbols) for a rotation-independent planetary magnetic field and the scaling law of Fig. 2. The approximate sensitivity of several instruments is shown (for 1 h of integration time and a bandwidth of 4 MHz). Frequencies below 10 MHz are not observable from the ground (ionospheric cutoff). Adapted from *[Griessmeier et al., 2011]*.

4.2 Observational modes and strategy toward a detection

NenuFAR will be able to operate in several complementary configurations : (i) either as a stand-alone instrument thanks to a dedicated receiver and/or coupled to LOFAR, and (ii) through imaging or beamforming observational modes.

(i) The configuration coupling NenuFAR to LOFAR (so called LOFAR super station or LSS) will provide the most sensitive observations and the highest spatial resolution for interferometry. However, the maximal

sensitivity reached by LSS will imply a huge data rate (and complex data processing) for a modest gain of sensitivity wrt NenuFAR alone, and the expected angular resolution of 2 arcsec will not be enough to resolve any star-exoplanet system while limiting the time-frequency resolution. Therefore, the most significant value-added of NenuFAR will rely on its standalone use, which will enable a high duty cycle with maximized time-frequency resolution.

(ii) Experience from LOFAR, that uses elementary dipole antennas seeing a large fraction of the sky at any time, taught us that imaging is generally more powerful than beamformed observations at detection stage, because it allows to better remove the contribution of sources around the target to obtain high dynamic range images. The low angular resolution of NenuFAR in standalone mode (~1°) will limit the imaging capability and imply a large confusion noise (see section 1). We will use both this coarse resolution imaging (in a broad field of view of 8°-60° diameter) and beamformed observations in order to monitor time variations revealing planetary bursts. Beating the confusion will require circularly polarized (or full Stokes) observations, accurate calibration of the beam shape versus pointing direction, and monitoring of the ionospheric distorsions of the effective beam, in order to reach a sensitivity as close as possible to the thermal noise limit.

Predictions of Figure 4 show that, similar to LOFAR, NenuFAR should be able to detect any radio emission (especially bursts) ~10^3 times stronger than Jupiter's up to ~10 pc, and any emission one order of magnitude stronger up to a distance of ~30 pc. The search strategy should concentrate on the most favourable targets (i.e. stars within 5 to 10 pc, known exoplanets for which a large radio flux is predicted *[Lazio et al., 2004; Griessmeier et al., 2007, 2011; Nichols, 2012]*, or for which hint of detection exist *[Lecavelier et al., 2013 ; Sirothia et al., 2014]*, and known exoplanets orbiting strongly magnetized stars) and by conducting systematic surveys (of multi-planetary systems, of the Kepler field-of-view etc.). For each target, several observations of several hours each should be performed to account for visibility effects (taking into account the expected location of radio sources – generally fixed in Local Time for SPI-driven emissions – together with the narrow beaming of CMI emission, simulated in Figure 3), or intrinsic variability.

Maximum sensitivity and circular or full-polarization measurements will be needed at all times. Modest temporal and spectral resolutions will be needed for meeting the physical objectives described above, typically $\delta f/f \approx 1\%$ (or ~1 MHz spectral channels) and $\delta t \approx 1$ sec to 1 min. Finer resolutions will be temporary required for the purpose of RFI mitigation before post-integration. The large number of targets to observe several times requires large duty cycles and large fields of view. The availability of several beams (or coarse imaging) will be a significant advantage for exoplanet search, as for searches or any other transient signals (exoplanetary radio emissions are slow transients).

5. Synergies with other observations

Besides LOFAR, the “natural complement” of NenuFAR, good sensitivity observations in a broad spectral range ≥70 MHz shoud be provided by the FAST radiotelescope in 2016+ (that will cover the declination range from -34° to 86°, almost similar to NenuFAR’s) *[Nan et al., 2011]*. In 2020+, SKA will improve by a factor 10 to 30 the sensitivity above 50 MHz,but cover mostly the southern hemisphere. NenuFAR will thus remai a complementary facility, e.g. for follow-on observations of SKA-Low candidates (in the overlapping part of the sky).

Measurements of stellar magnetic fields by Zeeman-Doppler imaging (with instruments such as CFHT/Espadons and TBL/Narval in visible light, and with CFHT/Spirou in the infrared in the near-future) are a key ingredient to assess SPI whose associated emission will be measured with NenuFAR/NenuFAR-1. Magnetic topology can impact on the direction of emission of CMEs and in turn their impact on orbiting exoplanets. Measurements of large magnetic fields will also motivate NenuFAR/NenuFAR-1 observations in search for unipolar inductor emissions *[Farès et al. 2010]*.

UV and X observations by HST, XMM-Newton, Chandra, and in the future the Athena+ X-ray observatory will characterize stellar outputs and allow to identify best exoplanet candidates for enhanced magnetosphere-ionosphere coupling *[Nichols, 2011, 2012]*. Observations of large flares can also motivate specific searches of radio emissions triggered by these flares (in parallel with spectroscopic studies of their impact on exoplanet's atmosphere), as it was done successfully to detect Uranus’ aurorae *[Lamy et al., 2012]*.

The number of known planets in the solar neighbourhood should increase substantially thanks to the missions PLATO (Planetary Transits and Oscillations of stars) and TESS (Transiting Exoplanet Survey Satellite), whereas Spirou will find Earth-like planets around nearby red dwarfs. The JWST will be able to characterize the atmospheres of these nearby planets, whereas magnetospheric studies with SKA will bring constraints to their habitability. Studies of lower mass planets will also provide insights to different regimes of planetary dynamos.

New surveys by the ESO-VLT instruments NGTS (Next-Generation Transit Survey) and ESPRESSO (Echelle SPectrograph for Rocky Exoplanet and Stable Spectroscopic Observations) will likely increase the number of confirmed exoplanets up to several tens per field of view of NenuFAR.

6. Conclusion

Thanks to our experience of solar system magnetospheres and radio emissions, and extensive theoretical studies, the interpretation frame of exoplanetary radio observations is ready, waiting for the first confirmed detections and measurements of dynamic spectra. Beyond the measurement of several exoplanet's parameters, including the magnetic field (with implications on dynamo theory and habitability) and rotation, radio detections will open the new field of comparative exoplanetary magnetospheric physics and permit to study flow-obstacle plasma interactions in various speed, density, magnetic field, mass regimes, from hot jupiters to low-mass planets around (M) dwarfs.

Up to now, detecting the signal is the most difficult step. But the characteristics of NenuFAR (probing the 10-85 MHz range, with a sensitivity of a few mJy, full-Stokes measurements) make it a powerful instrument able to detect intense Jupiter-like emission within a few parsecs, as predicted by scaling laws (and provided that Jupiter's magnetic field and radio flux density are not exceptionally high).

The context of these searches will be favoured by the expected rapid growth in the number of known exoplanets new years due to new instruments and space missions (PLATO, TESS, JWST, NGTS, EXPRESSO…). In order o take full advantage of this context, large duty-cycle are needed (repeated, hours-long observations). Observations will include targeted searches, commensal observations, and correlation of surveys to up-to-date exoplanet catalog. Radio flux densities of 1000 x Jupiter's will be detectable within 10 pc, where all stars should be observed. A large fraction of all stars within 30 pc should be observed, with a detection threshold one order of magnitude larger. All exoplanets should eventually be the subject of targeted searches, starting with systems with large stellar magnetic field or large X-UV flux.

Such synergies with observations at different wavelengths will be important. Eventually, radio detection may evolve as a discovery tool, e.g. adapted to finding planets (giant or terrestrial) around active, magnetic or variable stars. The realm that remains to explore is huge.

References

Berge, G.L. and S. Gulkis, S., in Jupiter, T. Gehrels el., Univ. Arizona Press, pp. 621–692, 1976

Bigg, E. K., Nature, 203, 1008–1010, 1964

Burke, B. F., and K. L. Franklin, J. Geophys. Res., 60, 213–217, 1955

de Pater, I., Planet. Space Sci., 52, 1449–1454, 2004

Farès, R., et al., MNRAS, 406, 409–419, 2010

Farrell, W. M. et al., J. Geophys. Res., 104, 14025–14032, 1999

Griessmeier, J.-M., et al., Astron. Astrophys., 425, 753–762, 2004

Griessmeier, J.–M., et al., Astrobiology, 5(5), 587–603, 2005

Griessmeier, J.–M., et al., Astron. Astrophys., 475, 359–368, 2007

Griessmeier, J.-M., et al., Radio Science, 46, RS0F09, 2011

Jardine, M., and A. C. Cameron, Astron. Astrophys., 490, 843, 2008

Hess, S. L. G., and P. Zarka, Astron. Astrophys., 531, A29, 2011

Lamy, L., et al., Geophys. Res. Lett., 39, L07105, 2012

Lazio, T. J. W., et al., Astrophys. J., 612, 511–518, 2004

Lecavelier des Etangs, A., et al., Astron. Astrophys., 552, A65, 2013

Nan, R., et al., Int. J. Modern Phys. D, 20 (6), 989, 2011

Nichols, J. D., MNRAS, 414, 2125–2138, 2011

Nichols, J. D., MNRAS, 427, L75–L79, 2012

Sirothia, S. K., et al., Astron. Astrophys., 562, A108, 2014

Treumann, R., Astron. Astrophys. Rev, 13, 229–315, 2006

Willes, A.J., and K. Wu, Astron. Astrophys., 432, 1091–1100, 2005

Zarka, P., et al., in Planetary Radio Emissions IV, H. O. Rucker et al. eds., Austrian Acad. Sci. Press, 51–63, 1997

Zarka, P., J. Geophys. Res., 103, 20159–20194, 1998

Zarka, P., et al., Astrophys. Space Sci., 277, 293-300, 2001

Zarka, P., Planet. Space Sci., 52, 1455-1467, 2004

Zarka, P., Planet. Space Sci., 55, 598-617, 2007

Zarka, P., in Pathways Towards Habitable Planets, ASP Conf. Ser., Vol. 430, V. Coudé du Foresto et al. eds., 175-180, 2010

Zarka, P., in Planetary Radio Emissions VII, H. O. Rucker et al. eds., Austrian Acad. Sci. Press, 287-302, 2011

Zarka, P., Lazio, T. J. W., Hallinan, G., & Astrobiology Science working group., in Advancing Astrophysics with the Square Kilometre Array, ed. SKAO, submitted, 2014

Zarka, P., Di Li, et al., Detecting exoplanets with FAST ?, Research in Astronomy and Astrophysics, submitted, 2014b

Observations of planetary lightning with NenuFAR

Jean-Mathias Grießmeier, Julien Girard, Philippe Zarka

Summary: Lightning on Saturn and Uranus have been discovered by the Voyager spacecraft in 1980–1981 and re-observed by Cassini. Ground-based observations using large dipole arrays have recently become possible, providing complementary information at high time resolution. Venus, Mars, Jupiter, and Neptune have been suggested to have occasional lightning activity, but no firm detection has been achieved. We assess the potential of NenuFAR-1 and NenuFAR to contribute to solar system planetary lightning studies.

Lightning is a transient, high-current electrostatic discharge resulting from macroscopic electric charge separation (by convection and gravitation combined), following small-scale particle electrification (via collisions and charge transfer). A large-scale electric field builds up, which may eventually lead to breakdown and ionise the ambient medium, causing a lightning stroke. A lightning discharge consists of many consecutive strokes of a few μs duration and lasts typically 1-100 msec. It may have an important role in the atmospheric chemistry (production of non-equilibrium trace organic constituents, potentially important for biological processes). Electromagnetic signatures include optical, VLF and LF radio emissions. The radio emission generated by lightning is broadband in nature; for example, the spectrum of terrestrial lightning peaks at 10s of kHz, but extends to much higher frequencies. The emission was found to extend to the VHF range (30-300 MHz) and above (cf. review by LeVine 1987).
Satellite observations showed that this phenomenon is not limited to our own planet, but takes place also for other planets in the solar system. However, because of the limited reach and lifetime of satellite missions, the amount of available data is rather limited. Recently, first ground-based observations became available, complementing the satellite observations. We review the main characteristics of lightning on the different solar system planets and evaluate the potential of LOFAR, NenuFAR-1 and the full NenuFAR array to contribute to this science field.

Lightning on Venus

On Venus, the existence of lightning has remained controversial for more than two decades (Zarka et al. 2004, 2008). Data obtained by Venera, Pioneer-Venus, Galileo and Cassini indicate that Venus lightning, if it exists, is either extremely rare (1 flash/hour, with long intervals of atmospheric electrical inactivity, as for Saturn), very weak (10^{2-3} times weaker than their terrestrial counterparts), or restricted to low frequencies (e.g. slow strokes with a very steep HF spectrum) which are unable to cross Venus' ionosphere. The whistler-mode waves detected by the Venus Express Magnetometer could either be associated to Venus lightning (Russell et al. 2007), or to local plasma waves, which are known to occur in a non magnetic ionosphere in interaction with the solar wind (see e.g. Strangeway 2004). The absence of lightning could be explained by a very low vertical convection inhibited by the strong horizontal atmospheric circulation.

Assuming that the non-detection of Venus lightning in radio comes from their intrinsically low intensity rather than from a low occurrence rate, one can infer an upper limit on their flux density spectrum at the Earth. This way, Zarka et al. (2004) calculated upper limits for the radio emission from that Venus, finding values between 2×10^{-4} and 0.7 Jy at 10 MHz. This is below the detection threshold of LOFAR and NenuFAR. However, the non-detection can also result from a low occurrence rate of Venus lightning. For this reason, monitoring with one beam is suggested to monitor Venus for potential rare and intense events.

Lightning on Earth

As noted above, terrestrial lightning is a source of intense, broadband radio emission. It peaks at 10s of kHz, but extends to much higher frequencies, with the power decreasing as a power-law. A power spectrum with a slope of f^{-2} at intermediate frequencies (up to 5 MHz) is observationally confirmed (Weidman et al. 1981, LeVine 1987, Willett et al. 1990). At high frequencies (> 10 MHz), the case it less clear: While some authors measure the same spectral slope of f^{-2} up to frequencies of almost 100 MHz (cf. review by LeVine 1987), others find spectral slopes decreasing as f^{-10} (Weidman et al. 1981, Willett et al. 1990).

Spectral measurements can be obtained with LOFAR or NenuFAR. Already with the first prototype station of LOFAR, LOFAR-ITS it was possible to detect terrestrial lightning discharges with a high temporal resolution, and to measure the broad-band spectrum between 10 and 35 MHz (Holleman et al. 2006). It was found that LOFAR-ITS already was an extremely sensitive detector, as it found a larger number of discharges than the SAFIR lightning detection network of KNMI. The main requirement thus is not sensitivity, but the availability of the instrument on a short notice (target of opportunity observation). Here, NenuFAR and even NenuFAR-1 can make an excellent contribution.

In addition to cloud-to-ground lightning and intracloud lightning, more extreme events are observed in the terrestrial atmosphere, such as Transient Luminous Events and Terrestrial Gamma-ray Flashes. These are described in the section “radio emissions associated with Terrestrial Gamma-ray Flashes” by S. Celestin and M. Fullekrug (this volume).

Lightning on Mars

Despite its thin atmosphere, atmospheric electric discharges can happen on Mars, via large scale dust storms and “dust devils” (localized dust storms) which are thought to be able to generate substantial charge via triboelectric processes, i.e. contact electrification (Farrell et al. 1999; Zarka et al. 2004, 2008, and references therein). Observations have been attempted, but reports of detection remain controversial (Ruf et al., 2009; Anderson et al., 2012).

The exact nature of the discharge (time scale, current flow, spatial size) is unknown. Because of the lower atmospheric pressure on Mars, the atmospheric breakdown voltage is about 1/100 that of Earth’s (or about 20 kV/m). Laboratory experiments involving tribo-electrified dust grains in low pressure Martian-like CO_2 atmosphere were found to generate both slow, sprite-like discharges and and fast discharges. Farrell et al. (1999) estimated incoherent HF radiation corresponding to flux densities at Earth of the order of 1 μJy for a peak emission frequency of 20 MHz ($\tau \approx 50$ nsec) to 1 mJy if the peak emission frequency is 200 MHz ($\tau \approx 5$ nsec). Discharges in Martian dust storms could also have a significant impact on the atmospheric chemistry (Farrell et al. 2006).

Due to the emission mechanism, the radio flux is expected to increase with frequency. Thus, HBA observations with LOFAR seem more promising than observations with NenuFAR, for which the expected radio flux caused is below the detection threshold. On the other hand, Mars is regularly searched for by the NASA/Deep Space Network, and joint observations during Mars' storm season could help constrain the emission, even in the case of a non-detection.

Lightning on Jupiter

No HF radio emission from lightning was detected at Jupiter by either Voyager, Galileo, or Cassini. Nevertheless, there is strong evidence for the presence of lightning on Jupiter, including optical

flashes (observed by Voyager, Galileo, and Cassini), low frequency whistlers (detected by Voyager, see Cook et al., 1979; Gurnett et al., 1979; and the review by Desch et al., 2002), and the signal recorded by the search coil on the Galileo descent probe at altitudes below the ionosphere (Lanzerotti et al., 1996). This discrepancy can be understood as emission at a frequency below below Jupiter's ionospheric cutoff, for which two different causes have been suggested: Either the cutoff frequency is increased by low-altitude ionospheric layers (at an altitude of a few hundred km above the 1 bar level) of (micro-)meteoritic origin (Zarka 1985), or the Jovian lightning discharges could have much longer time constants than their Terrestrial counterparts, which would imply a radio emission at a much lower frequency (Farrell et al. 1999).

These two possible causes can be converted into upper flux limits. If the current non-detections are explained by micro-meteorites, Jupiter's lightning emission would peak below 10–15 MHz at a flux density between ~ 4 Jy and 4 10^{-5} Jy at Earth. However, if the dense low altitude Jovian ionospheric layer is not permanent (e.g. due to a variable micrometeorite flux), then this upper limit could be relevant only part of the time, and exceeded at other moments (Zarka et al., 2004, 2008). On the other hand, if the current non-detections are caused by a slow discharge, at 10 MHz an upper limit for the flux density 7 10^{-6} Jy at Earth is obtained, decreasing to 10^{-6} Jy at 20 MHz (Zarka et al., 2004, 2008). In both cases, this is below the detection threshold of LOFAR and NenuFAR. However, if the micro-meteoritic explanation holds, this upper limit may not apply at all times, and stronger signals are possible. For this reason, monitoring with one beam is suggested to monitor Jupiter for potential rare and intense events.

Lightning on Saturn

HF (high-frequency) radio emission caused by planetary lightning was clearly observed for Saturn by Voyager 1 and 2 in 1980–1981 (Warwick et al., 1981). These events were soon suggested to be caused by lightning activity (Burns et al., 1983; Kaiser et al., 1983; Zarka and Pedersen, 1983). This has been confirmed by subsequent radio observations, and by the comparison to optical images of storm clouds and by imaging of single cloud flashes (Dyudina et al., 2010).

The flux densities of Saturn lightning varies from event to event and from one planetary rotation to another. Zarka et al. (2004) estimate the flux density that can be expected at Earth. They find that a good fraction of the events should reach at least 10 Jy at 20 MHz. Sometimes, even flux densities of up to 1000 Jy are reached. At higher frequencies, however, the flux density probably decreases as f^{-1} or f^{-2}, making their observation more difficult. Due to these low flux levels and due to its low occurrence rate, Saturn lightning emission has only recently become detectable for ground-based telescopes. Using the Cassini spacecraft in Saturn's orbit as a trigger for the observation, lightning radio emission was finally unambiguously detected at the giant Ukrainian radio telescope UTR-2 (Konovalenko et al. 2013, Grießmeier et al., 2010, 2011; Zakharenko et al., 2011). Saturn lightning was also recently observed by the WSRT, and during test observations with LOFAR (Grießmeier et al., 2010, 2011).

The stroke duration of Saturn lightning bursts is still unknown, but could be extremely short. It could be as low as 1 ms, while the terrestrial value is 70 ms (Farrell et al., 2007). This stroke duration is an important parameter required to estimate the discharge energy, which is uncertain by many orders of magnitude (Farrell et al., 2007). High time resolution profiles of Saturn lightning (up to 5 microseconds in standard mode for LOFAR or NenuFAR, and finer resolution when using the transient buffer boards) will be able to solve this open question.

In tied-array mode, NenuFAR-1 alone (possibly in correlation with optical surveys) will provide the sensitivity permitting to study lightning from Saturn, addressing questions such as the lightning

discharge timescales, spectral profile, and its energy budget, the electrification processes compared to the terrestrial case, the breakdown electric field (which depends on atmospheric pressure, composition and electron density), atmospheric dynamics and cloud structure, geographical and seasonal variations. In addition, NenuFAR can be combined with the LOFAR array (in "superstation mode") for high resolution imaging (Zarka et al. 2004, 2008). Saturn has an angular size of approximately 17″, whereas LOFAR can achieve an angular resolution of 1–2″ using the long baselines to its international stations, giving access to spatial information.

Lightning on Titan

No lightning from Titan was detected with either Voyager or Cassini flybys of Titan (Desch and Kaiser 1990; Fischer et al. 2011), implying an upper limit on the flux density at Earth $<2 \times 10^{-5}$ Jy at 500 kHz. Assuming a power spectrum in f^{-2}, this leads to $4\ 10^{-8}$ Jy at 10 MHz. As models based on atmospheric composition and dynamics predicted much higher flux densities especially from Titan's dayside (Lammer et al. 2001; Zarka et al. 2004), other reasons are invoked for the non-detection, including a very low flash rate ($<10^{-2}$ flash/h), long flash duration (0.25 msec) and thus a low HF radio flux, or very episodic activity. With the long data basis from Cassini, it seems now likely that Titan's lightning is either very rare, or non-existings (Fischer and Gurnett, 2011).

With the above upper limits, Titan's lightning is probably not observable with either LOFAR and NenuFAR.

Lightning on Uranus

Similarly to Saturn lightning, lightning-generated radio emission from Uranus was detected on by Voyager 2 in 1986 (Zarka and Pedersen, 1986). This emission had an occurrence rate much lower than Saturn lightning (~7 events/hour), a comparable duration of 30–250 msec per event, a steeper spectrum, and a weaker spectral power, corresponding to a flux density between ~0.4 and 40 Jy at the Earth. With this, lightning from Uranus are probably be detectable with LOFAR and NenuFAR. NenuFAR-1, however, is likely too limited in sensitivity.

Lightning on Neptune

At Neptune, only 4 weak events presenting characteristics similar to Saturn or Uranus lightning were detected by Voyager 2 during the fly-by (Kaiser et al. 1991), together with a few dispersed VLF whistlers supporting evidence for atmospheric lightning (Gurnett et al. 1990). Measurements of these 4 radio events was consistent with duration of 30–90 msec, a steep spectrum, and flux densities of 0.03 to 0.003 Jy at Earth. Even if one believes that these four events were due to lightning, their flux density is too weak to be detected by LOFAR. However, the Voyager 2 flyby may have occurred during a period of low activity. Occasional monitoring with LOFAR or NenuFAR with one beam has the potential of discovering lightning during periods of strong activity, or to set upper limits on the emission duty cycle. The sensitivity of NenuFAR-1, however, is probably not sufficient for this study.

NenuFAR design

As a fast transient, planetary lightning requires the tied-array beam observations in order to resolve the high temporal fine structure. For NenuFAR, the intrinsic time resolution will be 5, 10 or 20 μs, which is sufficient to resolve most of the temporal structure of planetary lightning. The currently planned backend will output such beam-formed data for analysis on a separate machine, either the ARTEMIS backend, or an improved version of this machine (see sections 1-6 and 16).

Table 1 compares the planned characteristics of NenuFAR-1 and NenuFAR to the capabilities of the LOFAR core (24 LOFAR core stations; there is currently no coherent tied array beam for the full LOFAR array, so that a comparision to the full array is not interesting) and of a single international LOFAR station when operated in standalone mode. Table 1 shows that NenuFAR is the most sensitive instrument for such observations, surpassing even the coherently added LOFAR core. NenuFAR-1 is less sensitive, but still a highly useful instrument. Under the assumption that the instrument will be flexible and support TOO observations on a short notice, both NenuFAR-1 and NenuFAR have the potential to become the leading ground-based observatory for solar system planetary lightning.

	LOFAR core	FR606	NenuFAR-1	NenuFAR
relative sensitivity	1	0.08	0.3	2.0
relative sensitivity at 15 MHz	0.23	0.02	0.08	0.5
frequency range	10/30-90	10/30-90	10/30-85	10/30-85
max. bandwidth	48 MHz (96 MHz in 8 bit)	48 MHz (96 MHz in 8 bit)	70 MHz	70 MHz
# beams	>100	4	2	2 or 4
time resolution	5.12 μs	5.12 μs	5, 10, 20 μs?	5, 10, 20 μs?
TOO support	yes	<10% of the time	yes	yes

Planetary lightning comparison

Based on the above, the detections prospects for solar system planetary lightning by NenuFAR-1 and NenuFAR are summarized in Figure 1 and Table 2. One notices that both instruments have the potential to make interesting discoveries in the field of solar system planetary lightning. Some studies are certainly accessible (Earth and Saturn); other studies may allow interesting discoveries (Venus, Mars, Jupiter), whereas the most distant planets (Uranus, Neptune) will probably require the full NenuFAR array.

planet	satellite data	ground-based data	NenuFAR-1 potential	NenuFAR potential
Venus	?	no	if emission intermittent	if emission intermittent
Earth	yes	yes	yes	yes
Mars	?	no	if combined to high-frequency observations	if combined to high-frequency observations
Jupiter	-	no	if ionosphere intermittent	if ionosphere intermittent
Saturn	Voyager 1&2, Cassini	UTR-2, WSRT?, LOFAR?	yes	yes
(Titan)	no	no	no	no
Uranus	Voyager 2	no	-	yes
Neptune	?	no	-	if emission intermittent

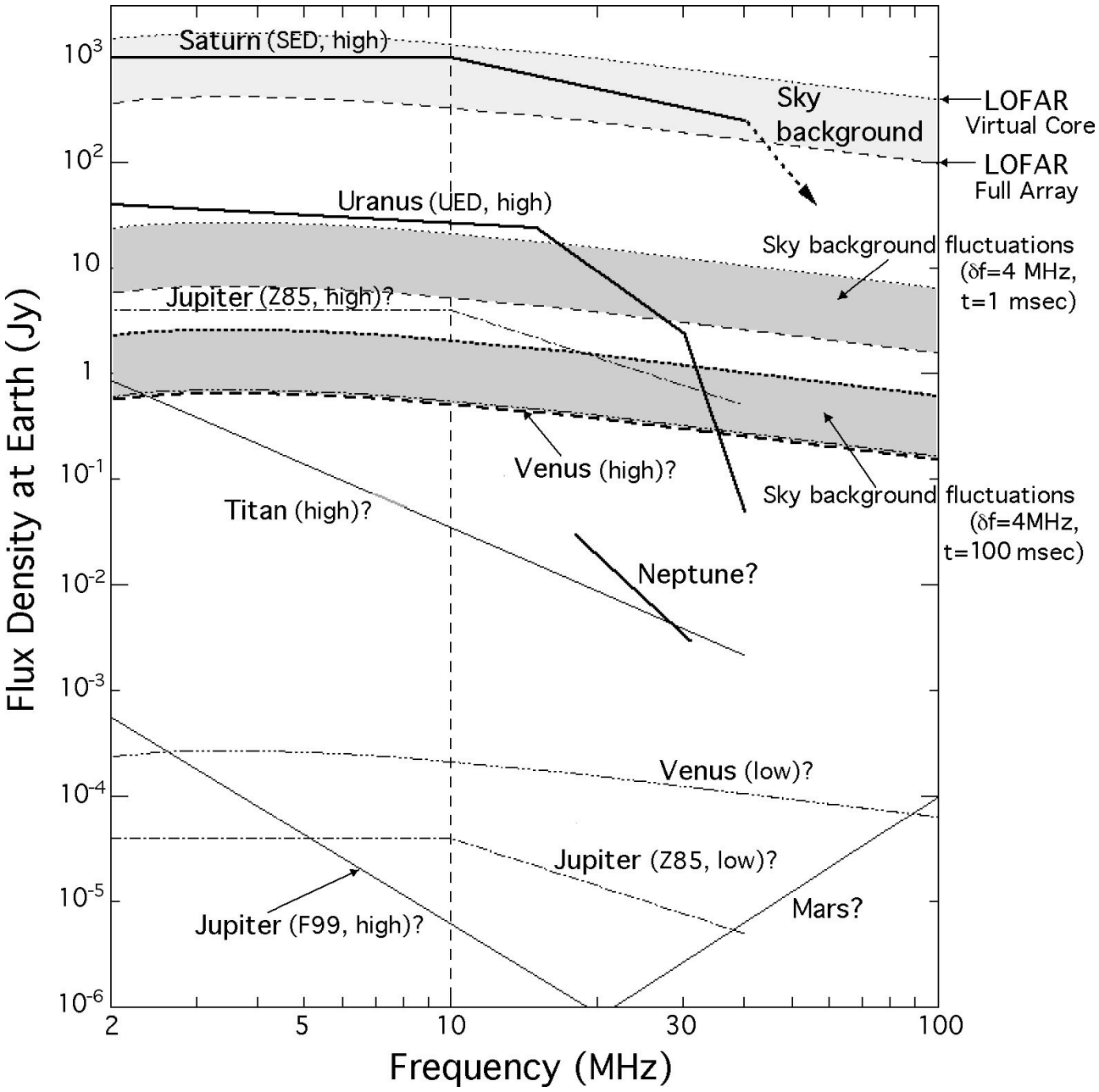

Figure 1 (from Zarka 2004): Summary of planetary lightning spectra (observed or predicted) compared with expected LOFAR sensitivity. The light grey-shaded region is the sky background noise spectrum that will be detected by LOFAR. The darker grey-shaded regions characterize the noise background fluctuations that will define the sensitivity (1σ) of the observations with a bandwidth of 4 MHz and an integration time of 1 or 100 msec. Boldface planetary lightning spectra (for Saturn, Uranus, and Neptune) correspond to extrapolations of Voyager observations. Lightface lines represent upper limits or models of unobserved planetary lightning radio spectra. The range accessible to ground-based observation is at the right of the dashed line (ionospheric cutoff). The detection threshold of NenuFAR is comparable to that of the LOFAR core.

References

- M. M. Anderson, A. P. V. Siemion, W. C. Barott, G. C. Bower, G. T. Delory, I. de Pater, and D. Werthimer (2012), Astrophysical Journal 744, 15.

- J. A. Burns, M. A. Showalter, J. N. Cuzzi, and R. H. Durisen (1983), Icarus 54, 280–295.
- A. F. Cook II, T. C. Duxbury, G. E. Hunt (1979), Nature 280, 794.
- S. J. Desch, W. J. Borucki, C. T. Russell, A. Bar-Nun (2002), Reports on Progress in Physics 65, 955–997.
- M. D. Desch, M. L. Kaiser (1990), Nature 343, 442–444.
- U. A. Dyudina, A. P. Ingersoll, S. P. Ewald, C. C. Porco, G. Fischer, W. S. Kurth, and R. A. West (2010), Geophysical Research Letters 37, L09205.
- W. M. Farrell, M. L. Kaiser, M. D. Desch (1999), Geophysical Research Letters 26, 2601–2604.
- W.M. Farrell, G.T. Delory, S.K. Atreya (2006), Geophys. Res. Lett. 33, L21203.
- G. Fischer and D. A. Gurnett (2011), Geophysical Research Letters 38, L08206.
- J.-M. Grießmeier, P. Zarka, J. Girard, S. ter Veen, H. Falcke (2010), in Proceedings of the ISKAF2010 Science Meeting, Proceedings of Science (http://pos.sissa.it/cgi-bin/reader/conf.cgi?confid=112), 022.
- J.-M. Grießmeier, P. Zarka, A. Konovalenko, G. Fischer, V. Zakharenko, B. W. Stappers, J. N. Girard, B. Ryabov, D. Vavriv, V. Ryabov, H. O. Rucker (2011), in Planetary Radio Emissions VII, (Editeurs) H. O. Rucker, W. S. Kurth, P. Louarn and G. Fischer, Austrian Academy of Sciences Press, Vienna, 145-154.
- D. A. Gurnett, R. R. Shaw, R.R. Anderson, W. S. Kurth, F. L. Scarf (1979), Geophysical Research Letters 6, 511–516.
- D.A. Gurnett, W.S. Kurth, I.H. Cairns, L.J. Granroth (1990), J. Geophys. Res. 95, 20967–20976
- I. Holleman, H. Beekhuis, S. Noteboom, L. Evers, H. Haak, H. Falcke & L. Bähren (2006), Validation of an operational lightning detection system , paper presented at the 19th International Lightning Detection Conference/1st International Lightning Meteorology Conference , Vaisala, Tucson, Arizona.
- M. L. Kaiser, J. E. P. Connerney, and M. D. Desch (1983), Nature, 303, 50–53.
- M.L. Kaiser, M.D. Desch, W.M. Farrell, P. Zarka (1991), J. Geophys. Res. 96, 19043–19047.
- A. A. Konovalenko, N. N. Kalinichenko, H. O. Rucker, A. Lecacheux, G. Fischer, P. Zarka, V. V. Zakharenko, K. Y. Mylostna, J.-M. Grießmeier, E.P. Abranin, I. S. Falkovich, K. M. Sidorchuk, W.S. Kurth, M. L. Kaiser, D. A. Gurnett (2013), Icarus 224, 4–23.
- H. Lammer, T. Tokano, G. Fischer et al. (2001), Planet. Space Sci. 49, 561–574.
- L. J. Lanzerotti, K. Rinnert, G. Dehmel, F. O. Gliem, E. P. Krider, M. A. Uman, J. Bach (1996), Science 272, 858–860.
- D. M. Le Vine (1987), Meteorol. Atmos. Phys. 37, 195–204.
- C. Ruf, N. O. Renno, J. F. Kok, E. Bandelier, M. J. Sander, S. Gross, L. Skjerve, and B. Cantor (1999), Geophysical Research Letters 36, L13202.
- R.J. Strangeway (2004), Adv. Space Res. 33(11), 1956–1967.
- J. W. Warwick, J. B. Pearce, D. R. Evans, T. D. Carr, J. J. Schauble, J.K. Alexander, M. L. Kaiser, M.D. Desch, B. M. Pedersen, A. Lecacheux, G. Daigne, A. Boischot, C. H. Barrow (1981), Science 212, 239–243.
- C. D. Weidman, E. P. Krider, and M. A. Uman (1981), Geophys. Res. Lett. 8(8):931–934.
- J. C. Willett, J. C. Bailey, C. Leteinturier, and E. P. Krider (1990), J. Geophys. Res., 95(D12):20367–20387.
- V. Zakharenko□, C. Mylostna, A. Konovalenko, P. Zarka, G. Fischer, J.-M. Grießmeier, G. Litvinenko, H. Rucker, M. Sidorchuk, B. Ryabov, D. Vavriv, V. Ryabov, B. Cecconi, A. Coffre, L. Denis, C. Fabrice, L. Pallier, J. Schneider, R. Kozhyn, V. Vinogradov, D. Mukha, R. Weber, V. Shevchenko, V. Nikolaenko (2012), Planet. Space Sci., 61, 53–59.
- P. Zarka (1985), Astronomy & Astrophysics 146, L15–L18.
- P. Zarka, W. M. Farrell, M. L. Kaiser, E. Blanc, and W. S. Kurth (2004), Planet. Space Sci., 52, 1435–1447.
- P. Zarka, W. Farrell, G. Fischer, and A. Konovalenko (2008), Space Sci. Rev., 137, 257–269.
- P. Zarka, B. M. Pedersen (1983), Journal of Geophysical Research 88, 9007–9018.
- P. Zarka, B. M. Pedersen (1986), Nature 323, 605–608.

Radio emissions associated with Terrestrial Gamma-ray Flashes

S. Celestin[1] and M. Fullekrug[2]

[1]Laboratory of Physics and Chemistry of the Environment and Space (LPC2E), University of Orleans, LPC2E / CNRS, 3A avenue de la Recherche Scientifique, 45071 Orleans Cedex 2, France
sebastien.celestin@cnrs-orleans.fr
[2]Dept. of Electronic and Electrical Engineering, Centre for Space, Atmospheric and Oceanic Science, University of Bath, Claverton Down, Bath, BA2 7AY, UK
eesmf@bath.ac.uk

Abstract :

NenuFAR offers novel opportunities to make fundamental contributions to our current understanding of the initiation of lightning discharges and terrestrial gamma ray flashes, the propagation of stepped leaders inside thunderclouds and the acceleration of electrons above thunderclouds associated with transient luminous events. These opportunities arise from the use of the NenuFAR's transient buffer boards and post-processing towards beam-steering to investigate radio emissions originating inside and above thunderclouds.

1- Terrestrial Gamma-ray Flashes

Terrestrial Gamma-ray Flashes (TGFs) are ~50 keV to 10s of MeVs photon bursts originating from terrestrial thunderstorms [Fishman et al., 1994; Smith et al., 2005; Tavani et al., 2011]. Observations identified TGFs with the initial development stages of normal polarity intracloud lightning that transports negative charge upward (+IC) (e.g., [Lu et al., 2011]).

In addition to space-based measurements, X-ray and gamma-ray bursts from lightning discharges have also been observed [Dwyer et al., 2005]. These X-ray and gamma-ray bursts have been linked to the production of high-energy electrons, so-called runaway electrons, in the Earth's atmosphere. Runaway electrons are electrons with high energy and consequently low probability of collision with gas molecules, propagating in an applied electric field so that the energy they acquire from the field is higher than the energy losses due to collisions. These electrons are therefore capable of efficiently gaining energy from an electric field in air. One can distinguish between thermal runaway processes, for which a very high electric field E exceeds the friction force at low-energy (>100 eV) and brings electrons to regimes where they continuously accelerate (E > 240 kV/cm in air at ground pressure), and relativistic runaway processes [Gurevich et al., 1992] for which initial high-energy electrons are already present (e.g., cosmic ray secondary electrons) and can initiate relativistic runaway electron avalanches (RREAs) in electric fields higher than 2.8 kV/cm in air at ground pressure (e.g., [Dwyer, 2008]).

X-ray bursts from lightning discharges have been clearly identified to result from the production of thermal runaway electrons [Dwyer, 2004] and although TGFs have been suggested to be related to thermal runaway processes in lightning leader tips [Celestin et al., 2011; Xu et al., 2012], the average TGF spectrum was very well reproduced by RREA models involving acceleration of runaway electrons in large-scale (at least several hundreds of meters) weak electric fields in thunderstorms [Dwyer and Smith, 2005]. Thus, there is now an urgent need to discriminate which of the proposed mechanisms is truly responsible for the production of TGFs.

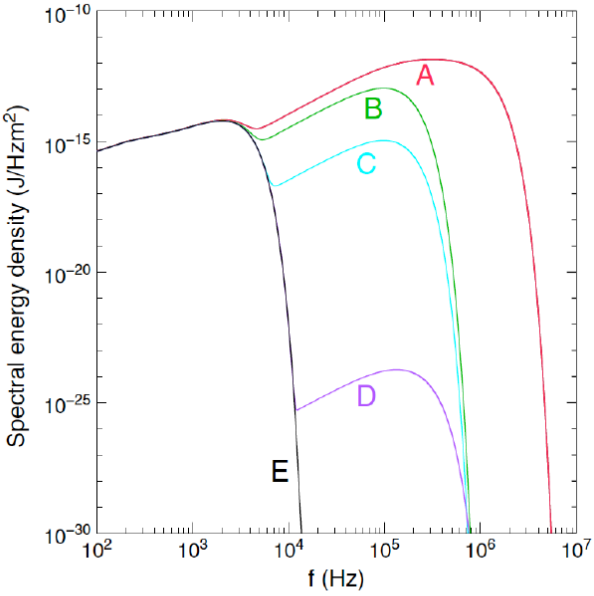

Table 2. TGF Model Parameters

Model	Name of Model
A	Fast lightning source (Celestin, Xu, and Pasko)
B	Slow lightning source 1
C	Slow lightning source 2
D	Relativistic feedback discharge
E	Infinite number of avalanche pulses

Figure 1. Spectral energy density from various sources associated with TGFs. Taken from [Dwyer and Cummer, 2013, Figure 4 and Table 2].

2- Radio emissions from TGF sources

Modeling efforts on radio emissions from TGF sources have been recently carried out to address the puzzle of the TGFs origin and it has been proposed that the observation of radio emissions from TGF-producing thunderstorms could validate or veto working theories [Dwyer and Cummer, 2013]. Figure 1 is taken from [Dwyer and Cummer, 2013, Figure 4]. This figure shows different spectral energy densities associated with different models of TGF production as observed from the ground at a radial distance of 500 km from the source. Dwyer and Cummer [2013] also noted that the observation at small angles (for which the thunderstorm is above the observation point) would enhance higher-frequency components due to relativistic beaming. In the range 10-80 MHz, NenuFAR is particularly well suited to observe these fast emissions.

TGF sources are believed to last from a few tens to a few hundreds of microseconds. Hence, the 5 µs temporal resolution of NenuFAR should be appropriate to capture the radio emission over the source duration. Additionally, very short temporal structures of a few tens of nanoseconds related to the stepping of lightning leaders might be present in TGF sources [Celestin et al., 2012]. NenuFAR with extended transient buffer boards (TBBs) (~5 sec continuous recordings from 96 mini-arrays of 1 to 19 active antennas simultaneously at 5 ns resolution) will enable post processing permitting beam steering at an extraordinary high sensitivity level.

TGFs will be directly studied by the French space agency (CNES) mission TARANIS (launch planned in November 2016) which is dedicated to the observation of transient electrodynamic couplings between thunderstorms and the atmosphere-ionosphere-magnetosphere

system. Additionally to high-energy photon and electron detectors, TARANIS will be equipped with instruments measuring the electric and magnetic field from DC to 35 MHz. Although the probability of observing the same TGF with NenuFAR and TARANIS is small, coincident satellite observations of TGFs and close range observation of radio emissions are possible [e.g., Lu et al., 2010; 2011; Marshall et al., 2013, Figure 1]. The future ESA space mission ASIM on board the International Space Station (launch planned in 2015) is dedicated to studying TGFs and will also be of great interest to NenuFAR. Apart from the planned missions ASIM and TARANIS, ongoing satellite missions currently detecting TGFs (AGILE, Fermi, RHESSI) cannot perform observations at high geographic latitudes corresponding to continental France.

3- Other thunderstorm-related radio emission sources

Lightning is a powerful source of radio emission, with a spectral peak in the 3-30 kHz range associated with the lightning return stroke current. The emissions with frequencies >MHz usually occur as a sequence of bursts associated with steps in the propagation of negative lightning leaders. Leader stepping is a poorly understood mechanism that needs to be further studied, especially concerning the initiation and propagation of intracloud discharges [Marshall et al., 2013; Pasko, 2014]. Lightning Mapping Arrays usually detect these impulsive radio signals in the range 30-100 MHz, the frequency range covered by NenuFAR is therefore well-suited to observe this phenomenon.

Moreover, NenuFAR will enable investigations of the radio emissions associated with sprites and other Transient Luminous Events (TLE), addressing their origin, distribution and dynamics, time and frequency scales, and physical mechanisms. For example, sprites have been associated with radio emissions in the frequency range ~50-350 kHz [Füllekrug et al., 2010, 2011], which could be produced by the acceleration of electrons above thunderclouds. Electron and positron beams above thunderstorms have been reported by space missions by re-interpreting unusually long-lasting TGFs [e.g, Briggs et al., 2011, and references therein]. It is currently thought that these energetic particles are generated by the electron-positron pair production of TGFs in the middle atmosphere. Alternatively, the electrons could be generated in the cosmic ray layer above thunderclouds [Füllekrug et al., 2010]. NenuFAR has the capability to detect these radio emissions above thunderclouds and determine their source height if their radio spectrum extends into the MHz range as predicted by theory. A negative result provided by NenuFAR would indicate that the observed radio emissions from ~50-350 kHz are related to the propagation mechanisms of expanding filaments (streamers) constituting especially powerful sprites [Qin et al., 2012], which would not extend into the frequency range of several MHz. The question of the possibility of higher frequency radio emission from TLEs is open, and can be further investigated using NenuFAR.

In order to better understand planetary lightning and thunderstorms, we note that it would be very important to compare radio signals from terrestrial and planetary thunderstorms as detected by the same instrument. Therefore, we plan on working in close collaboration with the contributors of Section 17 “Observations of planetary lightning with NenuFAR” (J.-M. Griessmeier et al.).

References

Briggs, M. S., V. Connaughton, C. Wilson-Hodge, R. D. Preece, G. J. Fishman et al. (2011), Electron-positron beams from terrestrial lightning observed with Fermi GBM, Geophys. Res. Lett., 38, L02808.

Celestin, S., and V. P. Pasko (2011), Energy and fluxes of thermal runaway electrons produced by exponential growth of streamers during the stepping of lightning leaders and in transient luminous events, J. Geophys. Res., 116, 2011, A03315.

Celestin, S., W. Xu, and V. P. Pasko (2012), Terrestrial gamma ray flashes with energies up to 100 MeV produced by nonequilibrium acceleration of electrons in lightning, J. Geophys. Res., 117, A05315.

Dwyer, J. R., (2004), Implications of X-ray emission from lightning, Geophys. Res. Lett., 31, L12102.

Dwyer, J. R., (2008), Source mechanisms of terrestrial gamma-ray flashes, J. Geophys. Res., 113, 2008, D10103.

Dwyer, J. R., et al. (2005), X-ray bursts associated with leader steps in cloud-to-ground lightning, Geophys. Res. Lett., 32, L01803.

Dwyer, J. R., and D. M. Smith (2005), A comparison between Monte Carlo simulations of runaway breakdown and terrestrial gamma-ray flash observations," Geophys. Res. Lett., 32, L22804.

Dwyer, J. R., and S. A. Cummer (2013), Radio emissions from terrestrial gamma-ray flashes, J. Geophys. Res., 118, 3769-3790.

Fishman, G. J., et al. (1994), Discovery of intense gamma-ray flashes of atmospheric origin, Science, 264, 1313.

Füllekrug, M., R. Roussel-Dupré, E. M. D. Symbalisty, O. Chanrion, A. Odzimek, O. van der Velde, and T. Neubert (2010), Relativistic runaway breakdown in low-frequency radio, J. Geophys. Res., 115, A00E09.

Füllekrug, M., R. Roussel-Dupré, E. M. D. Symbalisty, J. J. Colman, O. Chanrion, S. Soula, O. van der Velde, A. Odzimek, A. J. Bennett, V. P. Pasko, and T. Neubert (2011), Relativistic electron beams above thunderclouds, *Atmos. Chem. Phys.*, 11, 7747-7754.

Gurevich, A. V., G. M. Milikh, and R. A. Roussel-Dupré (1992), Runaway electron mechanism of air breakdown and preconditioning during a thunderstorm, Phys. Lett. A., 165, 463-468.

Lu, G., R. J. Blakeslee, J. Li, D. M. Smith, X.□M. Shao, E. W. McCaul, D. E. Buechler, H. J. Christian, J. M. Hall, and S. A. Cummer (2010), Lightning mapping observation of a terrestrial gamma−ray flash, Geophys. Res. Lett., 37, L11806.

Lu, G., S. A. Cummer, J. Li, F. Han, D. M. Smith, and B. W. Grefenstette (2011), Characteristics of broadband lightning emissions associated with terrestrial gamma ray flashes, J. Geophys. Res., 116, A03316.

Marshall, T., M. Stolzenburg, S. Karunarathne, S. Cummer, G. Lu, H.-D. Betz, M. Briggs, V. Connaughton, and S. Xiong (2013), Initial breakdown pulses in intracloud lightning flashes and their relation to terrestrial gamma ray flashes, J. Geophys. Res., 118, 10,907-10,925.

Pasko, V. P. (2014), Electrostatic modeling of intracloud stepped leader electric fields and mechanisms of terrestrial gamma ray flashes, Geophys. Res. Lett., 41, 179-185.

Qin, J., S. Celestin, and V. P. Pasko (2012), Low frequency electromagnetic radiation from sprite streamers, Geophys. Res. Lett., 39, L22803.

Smith, D. M., L. I. Lopez, R. P. Lin, and C. P. Barrington-Leigh (2005), Terrestrial gamma-ray flashes observed up to 20 MeV, Science, 307, 1085-1088.

Tavani, M., et al. (2011), Terrestrial gamma-ray flashes as powerful particle accelerators, Phys. Rev. Lett., 106, 018501.

Xu, W., S. Celestin, and V. P. Pasko (2012), Source altitudes of terrestrial gamma-ray flashes produced by lightning leaders, Geophys. Res. Lett., 39, L08801.

Meteor radio detection and motion estimation using NenuFAR

Contributors :
Sylvain Azarian - Onera - sylvain.azarian@onera.fr
Jeremie Vaubaillon - IMCCE - vaubaill@imcce.fr

People supporting this initiative :
Jean-Jacques MAINTOUX , Jeremy MAINTOUX , Frederic RIBLE - RETRAM - contact@retram.org

Introduction

Earth continuously crosses the orbit of meteoroids of different sizes, which can thus penetrate its atmosphere at velocities ranging from 11 to 72 km per second. These meteoroids can be single objects, dust clusters or asteroid trails. This last group cruises on deterministic orbits, crossing earth periodically.

When a high speed meteoroid enters atmosphere, its ablation produced by friction with the air molecules ionizes the surrounding gas into a plasma reflecting electromagnetic waves. This phenomenon is well known for radars where the plasma creates a moving target reflecting back the transmitted pulses. This reflection mechanism is also the key for point to point communications where specific wireless systems are designed to use these opportunistic reflectors to open obstructed channels. Most meteoroids fully ablate during their atmospheric entry, from which micrometeorites will eventually reach the ground.

We investigate here the possible outcomes in using the NenuFAR radio telescope as a radio sensor to detect and estimate the motion of meteoroids, using techniques traditionally applied in the Radar field. The document is organized in two sections: section 1 describes general principles and expected outcomes, while section 2 proposes practical scenarios for detection using NenuFAR.

Section 1 - Phenomenology and expected outcomes - Using radar techniques to detect and track meteors using NenuFAR

1.1 - Phenomenology

While entering upper layers of the atmosphere, the meteoroid starts ablating, ionizing the air molecules on its path. At the beginning of the entry, the meteor itself can be detected using classical radar techniques, as long as the power involved and used wavelength are compatible with the object shape and velocity.

The ionized remaining train acts as an electromagnetic reflector with a maximum reflectivity in the VHF band mainly (peak around 50 MHz), and less in the UHF range. This train is then extending downwards at the speed of the meteor head, and is moving according to the winds blowing in the atmosphere (in this following we will name 'meteor trail' the region of the atmosphere becoming ionized by the meteor). This trail will also be detected by radars, as long as the plasma will be reflective enough at the transmitted signal wavelength.

Different meteor detection experiments have been conducted using active radars, like the ARPA Long-Range Tracking and Instrumentation Radar (ALTAIR) or EISCAT. These trials have shown

head echo and trail can be detected efficiently, and provided a lot of useful data to understand the phenomenon. In such a scenario, a known high power radio signal is transmitted and echoes scattered back to a receiver are studied.

Another option to detect and estimate the motion of the meteoroids is to use 'passive radar techniques' : instead of transmitting a known signal towards the explored region, we use the existing signals broadcasted by ground transmitters, primarily used for other purposes like radio broadcast, data transmissions etc. These transmitters are called 'illuminators of opportunity'. A part of the signal power is reaching the upper layers of the atmosphere and will be reflected back to the ground by the meteor head or trail.

This technique is being used for many years now and specific beacons have been installed for meteors. For example the BRAMS (Belgian RAdio Meteor Stations) is a set of radio receiving stations using forward scattering techniques to study the meteoroid population. Well suited for an estimation of the frequency of this phenomenon, using a single source of illumination does not allow precise motion estimation. Because of scattering phenomenology and radar processing techniques, multiple measurements have to be performed to find the possible paths of the meteors.

1.2 - Using NenuFAR as a meteor passive radar system

We propose here to use NenuFAR as a passive radar receiver, collecting signals originally issued from ground transmitters, and apply radar signal processing to estimate the meteor location and motion parameters, as well as the trail position and motion.

NenuFAR, with its array of antennas and set of digital receivers, has important features that can help in meteor detection and tracking :

- Because of the number of antennas, it brings a high sensitivity and opens detection of small objects and meteor heads, usually requiring an important power for the incident radio signal,
- NenuFAR offers digital beam forming capabilities. This enables direction of arrival estimation techniques, hence simplifying the radar processing and removes ambiguities in the path estimation.

1.3 - Using the motion estimation for the solar system scientists

Natural meteor showers happen every month and it is estimated that 30,000 tons of grains fall on the Earth every year. Meteor storms happen a few times per century when the Earth enters a region of space populated with billions of grains, creating lots of meteors visible even to the naked eye. The most famous of them are the Perseids that are seen in the month of August. This is why it is well known that August is the month of meteors. However many other showers exist throughout the year. It is possible to predict the activity of the meteor showers and meteor storms, by knowing where they are coming from. The typical storm is caused by the ejection of the grains (Meteoroid) from a comet.

Calculating the exact time and strength of the shower in advance allows scientists to observe these major and rare events (the last meteor storms dates from 2002, and the next one is expected in 2032). Space agencies usually protect their satellites from meteor outbursts by re-orienting them. However this technique is expensive (estimated at 600,000 Euro). As a consequence, it is very important that the prediction of the meteor showers be accurate. Fortunately, this is possible by the computation of the past, present and future orbits of the comet and the ejected meteoroids. Due to the importance of this field of research the contributors have invested over 10 years in predicting the occurrence of meteor showers on Earth, as well as on other planets (Mars and Venus). These

predictions have proven to be extremely accurate, with less than 1 min of accuracy for the time of the maximum (for a total duration of 1 to 3 hours) and a level estimate better than 20%. Ephemeris of the meteor shower can be found at the lab website at: www.imcce.fr.

NenuFAR can here be used to monitor these showers for a better estimation of their path, leading to a more accurate estimation of their orbit. Using multiple beams can open the study of showers by tracking simultaneously multiple objects, giving a better knowledge of the shower intensity and density.

1.4 - Automatic classification of meteors by 'radar signature' analysis

Automatic Target Classification (ATR) is a popular field in Radar where one wants to estimate the detected object properties based on the returned signal characteristics. These algorithms are intensively used to estimate - for example - the type of aircraft detected by the radar. These techniques could be used on the falling meteor to estimate its size and composition, for example by analyzing the structure of the trail and the intensity of the reflected energy as a function of the wavelength.
One key requirement for such classification algorithm lies in the collection of a statistically significant amount of data to estimate the decision criteria to be used. Passive radar techniques using NenuFAR is a cost effective solution to build such a dataset.

1.5 - Collect data for meteor trail reflectivity estimation

As explained in the phenomenology section of this document, the meteor trail will follow meteor path and move according to existing winds. By tracking the trail at different altitudes, it is hence possible to estimate the wind speeds at different layers of the atmosphere.

NenuFAR offers the possibility the track multiple objects simultaneously (using digital beam forming), hence collecting speed measurements of multiple objects over a wide area. Following each objects at different moments lead to an estimation of the winds and their over a volume.

Another outcome of these measurements lies in the constitution of a model of reflectivity evolution over time. Intensive research is being conducted on using the trail reflectivity for data point to point communication. Telecommunication researchers are designing protocols adapted to the time evolution of the trail reflectivity using simple models, some taking into account ablation models and available statistics of the phenomenon.

Section 2 - Implementation and measurements

2.1 - Illuminators of opportunity

Passive radar techniques require the objects to be detected to be illuminated by an incoming RF signal. These signals can be AM radio broadcast, FM broadcast, TV etc. A survey has to be conducted to:

1. Study, based on the response of the antennas, amplifiers and digital receivers, the most appropriate frequencies,
2. Look for possible transmitters at a distance up to 60 Km around the radio telescope (a direct-path signal must be received from the telescope for cross-correlation and signal processing).
3. At the telescope, check the received levels for the selected transmitters and check their signal-to-noise ratio is appropriate for the processing.

The optimal frequency range for meteor detection is typically from 50 to 100 MHz. NenuFAR antennas have been optimized to work below 90 MHz.

2.2 - Signal processing

In meteor detection mode, no assumption can be made on the location of the event. This means the raw data from each antenna sub-array should not be combined to form beams as long as a no meteor as not been detected.

Typically, the processing could be :

- Configure the telescope to have one channel per antenna, narrow band (depends on selected illuminator of opportunity, typically from 100 to 200 KHz for FM broadcast);
- Queue incoming streams to have 'playback' for about 300 to 500 milliseconds,
- On a subset of streams (probably one would be sufficient), perform a threshold detection (cross-correlation).
- When an event is detected, keep all streams for meteor processing.

The meteor processing, ideally performed online, can also be done by post-processing the recorded data (snapshot of the antenna streams around the detection instant). This processing essentially combines antenna signals to form digital beams and then tries to detect the meteor in the resulting synthetic direction.
As an output, we have:

- Meteor bistatic distance,
- Meteor speed,
- Meteor reflectivity and trail reflectivity information at the working frequency,
- Meteor direction of arrival angle.

Note that a specific antenna / detector can be installed beside the telescope to perform the event triggering. In this case, this subsystem would send requests to freeze the previously received data, going up to 500 milliseconds back in time.

2.3 - When should be done the measurements ?

Except during known meteor showers, measurements can be performed daily, from the middle of the night up to the sun-rise. First trials should be conducted during main and known showers for performances estimation.

2.4 - Expected performances

Current systems use low gain, omni directional antennas. This opens 'full sky' detection but limits to biggest objects and require multiple points of observation to estimate meteor position (triangulation). This sets an important list of practical issues and technical challenges, like operating multiple receiving and processing sites, synchronizing detector for data fusion.

NenuFAR opens promising performances by offering multiple antennas at the same location with possible access to digital streams antenna by antenna, leading to high gain for detection, high directivity for a better position estimation. Performances comparable to a set of multiple interconnected detection stations can be expected from the radio telescope.

ExPRI: Experiment for Propagation of Radio waves in the Ionosphere

B. Cecconi, P. Zarka, D. Oberoi, J.-L. Pinçon

July 28, 2014

1 Introduction

ExPRI (Experience de Propagation Radio Ionosphérique / Experiment for Propagation of Radio waves in the Ionosphere) is a concept of a versatile embarked radio transmitter. This experiment would be providing a known radio source above the ionosphere, to be used as a calibrator from ground based low frequency radio interferometers. The propagation of radio waves in the range between 10 MHz to 30 MHz is strongly perturbed by the inhomogeneities of the ionosphere. A reference radio source, with known flux and polarization properties, is then necessary to remove this propagation effect, if we don't want to use a self-calibration. Such a calibration process is indeed an a posteriori deconvolution with hypotheses on the calibration radio sources in the field of view. This artificial radio source would provide an absolute calibrator that could be used in place or together with other calibration techniques.

2 Ionospheric perturbations

The earth ionosphere consists in a series of ionized layers with plasma frequency of the order of 10 MHz. Figure 1 summarizes its phenomenology regarding its structure depending on local time. It is reflecting radio waves at frequencies lower than its cutoff frequency. Radio frequency waves are also perturbed up to frequencies of a few tens of MHz, inducing various set of propagation effects: refraction, scintillation, caustics (focussing or defocussing, see Fig. 2), attenuation, phase perturbation. The isoplanetic patches (i.e., the horizontal range over which the phase perturbation is considered to be constant) are evaluated with a typical size of about 20 km [*Zarka*, 2010, and references therein].

Considerable progress has been made for correcting refraction effects, for example at 74 MHz at the VLA through a "self-cal" procedure using simultaneous observations at higher frequencies [*Kassim et al.*, 1993]. Accordingly, LOFAR calibration procedures is expected to depend upon λ^2 dependence of ionospheric effects in order to recognize and eliminate them [*Noordam*, 2001]. But this assumption breaks down when the paths traversed by waves at higher and lower frequencies are significantly different. This is likely to be the case when multiple scattering sets in towards the lower end of the LOFAR frequency range (typically below 50 MHz).

3 Experiment

ExPRI is a simple and cost-effective experiment intended to characterize, quantify, and understand the various above ionospheric perturbations and their time variations at low frequencies, using (i) a low-power satellite-embarked radio emitter, and (ii) a few receiving stations on the ground. It should allow us to estimate down to which frequency and during which fraction of time one can expect to correct these perturbations and usefully observe with LOFAR. A secondary objective is to measure the antenna diagrams (beam shapes, including polarization response) of the ground based receiving antennas.

The emitter consists of a radio transmitter that can be tuned to a number of frequencies in the range ∼5-50 MHz, embarked as a secondary passenger on a satellite (or even microsatellite) platform dedicated to other purposes (provided that the resources are available and the trajectory adequate — see below). The emitter should have a 2-channel output and be connected to 2 short dipole antennas (a few tens of cm each). This ensures a quasi-omnidirectional beam, the polarization of the emitted radiation being synthezised through the relative phasing of the 2 outputs. The altitude of the emitter should be

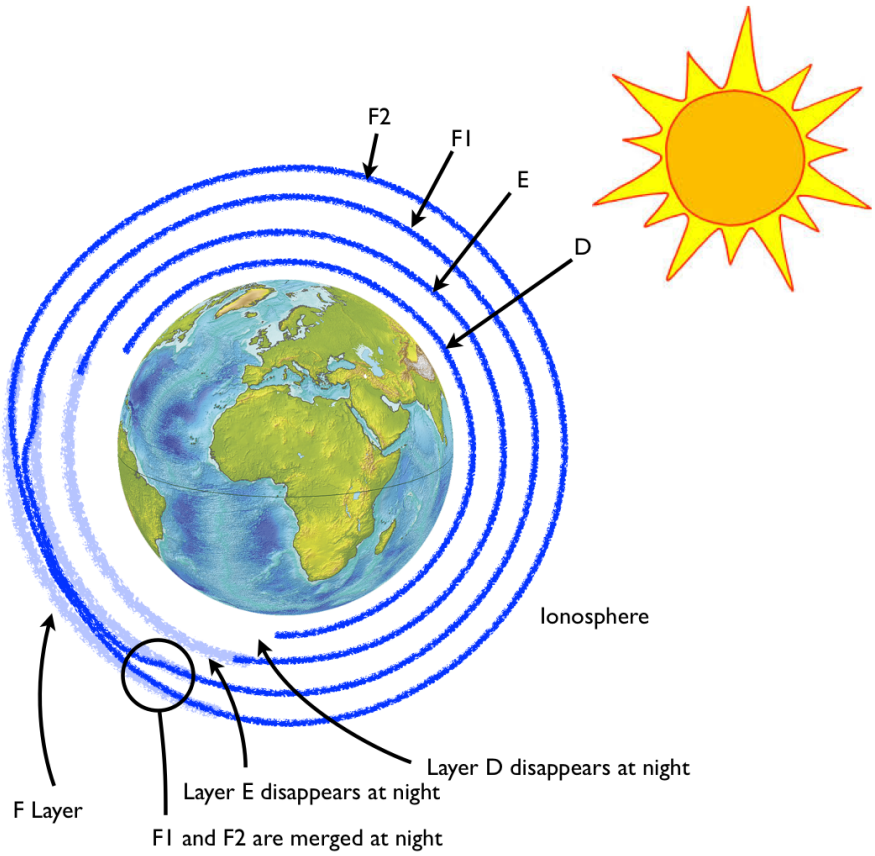

Figure 1: Schema of the various ionospheric layers around the Earth (distances not to scale).

at least 10 times that of the ionospheric layers causing the perturbations to the radio signal (100-300 km), i.e., larger than 3000 km, so that quasi-plane waves are incident on these layers. A Geostationnary Transfer Orbit (GTO, excluding perigee ; apogee at $\sim$6 R_E ; period $\sim$10.6 h) is well adapted and ensures continuous observation campaigns of 3-4 months.

The receiving stations could be models of low-frequency LOFAR stations [*Noordam*, 2001], possibly consisting of a fewer number of dipoles than the final stations planned, ensuring a >10 dB gain, broad beam, and full polarization measurements (S, Q, U, V Stokes parameters). Parts (antenna blocks) of the Nançay decameter array could be operated as one of the receiving stations. Ideally, 3 stations should be used to open the possibility for 2D interferometric measurements, allowing to study the non-isoplaneticity effects. Their separations should be of the order of the TID's horizontal length scales (a few tens of km). Possible locations where infrastructure is available include the Nançay radioastronomy station, CNRS Orléans and Garchy centers, and Meudon observatory.

4 Operations

The position and velocity (hence Doppler shift) of the satellite being available at any time, the field of view of the receiving stations will be dominated by a radio source of known (and selectable) characteristics (frequency, intensity, polarization) recurrently sweeping across the sky. As shown in Figure 3, a power of 100 mW emitted in a 10 kHz band by a source at 10000 km from the observer, detected by an antenna with 20 dB gain, provides a S/N $\sim$30 dB against the sky background. Little contamination by sky or terrestrial interference is thus expected. Note that such measurements would not be doable using the Sun or Jupiter as the emitter, due to the limited predictability of solar and jovian radio bursts, their lower S/N ratio (generally 10-20 dB), and unknown intensity and polarization.

We should be able to get authorizations to emit a low-power signal with a limited duty-cycle in selected frequency bands. Ideally these studies should have preceded LOFAR operation. However, it is still worth doing it in order to validate and enhance the current LOFAR processing pipelines. As the proposed experiment is cost-effective, and has low mass, low volume, low power consumption, a very

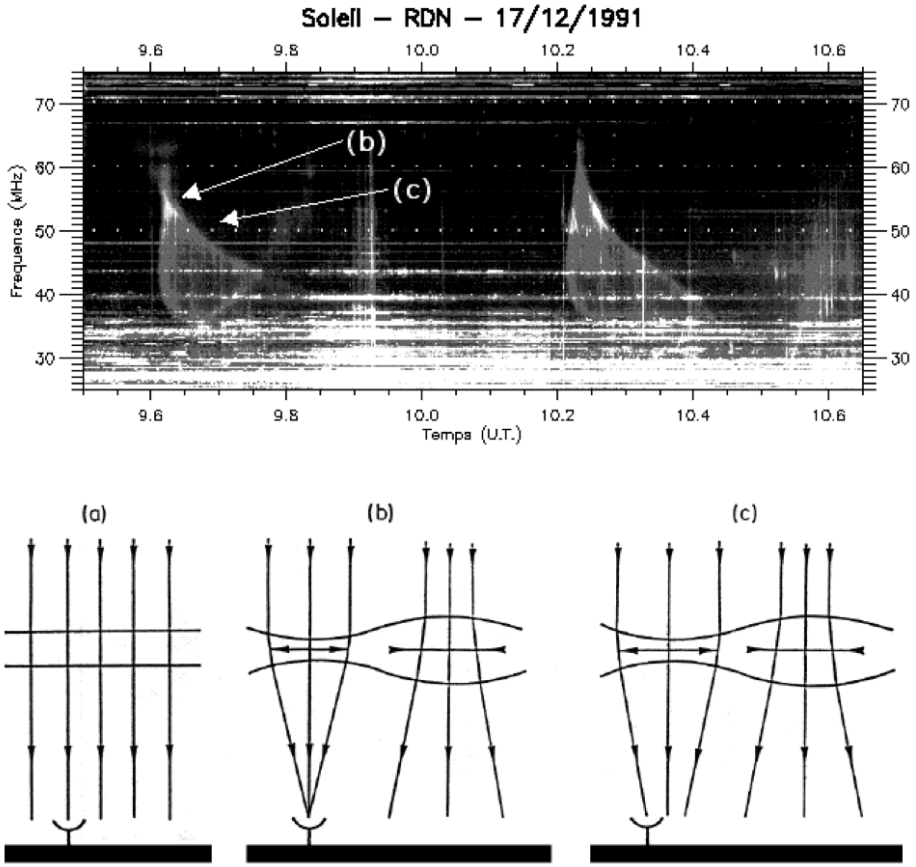

Figure 2: Upper panel: Example of ionospheric caustics affecting observations of solar radio burst in the range 25-75 MHz, recorded at the Nançay Decameter Array (France). They are usually attributed to Travelling Ionospheric Disturbances (TID's) [*Mercier and Jacobson*, 1997; *Jacobson and Erickson*, 1992]]. The lower panel provides explanations for labels (b) and (c). Lower Panel: Origin of ionospheric caustics: in presence of horizontally stratified ionosphere, as shown in (a), the radio waves are not perturbed, except for refraction for non-vertical incidence. In presence of ionospheric perturbations (plasma density inhomogeneities, especially due to gravity waves), ionosphere acts as a radio lens. The incident radiation may be perfectly focussed on the receiving antenna in some configurations, as shown in (b), causing a short-lived brightening. For neighboring frequencies, the focal length of the ionospheric radio lens is somewhat different and corresponds to an imperfect focussing and hence longer periods of brightening of lower intensity, as shown in (c).

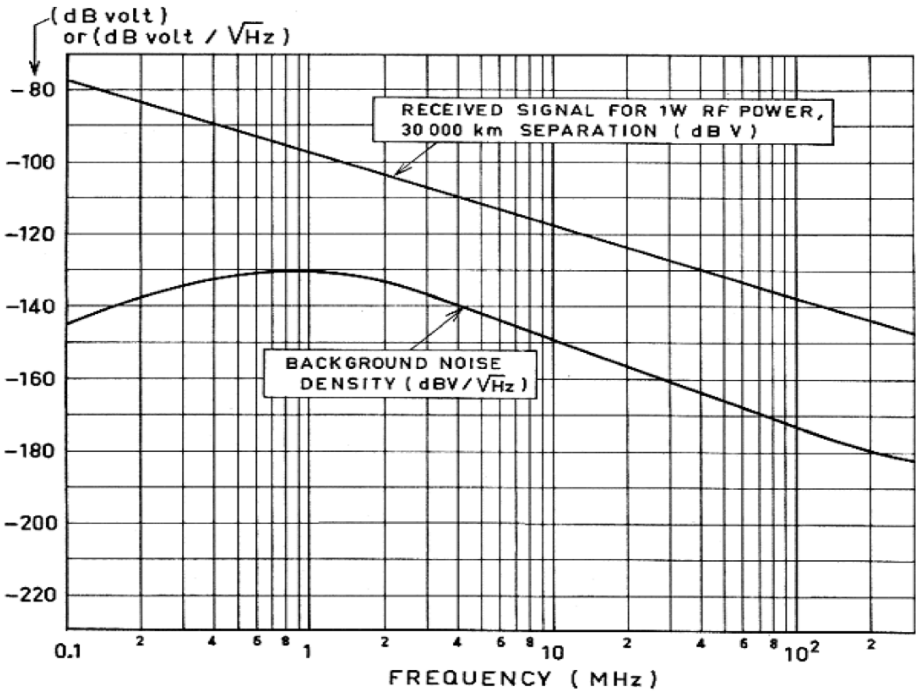

Figure 3: Estimating the RF power to be radiated : intensities of the background galactic noise level and of the received signal (for 1 W of RF power radiated at a distance of 30000 km) are plotted versus frequency. Hence a power of 100 mW emitted in a 10 kHz band by a source at 10000 km from the observer, detected by an antenna with 20 dB gain, provides a S/N ∼30 dB against the sky background.

low telecommand and practically no telemetry requirements, several copies could be flown successively or simultaneously as piggy-back payloads during LOFAR operational phase, and serve as calibration sources. The experiment can be build in laboratories such as Meudon Space Research Department, CNRS Orléans, etc.

References

Jacobson, A. R., and W. Erickson, Wavenumber-resolved observations of ionospheric waves using the very large array telescope, *Planet. Space Sci.*, *40*(4), 447–455, 1992.

Kassim, N. E., R. A. Perley, W. C. Erickson, and K. S. Dwarakanath, Subarcminute resolution imaging of radio sources at 74 MHz with the very large array, *The Astrophysical Journal*, *106*(6), 2218–2228, 1993.

Mercier, C., and A. R. Jacobson, Observations of atmospheric gravity waves by radio interferometry: are results biased by the observational technique?, *Annales Geophys.*, *15*, 430–442, 1997.

Noordam, J. E., LOFAR Calibration and Calibratability, *Tech. Rep. 00227*, ASTRON-LOFAR, 2001.

Zarka, P., Long Baseline Decameter Interferometry between Nançay and LOFAR, in *Measurements using Optic and RF Waves*, edited by F. de Fornel and P.-N. Favennec, pp. 291–304, ISTE & Wiley, 2010.

Synergies with other instruments

P. Zarka, L. Lamy, L. Guillemot, J.-M. Grießmeier, A. Konovalenko, M. Tagger et al.

NenuFAR will benefit from & to many synergies with other instruments. We provide below a non-exhaustive list of those :

On the ground

- UTR-2 / Kharkov (pulsars, Jupiter decametric emission, Sun, Saturn lightning, flare stars …)
- GURT / Kharkov (pulsars, Jupiter decametric emission, Sun, Saturn lightning, flare stars …)
- NDA / Nançay Decameter Array (Jupiter decametric emission, Sun),
- NRT / Nançay decimeter Radio Telescope (pulsars, stars/blazars/jets)
- LOFAR (NenuFAR as the LSS – LOFAR super station)
- SKA (NenuFAR as a precursor – see section 2)
- EPTA, IPTA, LEAP (pulsar timing arrays)
- IR telescopes (Jupiter's aurorae, exoplanets …)
- …

In space

- Cassini (Saturn lightning, Jupiter decametric emission),
- FERMI (Gamma-ray pulsars)
- TARANIS (TGF)
- JUNO (Jupiter)
- JUICE (Jupiter)
- HST – the Hubble Space Telescope (Jupiter's aurorae, exoplanets …)
- Chandra/XMM-Newton (exoplanets)
- JWST (Jupiter's aurorae, exoplanets …)
- …

NenuFAR – Art Project

Cyrille Courte, Philippe Zarka, et al.

By nature, the modern LF radioastronomy instruments, consisting of ~2m-high dipoles (Figure 1a), are less visually impressive that the massive radioastronomy dishes of the 1980's-1990's (Figure 1b). It is the distribution of a large number of dipoles (Figure 1c) that strikes the perception/imagination of the general public, illustrating the large means that must be deployed to detect tiny signals carrying the information about the vast Universe.

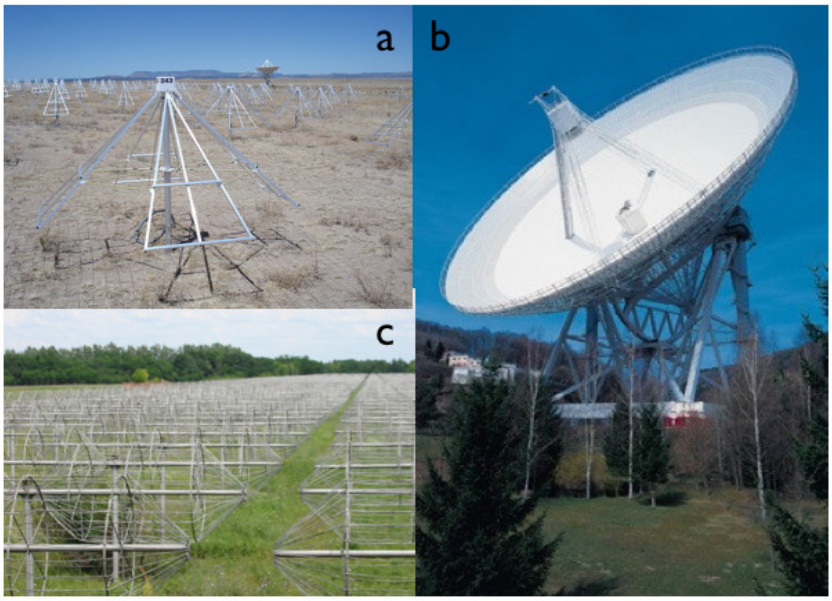

Figure 1 : (a) the Effelsberg 100 m diameter dish, near Bonn ;
(b) LWA antennas ~2m high ; (c) part of the UTR-2 Kharkov LF radio aray

NenuFAR will be a facility of international stature, and at the same time a large industrial-like development, covering almost 13 hectares of land within the Nançay Radioastronomy Observatory in région Centre with nearly 2000 crossed-dipoles antennas and their associated electronics (Figure 2). It will be visited by the radioastronomers from all around the world who will use it to observe, as well as by the general public at various occasions such as « open campus » or specific operations. We are convinced that such a large facility deserves an effort to integrate it with an art realization that will enhance its impact in the general public, attract its interest, and contribute thus to its public outreach.

In the frame of an internship work of the Master DNSEP of « Ecole Supérieure des Beaux-Arts de Tours », in March and June-July 2014, C. Courte studied an art project around NenuFAR. The present project includes 3 components :

- a large-scale ground marking making the instrument well visible from the sky (inspired by Nazca Geoglyphs and the Crop circles of Avebury Manor, UK) ; it could consist of a circular (or loop) path of white gravel, of ~300 m in diameter, immersed in the antenna array (Fig. 3a) ;
- a central structure of size comparable to a mini-array, self-supporting, without foundations, inspired by the ideas of the archirect and engineer D. G. Emmerich (Figs. 3b,c) ;
- a sound system inserted in this central structure providing an audio translation/illustration of the waves received by NenuFAR antennas (see e.g. http://www.lesia.obspm.fr/perso/philippe-zarka/SonsPZ.html)

More details can be found on http://nenufar.obs-nancay.fr/ (documentation→art project→ C. Courte).

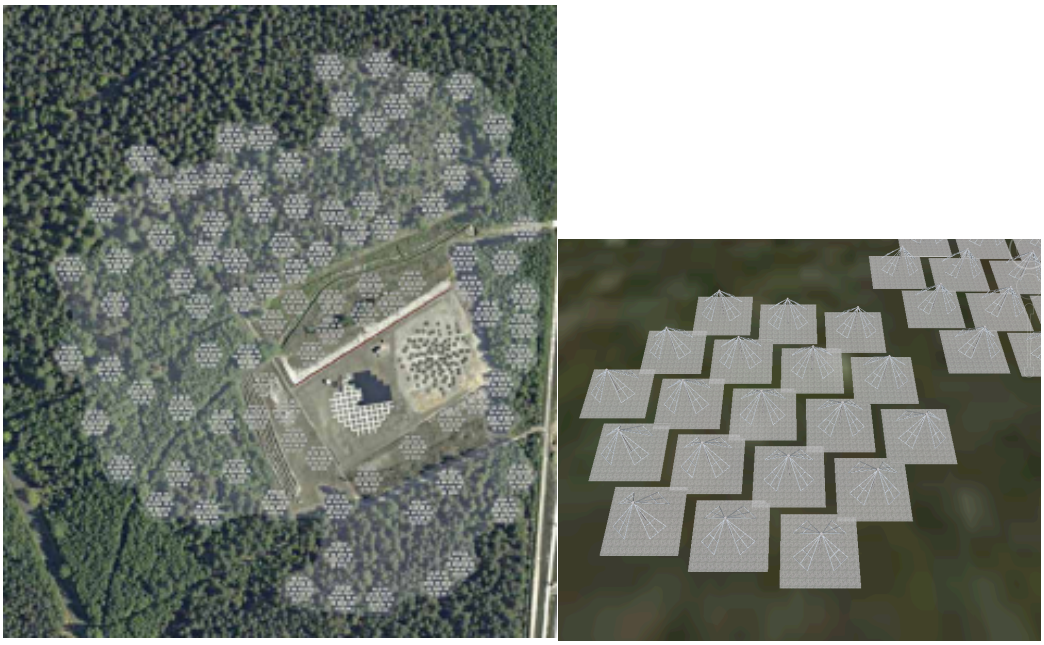

Figure 2 : (left) a possible layout of the 96 NenuFAR sub-arrays over 9 hectares in Nançay ; (right) zoom on onesub-array of 19 crossed dipole antennas.

The budget dedicated to this project should be of order of 1% of the construction cost of NenuFAR. Of course, special care will be taken in its realization so that it does not interfere in any way with the performances and exploitation of NenuFAR (no radio interference produced, no large metallic surface of electric currents in wires on the ground that may perturb the antennas response, etc.)

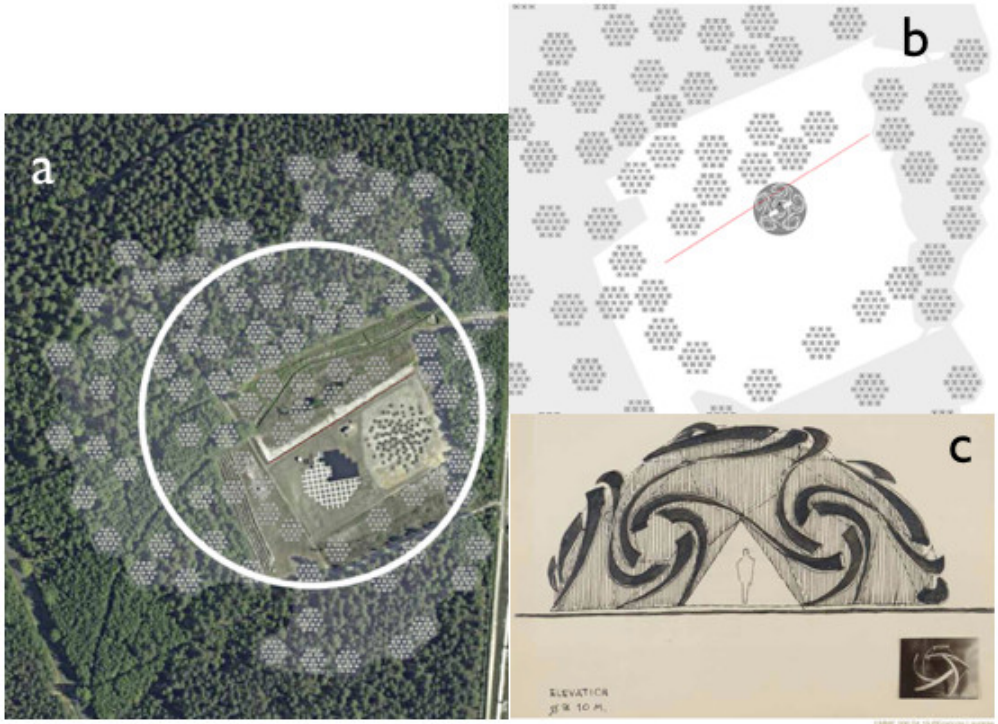

Figure 3 : (a) the white path around the array ; (b) location of the central structure, sketched in (c).

The management of the access of the general public to NenuFAR as an artwork might be set under the responsability of the Pôle des Etoiles / Centre Sciences.

Synthesis

Michel Tagger, Philippe Zarka, Laurent Denis

The NenuFAR project is the result of a long history, which has seen the French community develop an expertise in low-frequency radioastronomy with decades of dedicated observations of Jupiter and the Sun at Nançay with the decameter array (10-100 MHz) and the radioheliograph (discrete frequencies between 150 and 450 MHz). Some of its members participated in the definition and scientific case of the LOw Frequency ARray (LOFAR) since the initial stage of the project (2000). Following contacts between Nançay and LOFAR, and discussions within the French scientific community, the INSU prospective of 2003 provided the initial momentum to LOFAR/SKA/FASR activities in France. Year 2006 was a key date in the french implication in LOFAR: the FLOW consortium was formed and held its first meeting in march in CIAS/Meudon, resulting in the LOFAR/FLOW science case (*Tagger et al. , 2006*). On this basis CNRS/INSU and Observatoire de Paris decided to fund the French LOFAR station in Nançay. They were joined by Université d'Orléans, which made this the first large project of its Observatoire des Sciences de l'Univers en region Centre (OSUC) and brought regional support for it.

In parallel, the formation and P.I.-ship of a planet-exoplanet working group was proposed to P. Zarka by the "Transients" Key Science Project of LOFAR (`http://www.transientskp.org/`). First long baselines LF fringes were obtained on Jupiter between the Nançay decameter array and LOFAR's test Core Station 1 (*Nigl et al., 2014*). LOFAR commissioning observations extended over 2009-2011. The Nançay LOFAR station (FR606) was inaugurated in may 2011.

LOFAR is an interferometer of phased arrays centered in The Netherlands but extending across Europe, with maximum baselines of (presently) 1300km. As the first real LF spectro-imager and the first truly "digital radiotelescope", gathering thousands of antennas in the band 30-80 MHz (down to 10 MHz with reduced sensitivity) and tens of thousands in the range 110-250 MHz, LOFAR brings an increase > 1 order of magnitude in sensitivity and > 2 orders of magnitude in angular resolution over all existing instruments. LOFAR's philosophy is based on (relatively) simple but numerous antennas, coupled via powerful and complex software. As a consequence, its capabilities improve permanently with new versions of the central correlator and of the real-time and analysis software.

LOFAR scientific operations started in December 2012, with the (near-) complete instrument described in (*van Haarlem et al., 2013*), and proceeds now with semester calls for observations. Several tens of scientific papers have already been published in refereed journals. The FR606 station is regularly used within the LOFAR telescope (see e.g. *Moldon et al., 2014*) as well as in "standalone mode" (`http://www.obs-nancay.fr/Observer-avec-LOFAR-FR606.html`).

The French community is signficantly involved in LOFAR observation programs (5 to 10% of P.I.'s and Co.I.'s in cycles 0-2), and its contribution is especially remarkable concerning the LOFAR imaging tools (direction-dependent imager by *Tasse et al. (2013)*, and advanced methods such as nonlinear Kalman filters (*Tasse , 2014*) and compressed sensing (*Garsden et al. 2014*)). In parallel with this involvement of French scientists in LOFAR, the original concept of a LOFAR superstation was developed in Meudon and Nançay, and became NenuFAR. It consists in a large array antennas in the range 10-85 MHz. The instrument and its foreseen science are described in (*Zarka et al., 2012*) and (*NenuFAR, 2014*).

NenuFAR has a hierarchical structure, being composed of 96 mini-arrays of 19 dual polarization antennas. Each mini-array is analog-phased and the 96 units feed at the same time the LOFAR backend (and telescope) and a dedicated receiver (fiat a beamformer and soon a correlator),

permitting it to be used at the same time and near-independently as a major addition to the international LOFAR telescope and as a large standalone instrument.

NenuFAR will permit observations with high instantaneous sensitivity, coarse resolution imaging for transient searches in Standalone mode, and ultra-sensitive long (and short) baselines within LOFAR (possibly also acting as a second LOFAR core). In addition to significantly improving LOFAR's capabilities, NenuFAR in standalone mode will be a large LF instrument with privileged access to the French community, but driven by a program committee and open to international use.

The NenuFAR proposal thus offers a unique opportunity on three fronts:

- it promises important, original, timely and highly visible new scientific results, in many different fields of astrophysics and cosmology now accessible thanks to the progress in low-frequency radio observation technologies, according to the science case presented in this document ;
- it marks the achievement of a long effort by CNRS, Observatoire de Paris and Université d'Orléans, to consolidate on the Nançay-Orléans-Paris axis a world-class pole of reference for the radioastronomy of the 21st century, in the SKA era;
- and it is a means to foster, expand, train and qualify the new generation of scientists and engineers, ready to tackle the challenges of that era.

The first point is illustrated by the present document. Thanks to its dual nature as both a LOFAR superstation and a stand-alone instrument NenuFAR will permit to address most of the scientific fields covered by SKA, with capabilities that are of course lower but quite different and complementary– in particular the optimization for the lowest range of radio frequencies accessible from the ground. Note that the present document is by no means "final". It will remain a live document and be updated alobg with the development of the project, especially when implementing distant mini-arrays. Science cases will be added as they appear, such as SETI – for which NenuFAR can obviously be used – that we did not develop here.

The second challenge was already the driving ambition for the creation in 2006 of the FLOW scientific consortium. NenuFAR makes the best use of the technical skills of the Nançay engineers to create a new and original instrument, unique and highly visible among the SKA pathfinders (a status LOFAR has been granted, and for which we have applied); it thus ensures the future of Nançay as a modern observatory and a center of expertise in the design and operation of radioastronomy instruments. NenuFAR will also be a precious and versatile tool for the training of new students and engineers, and for future developments.

NenuFAR phase 1, representing 1/4 of the instrument (24 mini-arrays) and 1/3 of its cost, is presently funded and will be built and operational in 2015. It is no coincidence that its funding was obtained from regional funds (both Région Centre and Région Ile-de-France), just as LOFAR in the Netherlands was first seeded by the Drendt Region, matched by national funding. For the Regions such a development appears as a strategic investment for the future in scientific research and education.

Answering the third challenge is already largely under way: the breadth of the present science case shows that around LOFAR and now NenuFAR we have already been able to attract a large community of astronomers and cosmologists, going far beyond the traditional fields of low-frequency radioastronomy. Less visible is also the fact that the design of NenuFAR has involved contributions from top research engineers (in particular its has permitted to rebuild in Nançay a technical expertise on all aspects of radiotelescope design) and from high-tech companies whose expertise in radio technologies of the future is thus also developed.

On the other hand we hope that we have made visible enough in this document the very strong support we have received from colleagues abroad: a financial contribution from University of Graz, but also extremely positive inputs on the science case, some of which have had a direct impact on the design of NenuFAR.

This is a guarantee that we will produce the best possible scientific return; but it is also a guarantee that NenuFAR already is, and will be even more once it is built, a powerful tool to expand the French scientific teams, their contribution, their role and their visibility in the international community. Our community has a recognized scientific expertise in many fields for which LF radio observations are relevant (cf. (Goutelas, 2011) and the other chapters in this White Book). With NenuFAR expertise will be gathered in advanced interferometric imaging, beamformed and waveform (time domain) observations. This interdisciplinary community will then have the possibility to fully prepare a strong scientific involvement in SKA.

Indeed, given the prospects offered by SKA, but already also LOFAR and its other pathfinders, and the immense field to explore with them, the development or renewal of a strong LF radio community in France should now be seen as strategic. This development of expertise should go along with hiring young scientists. 3 have already been hired on LOFAR-SKA by the CNAP ; more are needed and the scientific exploitation of LOFAR and NenuFAR will permit us to prepare and train them.

References

Garsden, H., et al., LOFAR Sparse Image Reconstruction, A&A, submitted (2014)

Moldon, J., et al., The LOFAR long baseline snapshot calibrator survey, Astron. Astro- phys., submitted (2014)

The NenuFAR collaboration, NenuFAR : instrument description and science case, CNRS/INSU Prospective, 2014, http://nenufar.obs-nancay.fr/IMG/pdf/ nenufar-science-case.pdf (2014)

Nigl, A., P. Zarka, J. Kuijpers, H. Falcke, L. Bahren, and L. Denis, VLBI observations of Jupiter with the Initial Test Station of LOFAR and the Nanay Decametric Array, Astron. Astrophys., 471, 10991104 (2007)

Tagger, M., and FLOW (The French LOFAR consortium), Science Case for a French participation in LOFAR, http://www.lesia.obspm.fr/plasma/LOFAR2006/ FLOW_Science_Case_r.pdf (2006)

"Radioastronomie Basses Fréquences : Instrumentation, Thématiques scientifiques, Projets", XXX^{ème} Ecole de Goutelas, CNRS/INSU/SF2A, 4-8/6/2007, edited by P. Zarka, M. Tagger, and B. Cecconi, http://www.lesia.obspm.fr/plasma/Goutelas2007/ #Presentations (2011)

Tasse, C., et al., Applying full polarization A-Projection to very wide field of view instru- ments: An imager for LOFAR, A&A 553, A105 (2013)

Tasse, C., Nonlinear Kalman filters for calibration in radio interferometry, A&A 566, A127 (2014)

van Haarlem, M. P., et al., LOFAR: The Low Frequency Array, Astron. Astrophys., 556, A2 (2013)

Zarka, P., J.N. Girard, M. Tagger, L. Denis and the LSS team, "LSS/NenuFAR: The LOFAR Super Station Project in Nançay", 2012, Proc. Société française d'Astronomie Astrophysique http://nenufar.sciencesconf.org/conference/nenufar/pages/LSS.pdf